ASSESSMENT OF MEMBRANE FOULING BEHAVIOR OF NANOFILTRATION AND MEMBRANE DISTILLATION FOR WATER REUSE

By
NGO THI TRA MY

A thesis submitted in partial fulfillment of the requirements for
the degree of Doctor of Engineering

Graduate School of Engineering
Nagasaki University
Division of Water and Environmental Science

December, 2021

Abstract

Dissolved organics and trace organic compounds (TOrCs) have been recently found in treated effluent of municipal wastewater treatment plants and recipient waters. This can pose a serious threat to the safeness of reusing water due to the insufficiency of the conventional treatment train against these emerging pollutants. Although membrane-based treatment becomes an attractive option to address contaminated water, membrane fouling remains a major challenge for the sustainable operation of wastewater treatment as it increases the operating cost and shortens the membrane lifetime. This research aimed to establish a membrane selection strategy with different wastewater sources for removing contaminants and minimizing membrane fouling. The direct treatment of secondary wastewater effluent using nanofiltration (NF) membranes was applied for non-potable water reuse while reverse osmosis (RO) and membrane distillation (MD) membranes were used in the treatment of RO concentrate containing high concentrations of salts and organics for potable purposes.

For the NF membrane, a submerged membrane module was adopted at low permeate flux (3 L/m^2h) for alleviating membrane fouling. The separation performance of the NF system was assessed by periodically measuring the color, turbidity, UV light absorbance at the wavelength of 254 nm (E_{254}), and total organic carbon (TOC) of the NF feed water and permeate. During a 48-d test, direct NF treatment of secondary wastewater effluent resulted in a negligible membrane fouling with the transmembrane pressure increase of only 3 kPa. The fouling speed is far less than the case with a typical permeate flux of 40 L/m^2h (an 18 % permeability drop within the first 4 h), which can require chemical cleaning every few hours. The substances deposited on the membrane surface were readily removed by a polyurethane sponge, which fully recovered the membrane permeability. The cake layer on the membrane surface is the major source of the increased hydraulic resistance. The direct NF treatment stably achieved high removal of organics during the test period with the rejection of color, $E_{254,}$ and TOC at over 93, 84, and 67%, respectively. The excitation-emission matrix fluorescence spectra showed that direct NF treatment considerably reduced the intensity of humic acid-like substances. This study demonstrated the efficacy of the direct nanofiltration treatment using a submerged NF module for achieving a stable operation and producing high-quality recycled water.

The membrane fouling propensity and water quality were compared during the treatment of the reverse osmosis (RO) concentrate by membrane distillation (MD) and RO membranes at a permeate flux of 25 L/m^{2}h. Increasing overall water recovery from 85% to 98% did not significantly reduce the permeate flux (~4%) for MD treatment. However, the considerable increase in transmembrane pressure in only 1.5 h indicates that the treatment of the RO concentrate by RO allowed only 88% of overall water recovery. A reduction in pure water permeability of up to 73% was found after the treatment by RO while MD treatment did not reduce the permeance. This indicates that membrane fouling might occur for the RO membrane. The significant formation of the foulant layer on the membrane surface of the RO membrane was also found. In addition, the MD membrane shows superior retention of almost all the ions and TOrCs. Electrical conductivity rejection was very high (99.8%) for MD, but the treatment led to high permeation of trace organic compounds with high volatility, particularly *N*-nitrosodimethylamine. Post-treatment (e.g., advanced oxidation) after reverse osmosis and membrane distillation may be needed to comply with the *N*-nitrosodimethylamine regulations. This study suggests that MD will be a more feasible choice than RO membrane for increasing water recovery in wastewater treatment. A considerably higher energy requirement in MD highlights the necessity of abundant waste heat or renewable energy sources to enable the applicability of MD treatment.

In general, this doctoral dissertation addresses membrane fouling in advanced water treatment processes as well as ensures treated water quality for potable or non-potable water reuse. The results demonstrate the efficacy of the direct NF treatment using a submerged NF membrane module and the feasibility of MD in RO concentrate treatment for achieving a stable operation and producing high-quality recycled water. Further pilot-scale studies may be conducted to enhance the permeate flux and to minimize the energy consumption for potable or non-potable water reuse. This can be achieved by improving membrane module design in NF and membrane properties in MD.

Acknowledgment

Throughout my research at Nagasaki University as well as the life in Japan, I have received many supports from my supervisor, my labmates, and other scientists:

- First and foremost, I am grateful to my supervisor - Associate Professor Takahiro Fujioka (Nagasaki University, Japan) who helped me a lot in my research process.
- I would like to thank Dr. Tetsuro Ueyama and Mr. Ryo Makabe (Kyowakiden Industry Co., Japan) who supported me in the analysis.
- I would like to thank Dr. Tetsuji Okuda (Ryukoku University, Japan) who supported me with research materials.
- I would like to thank Dr. Hideaki Sano (Nagasaki University, Japan) who taught me to analyze membrane surface characteristics.
- I would like to thank my labmates (Ms. Sandrine Boivin and Mr. Binh Quoc Diep) who supported me get used to new equipment and give the hand in lab work.

Finally, I am grateful that the Japanese Government provided me with a MEXT scholarship so that I can focus on the research to complete the Ph.D. program in Japan.

Table of Contents

Chapter 1. Introduction

1.1. General backgrounds

1.1.1. Water pollution

The rapid growth of the population has put tremendous pressure on water resources in both quality and quantity (Chen et al., 2020b; Jia et al., 2020). In some parts of the world, reusing water has re-emerged as a promising water source to compensate for freshwater scarcity (Ali et al., 2018). The contamination of water sources with organics, ions, or microbial contaminants has become a serious issue in potable or non-potable water reuse. Not only the formation of disinfection by-products caused by organic fractions in treated water through post-chlorination (Rodriguez-Narvaez et al., 2017; Mohd Zainudin et al., 2018) but also a high concentration of toxic ions can cause health problems in drinking water treatment (Liu et al., 2020). Hence, the removal of chemical and microbial contaminants from water sources is of paramount importance in water treatment to protect public health (WHO, 2011). Security of drinking water is ensured by providing drinking water treatment and complying with the drinking water quality standards. Conventional drinking water treatment—a rapid sand filtration system—typically comprises coagulation, flocculation, sedimentation, rapid sand filter, and post-chlorination. With relatively clean drinking water sources, conventional drinking water treatment can readily achieve the water quality goals. However, it can be insufficient to address contaminated water with high concentrations of salts and organics and specially with trace organic compounds that have low molecular weight in municipal wastewater.

1.1.2. Trace organic compounds (TOrCs)

Due to the rapid industrialization and urbanization around the world, a growing amount of trace organic compounds (TOrCs) is produced and released into the aquatic environment and causes critical concerns on human health (Bellona et al., 2004; Khetan and Collins, 2007; Yang et al., 2017; Golovko et al., 2021). These chemicals have been found in drinking water from several countries, particularly in South Africa (Van Zijl et al., 2017; Kasonga et al., 2021). TOrCs compounds consist of various chemicals, such as pharmaceuticals and personal care products (PPCPs), surfactants, endocrine-disrupting compounds, and persistent organics

(e.g., fertilizers, pesticides, or biocides). They can enter the aquatic environment via many different pathways (Fig. 1-1), such as pharmaceutical waste, agricultural and industrial sectors, human activities from households, or inadequately treated effluents from wastewater treatment plants (Van Zijl et al., 2017).

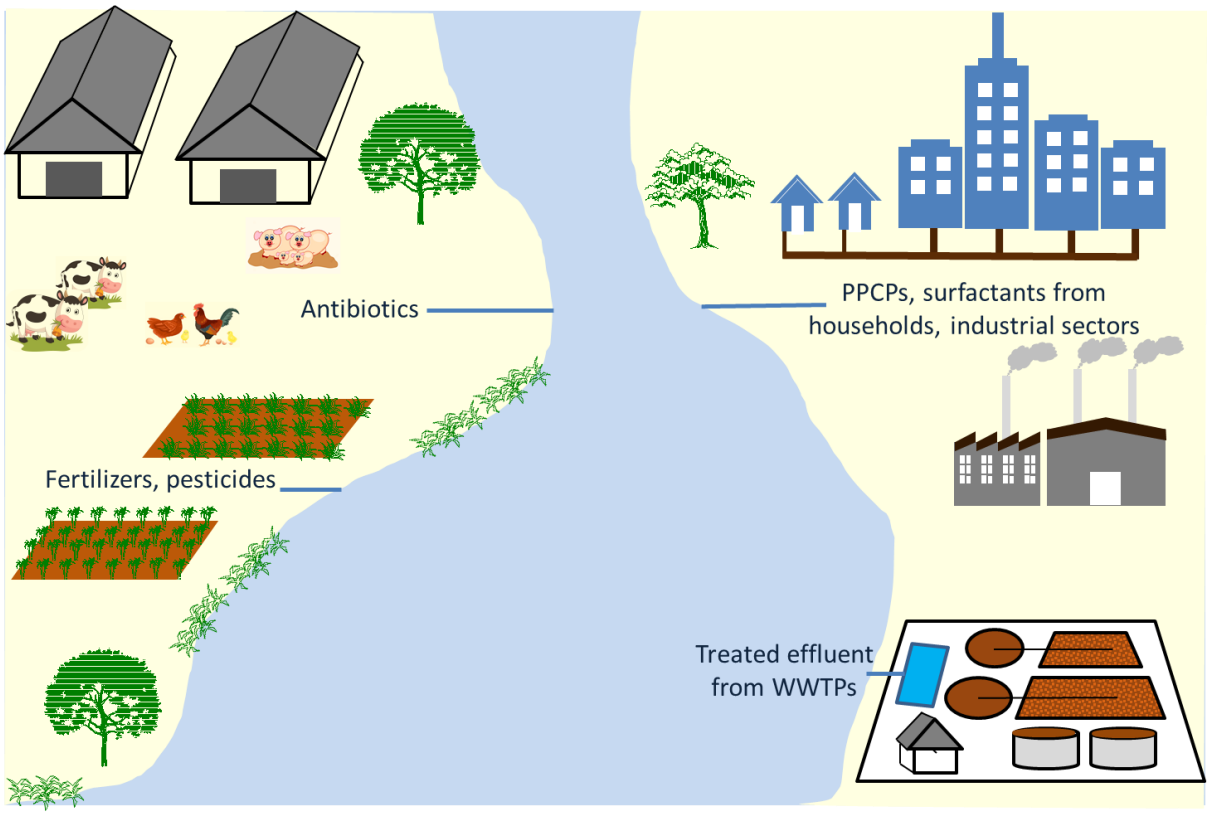

Fig. 1-1. Sources of trace organic compounds (TOrCs).

These TOrCs can easily dissolve in water and tend to accumulate in the food chain (Escher et al., 2011; Sui et al., 2015). Although some TOrCs can deteriorate upon release into the environment, most of them are persistent. Moreover, conventional wastewater treatment is not capable of removing TOrCs chemicals and their metabolites (Wang and Wang, 2016; Golovko et al., 2021). As a result, TOrC concentrations in downstream recipient samples of the wastewater treatment plant were 50% higher than upstream. Their concentrations of TOrCs were detected from a few ng/L to 19 µg/L in surface water and 64 µg/L in wastewater (Golovko et al., 2021). Therefore, these chemicals become a high risk to the environment as well as human health. It should be noted that some TOrCs compounds can be active even in very low concentrations from a few µg/L (Kasonga et al., 2021). Prolonged exposure to

pharmaceuticals and personal care products can increase antibiotic resistance and break the balance of the human body (Hernando et al., 2006). Some endocrine-disrupting compounds can copy or offend hormones' effects, change the model of synthesis of hormones, and modify hormone receptor levels (Tapia-Orozco et al., 2017). They can cause thyroid problems, Alzheimer, obesity, and cancer in humans (Kasonga et al., 2021). The presence of antibiotics in the aquatic environment can lead to an increase in harmful bacteria species and endanger human health (Pan and Chu, 2017).

1.1.3. Membrane technologies in drinking water treatment and challenges

Various advanced water technologies have been developed for removing contaminants that persisted after conventional treatment (Chen et al., 2020a; Zhao et al., 2022). The removal of organic matters can be achieved by deploying advanced drinking water treatment processes such as ozonation and biological activated carbon (Fan et al., 2014; Hu et al., 2019). However, the addition of these advanced processes makes the overall water treatment system complex; therefore, it is unlikely feasible for small water utilities that typically have less skilled labor and insufficient funding. The high-pressure membrane treatments including reverse osmosis (RO) and nanofiltration (NF) are powerful water treatment processes that can achieve high removal of small organics and ions (Van der Bruggen and Vandecasteele, 2003; Owusu-Agyeman et al., 2019). Among membrane processes, RO has the highest separation performance, but it requires high energy according to its high-pressure requirement. In contrast, NF membrane, which has a molecular weight cut-off of 200–1000 Da, requires less energy than RO membrane due to its looser membrane structure, whereas their separation capability for monovalent ions (i.e., NaCl) is far less than RO and can vary considerably depending on the membrane selection. However, the main problem in both NF and RO membranes is membrane fouling that reduces permeate flux, increases operation cost, and shortens membrane lifetime (Jiang et al., 2017).

In addition to RO and NF, membrane distillation (MD), which is a thermally driven membrane separation process using hydrophobic membranes, is capable of removing almost all non-volatile contaminants (Wang and Chung, 2015). Although MD technology has not started to be applied in water and wastewater treatment plants, studies on both MD theories and experiments have remarkably increased over the past few decades (Laganà et al., 2000; Wang and Chung, 2015; Khalifa et al., 2017). Membrane wetting and fouling are also the

potential issues that constraint the applications of hydrophobic MD membranes for treating feed water containing surfactants (Wang and Lin, 2017; Rezaei et al., 2018). However, since MD is less susceptible to fouling, the effects of membrane fouling on both permeate flux and water quality are insignificant while membrane fouling in RO/NF treatment can significantly reduce the quantitative of pure product water (Lee et al., 2016).

1.2. The aims and study flow of the doctoral dissertation

The main objectives of the dissertation were to establish a membrane selection strategy with low fouling for removing contaminants by providing an in-depth understanding of their separation mechanisms according to the properties of the membrane and contaminants (e.g., pore size, surface charge, and hydrophobicity) and required operating conditions related to cost factor (e.g., transmembrane pressure and recovery). Membrane fouling propensity and treated water quality were assessed via membrane-based water treatment processes for potable or non-potable water reuse. Small coupons of various NF/RO/MD membranes and a variety of wastewaters generated from municipal wastewater treatment plants (e.g., secondary wastewater effluent and reverse osmosis concentrate) were used at the laboratory scale. The outcome of this study will help the poor in water shortage areas to be able to access clean water. The main contents of the doctoral dissertation are presented in Fig. 1.2. Herein, chapters 3 and 4 are published papers.

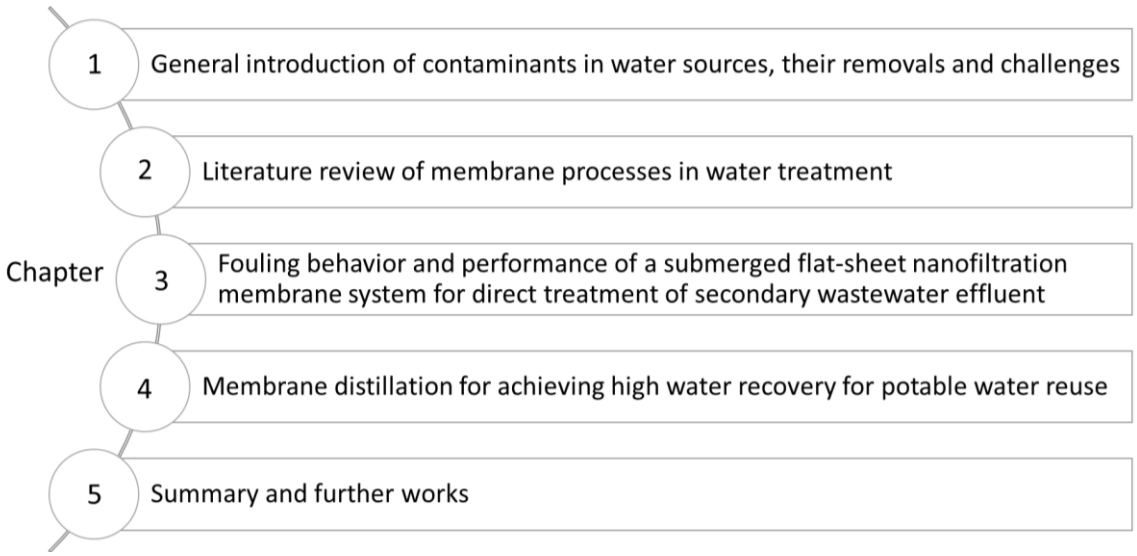

Fig. 1-2. Main contents of the doctoral dissertation.

References

Ali, A., Tufa, R.A., Macedonio, F., Curcio, E., Drioli, E., 2018. Membrane technology in renewable-energy-driven desalination. Renewable and Sustainable Energy Reviews 81, 1-21.

Bellona, C., Drewes, J.E., Xu, P., Amy, G., 2004. Factors affecting the rejection of organic solutes during NF/RO treatment—a literature review. Water Res. 38, 2795-2809.

Chen, A.S.C., Wang, L., Sorg, T.J., Lytle, D.A., 2020a. Removing arsenic and co-occurring contaminants from drinking water by full-scale ion exchange and point-of-use/point-of-entry reverse osmosis systems. Water Res. 172, 115455.

Chen, L., Huang, K., Zhou, J., Duan, H.-F., Zhang, J., Wang, D., Qiu, H., 2020b. Multiple-risk assessment of water supply, hydropower and environment nexus in the water resources system. Journal of Cleaner Production 268, 122057.

Escher, B.I., Baumgartner, R., Koller, M., Treyer, K., Lienert, J., McArdell, C.S., 2011. Environmental toxicology and risk assessment of pharmaceuticals from hospital wastewater. Water Res. 45, 75-92.

Fan, X., Tao, Y., Wang, L., Zhang, X., Lei, Y., Wang, Z., Noguchi, H., 2014. Performance of an integrated process combining ozonation with ceramic membrane ultra-filtration for advanced treatment of drinking water. Desalination 335, 47-54.

Golovko, O., Örn, S., Sörengård, M., Frieberg, K., Nassazzi, W., Lai, F.Y., Ahrens, L., 2021. Occurrence and removal of chemicals of emerging concern in wastewater treatment plants and their impact on receiving water systems. Sci. Total Environ. 754, 142122.

Hernando, M.D., Mezcua, M., Fernández-Alba, A.R., Barceló, D., 2006. Environmental risk assessment of pharmaceutical residues in wastewater effluents, surface waters and sediments. Talanta 69, 334-342.

Hu, Y., Zhang, T., Jiang, L., Luo, Y., Yao, S., Zhang, D., Lin, K., Cui, C., 2019. Occurrence and reduction of antibiotic resistance genes in conventional and advanced drinking water treatment processes. Sci. Total Environ. 669, 777-784.

Jia, X., Klemeš, J.J., Alwi, S.R.W., Varbanov, P.S., 2020. Regional Water Resources Assessment using Water Scarcity Pinch Analysis. Resources, Conservation and Recycling 157, 104749.

Jiang, S., Li, Y., Ladewig, B.P., 2017. A review of reverse osmosis membrane fouling and control strategies. Sci. Total Environ. 595, 567-583.

Kasonga, T.K., Coetzee, M.A., Kamika, I., Ngole-Jeme, V.M., Momba, M.N.B., 2021. Endocrine-disruptive chemicals as contaminants of emerging concern in wastewater and surface water: A review. J. Environ. Manage. 277, 111485.

Khalifa, A., Ahmad, H., Antar, M., Laoui, T., Khayet, M., 2017. Experimental and theoretical investigations on water desalination using direct contact membrane distillation. Desalination 404, 22-34.

Khetan, S.K., Collins, T.J., 2007. Human pharmaceuticals in the aquatic environment: a challenge to green chemistry. Chem. Rev. 107, 2319-2364.

Laganà, F., Barbieri, G., Drioli, E., 2000. Direct contact membrane distillation: modelling and concentration experiments. J. Membr. Sci. 166, 1-11.

Lee, S., Kim, Y., Kim, A.S., Hong, S., 2016. Evaluation of membrane-based desalting processes for RO brine treatment. Desalination and Water Treatment 57, 7432-7439.

Liu, X., Chen, L., Yang, M., Tan, C., Chu, W., 2020. The occurrence, characteristics, transformation and control of aromatic disinfection by-products: A review. Water Res. 184, 116076.

Mohd Zainudin, F., Abu Hasan, H., Sheikh Abdullah, S.R., 2018. An overview of the technology used to remove trihalomethane (THM), trihalomethane precursors, and trihalomethane formation potential (THMFP) from water and wastewater. Journal of Industrial and Engineering Chemistry 57, 1-14.

Owusu-Agyeman, I., Reinwald, M., Jeihanipour, A., Schäfer, A.I., 2019. Removal of fluoride and natural organic matter from natural tropical brackish waters by nanofiltration/reverse osmosis with varying water chemistry. Chemosphere 217, 47-58.

Pan, M., Chu, L., 2017. Transfer of antibiotics from wastewater or animal manure to soil and edible crops. Environ. Pollut. 231, 829-836.

Rezaei, M., Warsinger, D.M., Lienhard V, J.H., Duke, M.C., Matsuura, T., Samhaber, W.M., 2018. Wetting phenomena in membrane distillation: Mechanisms, reversal, and prevention. Water Res. 139, 329-352.

Rodriguez-Narvaez, O.M., Peralta-Hernandez, J.M., Goonetilleke, A., Bandala, E.R., 2017. Treatment technologies for emerging contaminants in water: A review. Chem. Eng. J. 323, 361-380.

Sui, Q., Cao, X., Lu, S., Zhao, W., Qiu, Z., Yu, G., 2015. Occurrence, sources and fate of pharmaceuticals and personal care products in the groundwater: a review. Emerging Contaminants 1, 14-24.

Tapia-Orozco, N., Santiago-Toledo, G., Barrón, V., Espinosa-García, A.M., García-García, J.A., García-Arrazola, R., 2017. Environmental epigenomics: Current approaches to assess epigenetic effects of endocrine disrupting compounds (EDC's) on human health. Environmental toxicology and pharmacology 51, 94-99.

Van der Bruggen, B., Vandecasteele, C., 2003. Removal of pollutants from surface water and groundwater by nanofiltration: overview of possible applications in the drinking water industry. Environ. Pollut. 122, 435-445.

Van Zijl, M.C., Aneck-Hahn, N.H., Swart, P., Hayward, S., Genthe, B., De Jager, C., 2017. Estrogenic activity, chemical levels and health risk assessment of municipal distribution point water from Pretoria and Cape Town, South Africa. Chemosphere 186, 305-313.

Wang, J., Wang, S., 2016. Removal of pharmaceuticals and personal care products (PPCPs) from wastewater: a review. J. Environ. Manage. 182, 620-640.

Wang, P., Chung, T.-S., 2015. Recent advances in membrane distillation processes: Membrane development, configuration design and application exploring. J. Membr. Sci. 474, 39-56.

Wang, Z., Lin, S., 2017. Membrane fouling and wetting in membrane distillation and their mitigation by novel membranes with special wettability. Water Res. 112, 38-47.

WHO, G., 2011. Guidelines for drinking-water quality. World Health Organization 216, 303-304.

Yang, Y., Ok, Y.S., Kim, K.-H., Kwon, E.E., Tsang, Y.F., 2017. Occurrences and removal of pharmaceuticals and personal care products (PPCPs) in drinking water and water/sewage treatment plants: A review. Sci. Total Environ. 596, 303-320.

Zhao, Q., He, H., Gao, K., Li, T., Dong, B., 2022. Fate, mobility, and pathogenicity of drinking water treatment plant resistomes deciphered by metagenomic assembly and network analyses. Sci. Total Environ. 804, 150095.

Chapter 2. Reviews of membrane processes in water treatment

2.1. Nanofiltration (NF)

Nanofiltration (NF) and reverse osmosis (RO) are classes of pressure-driven membrane filtration technologies which has been increasingly employed as advanced treatment processes for potable water (Matin et al., 2021; Oatley-Radcliffe et al., 2017). NF and RO are closely resemblant in terms of membrane structure and operation but differ in their pore size and the target substance for removal. As the intermediate between ultrafiltration (UF) and RO membranes, the pore size of the NF membrane is in the sub-nanometer range which corresponds to a molecular weight cut-off (MWCO) of about 200 – 1000 Da (Mohammad et al., 2015). Typically operated under a pressure of 5–35 bars, NF is of particular interest for its ability to reject low MWCO solutes such as natural organic matters and partial salt rejection (Abdel-Fatah, 2018).

2.1.1. Removal mechanisms

The rejection of solutes in NF processes results from a complex mechanism including molecular sieving, charge repulsion, and adsorption/diffusion. Molecular sieving is the key influencing factor in the removal of uncharged solutes and usually the higher the molecular weight the better rejection. On the other hand, charge separation governs the separation of charged solutes and ions. In NF, monovalent ions can permeate through the membrane but multivalent ions are retained (up to above 95% can be achieved (Van der Bruggen, 2013)) due to the higher electrostatic repulsion force. For charged organic matters, electrostatic interaction with membranes can lead to higher or lower retention than expected based purely on size exclusion (Van Der Bruggen et al., 1999). Besides two main mechanisms, in the case of organic matters, retention can also be affected by adsorption and diffusion. Hydrophobic compounds are more likely to attach to the membrane than hydrophilic counterparts, thus resulting in higher initial retention of the hydrophobic fraction (Kimura et al., 2003). The same initial adsorption was observed by Nghiem et al. (2004) in the NF of natural hormones. However, in the later phase, as adsorption reached saturation, overall lower retention than predicted by size exclusion was reported, suggesting that diffusion of these hormones through

the active layer of the NF membrane had happened. This solute diffusion pathway resembles the transport mechanism of RO membranes.

2.1.2. Fouling mechanisms

A rough definition of membrane fouling is the accumulation of organic, inorganic, and biological substances on the membrane surface (external fouling) and membrane pores (internal fouling) causing a reduction of permeate flux in constant pressure filtration or an increase of transmembrane pressure in constant flux operation. External fouling is the result of solutes larger than membrane pore size depositing on the membrane surface forming cake/gel layers. On the other hand, internal membrane fouling is caused by the adsorption/deposition of solutes similar or smaller than membrane pores. Depending on the type of pore blocking, the permeate flux decline may be gradual as in standard blocking, abrupt as in complete blocking, or somewhere in between as in intermediate blocking (Guo et al., 2012). There are four mechanisms of membrane fouling that happen in water treatment using membranes (Fig. 2-1). Among these, cake formation has been suggested to be more common on tight membranes (NF and RO) due to their dense structure, while pore-blocking is more relevant in loose membranes (microfiltration and ultrafiltration) (Jiang et al., 2017). However, external fouling is generally more accessible and can be reversed by physical and chemical cleaning. In NF where pore structure still exists, permeate flux may be greatly impacted by the adsorption and clogging of foulants inside the membrane pores (Al-Amoudi and Lovitt, 2007). Due to the small, asymmetric pores of NF membranes, pore-blocking is usually irreversible. Another important phenomenon contributing to permeate flux decline in membrane filtration is concentration polarization, which is the accumulation of retained solutes near the membrane surface, resulting in a high solute concentration layer at the membrane surface compared to the bulk solution (Schäfer et al., 2006). This phenomenon is more severe in the NF and RO due to their capability to effectively retain a wide range of solutes including ions. Concentration polarization in NF and RO can cause a significant increase in osmosis pressure, leading to a high degree of flux decline. The high retention of divalent ions also makes scaling more relevant to NF and RO than to microfiltration and ultrafiltration. Although concentration polarization is reversible, it can serve as the precursor of other fouling mechanisms such as adsorption and cake/gel layer formation (Mohammad et al., 2015).

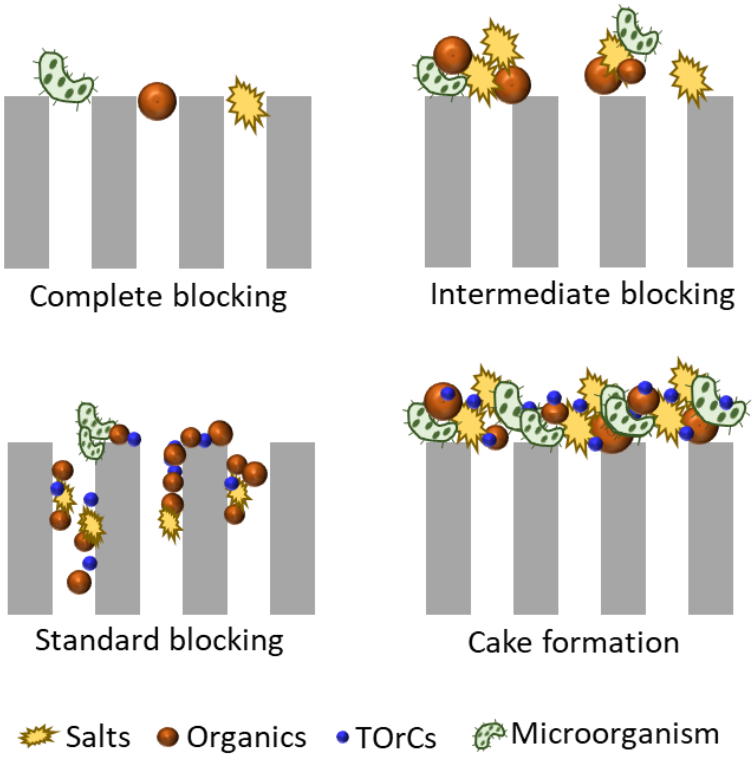

Fig. 2-1. Illustration of different fouling mechanisms.

2.1.3. Membrane fouling mitigation

Numerous measures have been applied or proposed to address membrane fouling. Pre-treatment such as coagulation/flocculation (Chon and Cho, 2016; Racar et al., 2017), granular prefiltration (Meier and Melin, 2005; Zahrim and Hilal, 2013), microfiltration/ultrafiltration (Bodzek et al., 2011; Chon and Cho, 2016), and advanced oxidation processes (Lin et al., 2019; Vatankhah et al., 2018) are among common practices for minimizing membrane fouling. Regardless of intensive pre-treatments, the accumulation of foulants on the membrane surface is unavoidable; hence, periodical membrane cleaning is an essential practice for substantial operation. Despite being very effective in removing foulants and recovering permeate flux is generally not desirable because of the longer downtime required. Moreover, the chemical involved cleanings should be carried out conservatively as excessive use of chemicals and a high cleaning frequency not only are costly but also can alternate the membrane structure, resulting in lower selectivity and potentially damaging the membrane (Andrade et al., 2017; Simon et al., 2013). The techniques that can reduce the progress of membrane fouling include the application of low permeate flux (Kim et al., 2007; Fujioka et al., 2019). The low

permeate flux has the advantage of necessitating low transmembrane pressure in exchange for membrane surface areas to treat a specific volume of water, and it allows to apply a submerged membrane orientation, which can have a transmembrane pressure (TMP) of up to 100 kPa. Another alternative approach to prolong the chemical cleaning frequency is to apply simple surface cleaning using sponges. It has been demonstrated that transmembrane pressure progression could be well delayed by applying moving sponges for both hollow fiber polymer membrane and flat-sheet non-woven membrane in submerged configuration (Xue et al., 2019). Another study reported that the addition of sponge carriers to the membrane tank was capable of mitigating cake layer formation and pore blocking (Deng et al., 2014). For flat-sheet membranes, manual cleaning of the membrane surface by a soft sponge can also be carried out after a period of filtration. Almost complete removal of fibrous extracellular matrix structure and microorganisms on the membrane surface was observed after the sponge cleaning (Kimura et al., 2016).

2.2. Membrane distillation (MD)

Membrane distillation (MD) is the combination of distillation and membrane processes in only one process. It is a thermally driven separation process, where the applied membrane must be porous and hydrophobic (Wang and Chung, 2015). There are four basic MD configurations, namely direct contact membrane distillation, vacuum membrane distillation, air gap membrane distillation, and sweeping gas membrane distillation. Among these configurations, direct contact MD is the simplest with direct contact between feed (hot) and permeate (cold) sides via a hydrophobic membrane. Therefore, much previous research has focused on this configuration to investigate the application potential in the future (González et al., 2017).

2.2.1. Removal mechanisms

In membrane distillation, water or other volatile components evaporate in the feed side, pass through the microporous membrane, and condensate in permeate side (Fig. 2-2). It is noted that the hydrophobicity of MD membranes disallows the feed liquid to directly penetrate the hydrophobic layer because of surface tension (Wang and Chung, 2015). Non-volatile contaminants or compounds with high volatile temperatures are retained in feed solution

while vapors penetrate membrane pores, which produces high-quality treated water. The driving force of this phenomenon is the difference of vapor pressure through the membrane, which is caused by the differential temperature between two sides of the membrane (Alkhudhiri et al., 2012).

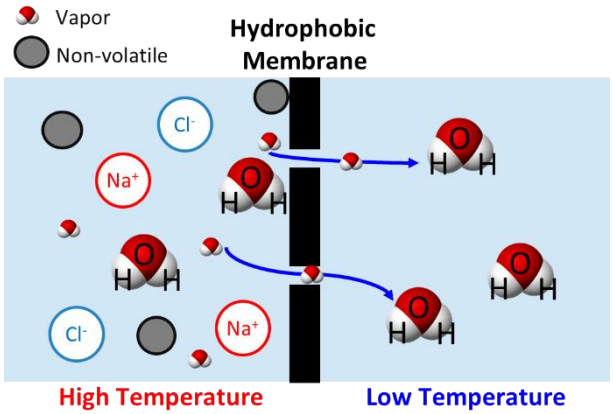

Fig. 2-2. Mechanism of vapor transportation through the hydrophobic membrane.

The removal of contaminants in MD has been found to be dependent on their volatility and hydrophobicity. A low removal of trace organic compounds was reported in MD treatment, such as industrial chemicals (e.g., aniline and phenol, 14–60%), some household products, drugs, hormones, or herbicides with the removal of <88% (Naidu et al., 2017; Li et al., 2018). In particular, during the RO concentrate treatment using a polytetrafluoroethylene (PTFE) membrane, a direct contact MD system showed a high removal of ions (99%) and micropollutants (96–99%). However, only 50–88% of rejection was observed for hydrophobic compounds and compounds with high volatility, such as salicylic acid, propylparaben, benzophenone, triclosan, bisphenol A and atrazine (Naidu et al., 2017). Also, in olive mill wastewater treatment, phenolic compounds including hydroxytyrosol, 3,4-dihydroxyphenylglycol, gallic acid, p-dihydroxyphenyl acetic acid, tyrosol, ferulic acid were detected in the permeate with very low concentration after 76h treatment of olive mill wastewater (El-Abbassi et al., 2013). These detected phenolics were monocyclic with small molecular weight and more volatility. Therefore, the low rejection of volatile compounds can be mainly attributed to their volatility. In addition, hydrophobic compounds can attach to the surface of MD membranes, thus this can cause adverse effects on separation performance.

2.2.2. Membrane wetting and fouling

In membrane distillation, membranes must be hydrophobic to prevent the direct penetration of feed liquid through the microporous membrane. When the transmembrane hydrostatic pressure exceeds liquid entry pressure (LEP) of the membrane, pore wetting occurs. In the case of pore wetting, the direct penetration of liquid reduces the rejection and makes the whole process fail (Guillen-Burrieza et al., 2016). Four levels of pore wetting consist of non-wetted, surface wetted, partially wetted, and fully wetted (Fig. 2-3). In the long-term treatment, surface wetting happens on the membrane surface, but gaps for transporting only vapor still exist. When some membrane pores are open for water liquid passing through the hydrophobic membrane, the phenomenon is called partial wetting. In case of full wetting, liquid can penetrate through almost all membrane pores (Tijing et al., 2015).

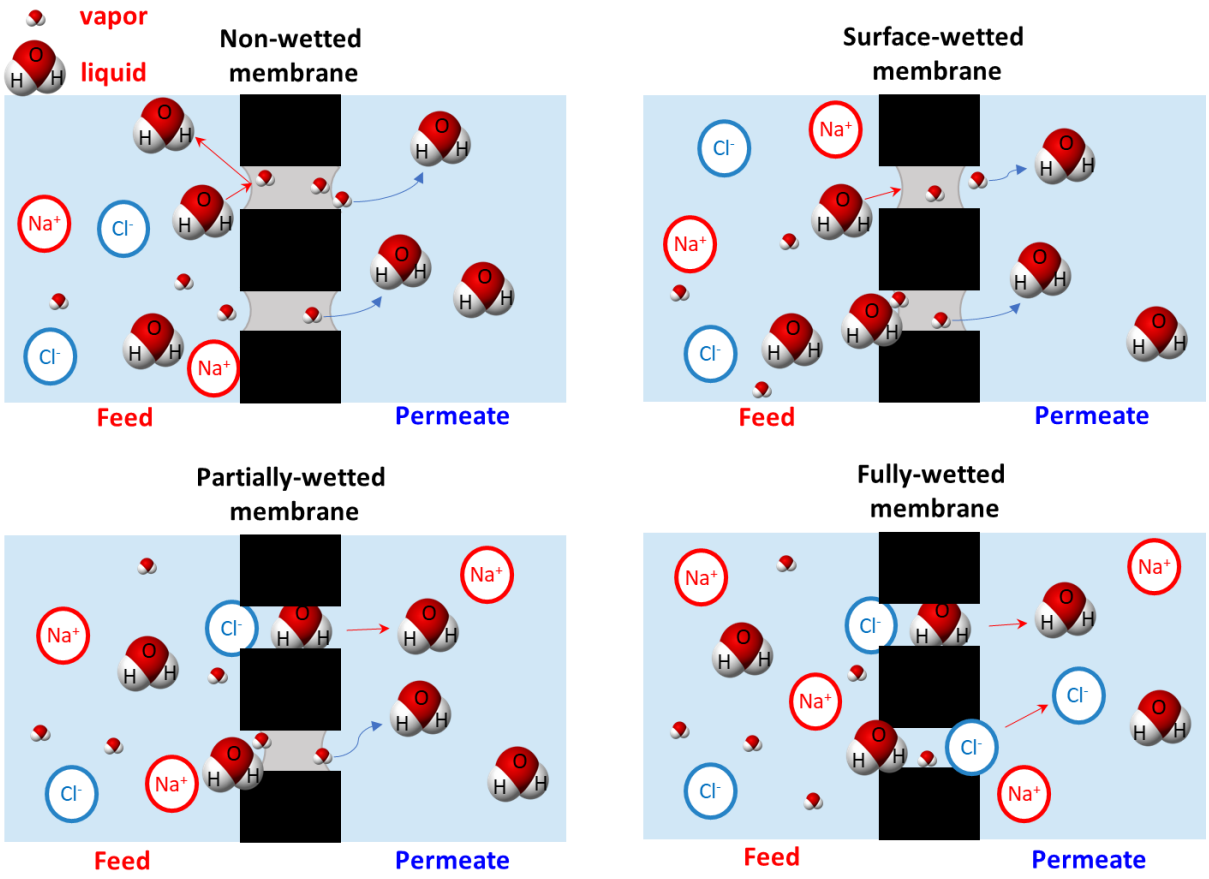

Fig. 2-3. The levels of pore wetting in membrane distillation.

The wetting phenomenon happens when the feed solution contains high concentrations of salts, organics, and nutrients. The deposition of these compounds on the surface and in the pores of the membrane results in the loss of hydrophobicity (Rezaei et al., 2018; Tibi et al., 2020). Moreover, the presence of surfactants and oil in wastewater sources promotes membrane wetting and fouling (Han et al., 2017). To have high wetting resistance of the membranes, LEP should be higher than applied pressure. In addition to the effects of contaminants (e.g., low surface tension liquids) presented in wastewater, the LEP of hydrophobic membranes is also influenced by the surface energy of membrane material, membrane pore size, and geometry (Table 1-1). The effects of these membrane characteristics on LEP were expressed by the Laplace-Young equation (Alkhudhiri et al., 2012):

$$\mathrm{LEP} = \frac{-4B_g \sigma \cos\theta}{d_{\max}} \tag{2-1}$$

where, B_g is the pore geometric factor, θ is the contact angle, d_{max} is the maximum diameter of membrane pores, and σ is the surface tension of the solution.

Table 1-1. Effects and recommended values for membrane distillation.

Membrane characteristics	Effects	Given value	Recommended value	References
Liquid entry pressure (LEP)	High LEP can prevent the entry of feed solution into the membrane.	0.5−4.6 bar	>2.5 bar	(Swaminathan et al., 2018)
Contact angle	High contact angle leads to high wetting resistance.	80−160°	>105°	(Eykens et al., 2016)
Pore size	Bigger size leads to less mass resistance and higher flux, but less wetting resistance.	0.1–1 μm	~0.3 μm	(Khalifa et al., 2017; Swaminathan et al., 2018)
Porosity	Higher porosity results in less heat loss and higher flux, but lower mechanical strength.	30–90%	80–90%	(Eykens et al., 2016)
Tortuosity	Low tortuosity leads to high permeate flux.	1.1–3.9	1.1–1.2	(Khayet et al., 2004; Ullah et al., 2018)
Thickness	Thicker membranes have larger heat loss and higher resistance to mass transfer.	5–700 μm	30–60 μm	(Laganà et al., 2000; Swaminathan et al., 2018)
Thermal conductivity	Low thermal conductivity leads to high permeate flux and high energy efficiency.	0.031–0.057 W/mK	<0.06 W/mK	(Ullah et al., 2018)

While pore wetting can reduce the treated water quality, membrane fouling happened on the feed side of the membrane can lead to a low permeate flux (Choudhury et al., 2019). As foulants adhere to the hydrophobic membrane and block the membrane pores, permeate flux is reduced. The fouling of hydrophobic membrane is affected by the foulant characteristics, membrane properties, operating conditions, and feed solution characteristics (Tijing et al., 2015). In MD, membrane fouling is classified into inorganic fouling, organic fouling, and biological fouling. The presence of inorganic compounds in wastewater causes the growth of precipitates (e.g., calcium and phosphate) on the membrane surface (Khan et al., 2014) while the existence of organic compounds leads to the drop of surface tension of the solution (Rezaei et al., 2018). Hence, the membrane hydrophobicity can be reduced, leading to membrane wetting and fouling. On the other hand, the growth of microorganisms in MD is limited by high salinity and high temperature of feed solution (Gryta, 2002), thus biological fouling could be lower than that of other membrane technologies (e.g., reverse osmosis, nanofiltration, or microfiltration). However, microorganisms can still persist at the feed temperature of <60 °C even in the very low concentrations of nutrients (Tijing et al., 2015).

References

Abdel-Fatah, M.A., 2018. Nanofiltration systems and applications in wastewater treatment: Review article. Ain Shams Eng. J. 9, 3077-3092.

Al-Amoudi, A., Lovitt, R.W., 2007. Fouling strategies and the cleaning system of NF membranes and factors affecting cleaning efficiency. J. Memb. Sci. 303, 4-28.

Alkhudhiri, A., Darwish, N., Hilal, N., 2012. Membrane distillation: A comprehensive review. Desalination 287, 2-18.

Andrade, L.H., Ricci, B.C., Grossi, L.B., Pires, W.L., Aguiar, A.O., Amaral, M.C.S., 2017. Nanofiltration applied in gold mining effluent treatment: Evaluation of chemical cleaning and membrane stability. Chem. Eng. J. 323, 545–556.

Bodzek, M., Konieczny, K., Kwiecińska, A., 2011. Application of membrane processes in drinking water treatment–state of art. Desalin. Water Treat. 35, 164–184.

Chon, K., Cho, J., 2016. Fouling behavior of dissolved organic matter in nanofiltration membranes from a pilot-scale drinking water treatment plant: An autopsy study. Chem. Eng. J. 295, 268–277.

Choudhury, M.R., Anwar, N., Jassby, D., Rahaman, M.S., 2019. Fouling and wetting in the membrane distillation driven wastewater reclamation process – A review. Advances in Colloid and Interface Science 269, 370-399.

Deng, L., Guo, W., Ngo, H.H., Zhang, J., Liang, S., Xia, S., Zhang, Z., Li, J., 2014. A comparison study on membrane fouling in a sponge-submerged membrane bioreactor and a conventional membrane bioreactor. Bioresour. Technol. 165, 69–74.

El-Abbassi, A., Hafidi, A., Khayet, M., García-Payo, M.C., 2013. Integrated direct contact membrane distillation for olive mill wastewater treatment. Desalination 323, 31-38.

Eykens, L., De Sitter, K., Dotremont, C., Pinoy, L., Van der Bruggen, B., 2016. How to optimize the membrane properties for membrane distillation: a review. Ind. Eng. Chem. Res. 55, 9333-9343.

Fujioka, T., Takeuchi, H., Tanaka, H., Kodamatani, H., 2019. A surrogate-based approach for trace organic chemical removal by a high-rejection reverse osmosis membrane. Sci. Total Environ. 696, 134002.

González, D., Amigo, J., Suárez, F., 2017. Membrane distillation: Perspectives for sustainable and improved desalination. Renewable and Sustainable Energy Reviews 80, 238-259.

Gryta, M., 2002. The assessment of microorganism growth in the membrane distillation system. Desalination 142, 79-88.

Guillen-Burrieza, E., Mavukkandy, M.O., Bilad, M.R., Arafat, H.A., 2016. Understanding wetting phenomena in membrane distillation and how operational parameters can affect it. J. Membr. Sci. 515, 163-174.

Guo, W., Ngo, H.H., Li, J., 2012. A mini-review on membrane fouling. Bioresour. Technol. 122, 27–34.

Han, L., Tan, Y.Z., Netke, T., Fane, A.G., Chew, J.W., 2017. Understanding oily wastewater treatment via membrane distillation. J. Membr. Sci. 539, 284-294.

Jiang, S., Li, Y., Ladewig, B.P., 2017. A review of reverse osmosis membrane fouling and control strategies. Sci. Total Environ.

Khalifa, A., Ahmad, H., Antar, M., Laoui, T., Khayet, M., 2017. Experimental and theoretical investigations on water desalination using direct contact membrane distillation. Desalination 404, 22-34.

Khan, M.T., Busch, M., Molina, V.G., Emwas, A.-H., Aubry, C., Croue, J.-P., 2014. How different is the composition of the fouling layer of wastewater reuse and seawater desalination RO membranes? Water Res. 59, 271-282.

Khayet, M., Khulbe, K.C., Matsuura, T., 2004. Characterization of membranes for membrane distillation by atomic force microscopy and estimation of their water vapor transfer coefficients in vacuum membrane distillation process. J. Membr. Sci. 238, 199-211.

Kim, E.S., Liu, Y., El-Din, M.G., 2011. The effects of pretreatment on nanofiltration and reverse osmosis membrane filtration for desalination of oil sands process-affected water. Sep. Purif. Technol.

Kim, H.-A., Choi, J.-H., Takizawa, S., 2007. Comparison of initial filtration resistance by pretreatment processes in the nanofiltration for drinking water treatment. Sep. Purif. Technol. 56, 354-362.

Kimura, K., Amy, G., Drewes, J., Watanabe, Y., 2003. Adsorption of hydrophobic compounds onto NF/RO membranes: An artifact leading to overestimation of rejection. J. Memb. Sci. 221, 89–101.

Kimura, K., Okazaki, S., Ohashi, T., Watanabe, Y., 2016. Importance of the co-presence of silica and organic matter in membrane fouling for RO filtering MBR effluent. J. Memb. Sci. 501, 60–67.

Laganà, F., Barbieri, G., Drioli, E., 2000. Direct contact membrane distillation: modelling and concentration experiments. J. Membr. Sci. 166, 1-11.

Li, F., Huang, J., Xia, Q., Lou, M., Yang, B., Tian, Q., Liu, Y., 2018. Direct contact membrane distillation for the treatment of industrial dyeing wastewater and characteristic pollutants. Sep. Purif. Technol. 195, 83-91.

Lin, D., Tang, X., Xing, J., Zhao, J., Liang, H., Li, G., 2019. Application of peroxymonosulfate-based advanced oxidation process as a novel pretreatment for nanofiltration: Comparison with conventional coagulation. Sep. Purif. Technol. 224, 255–264.

Matin, A., Laoui, T., Falath, W., Farooque, M., 2021. Fouling control in reverse osmosis for water desalination & reuse: Current practices & emerging environment-friendly technologies. Sci. Total Environ. 765, 142721.

Meier, J., Melin, T., 2005. Wastewater reclamation by the PAC-NF process. Desalination 178, 27-40.

Mohammad, A.W., Teow, Y.H., Ang, W.L., Chung, Y.T., Oatley-Radcliffe, D.L., Hilal, N., 2015. Nanofiltration membranes review: Recent advances and future prospects. Desalination 356, 226-254.

Nghiem, L.D., Schäfer, A.I., Elimelech, M., 2004. Removal of Natural Hormones by Nanofiltration Membranes: Measurement, Modeling and Mechanisms. Environ. Sci. Technol. 38, 6, 1888-1896.

Naidu, G., Jeong, S., Choi, Y., Vigneswaran, S., 2017. Membrane distillation for wastewater reverse osmosis concentrate treatment with water reuse potential. J. Membr. Sci. 524, 565-575.

Oatley-Radcliffe, D.L., Walters, M., Ainscough, T.J., Williams, P.M., Mohammad, A.W., Hilal, N., 2017. Nanofiltration membranes and processes: A review of research trends over the past decade. J. Water Process Eng. 19, 164–171.

Racar, M., Dolar, D., Špehar, A., Kraš, A., Košutić, K., 2017. Optimization of coagulation with ferric chloride as a pretreatment for fouling reduction during nanofiltration of rendering plant secondary effluent. Chemosphere 181, 485-491.

Rezaei, M., Warsinger, D.M., Lienhard V, J.H., Duke, M.C., Matsuura, T., Samhaber, W.M., 2018. Wetting phenomena in membrane distillation: Mechanisms, reversal, and prevention. Water Res. 139, 329-352.

Schäfer, A.I., Fane, A.G., Waite, T.D., 2006. Nanofiltration : principles and applications. Elsevier.

Simon, A., McDonald, J.A., Khan, S.J., Price, W.E., Nghiem, L.D., 2013. Effects of caustic cleaning on pore size of nanofiltration membranes and their rejection of trace organic chemicals. J. Memb. Sci. 447, 153–162.

Tibi, F., Charfi, A., Cho, J., Kim, J., 2020. Fabrication of polymeric membranes for membrane distillation process and application for wastewater treatment: Critical review. Process Saf. Environ. Prot. 141, 190-201.

Swaminathan, J., Chung, H.W., Warsinger, D.M., Lienhard V, J.H., 2018. Energy efficiency of membrane distillation up to high salinity: Evaluating critical system size and optimal membrane thickness. Applied Energy 211, 715-734.

Tijing, L.D., Woo, Y.C., Choi, J.-S., Lee, S., Kim, S.-H., Shon, H.K., 2015. Fouling and its control in membrane distillation—A review. J. Membr. Sci. 475, 215-244.

Ullah, R., Khraisheh, M., Esteves, R.J., McLeskey, J.T., AlGhouti, M., Gad-el-Hak, M., Vahedi Tafreshi, H., 2018. Energy efficiency of direct contact membrane distillation. Desalination 433, 56-67.

Van der Bruggen, B., 2013. Nanofiltration, in: Encyclopedia of Membrane Science and Technology. John Wiley & Sons, Inc., Hoboken, NJ, USA.

Van Der Bruggen, B., Schaep, J., Wilms, D., Vandecasteele, C., 1999. Influence of molecular size, polarity and charge on the retention of organic molecules by nanofiltration. J. Memb. Sci. 156, 29–41.

Vatankhah, H., Murray, C.C., Brannum, J.W., Vanneste, J., Bellona, C., 2018. Effect of pre-ozonation on nanofiltration membrane fouling during water reuse applications. Sep. Purif. Technol. 205, 203–211.

Xue, J., Jiao, Z., Bi, R., Zhang, R., You, X., Wang, F., Zhou, L., Su, Y., Jiang, Z., 2019. Chlorine-resistant polyester thin film composite nanofiltration membranes prepared with B-cyclodextrin. J. Memb. Sci. 584, 282–289.

Wang, P., Chung, T.-S., 2015. Recent advances in membrane distillation processes: Membrane development, configuration design and application exploring. J. Membr. Sci. 474, 39-56.

Zahrim, A.Y., Hilal, N., 2013. Treatment of highly concentrated dye solution by coagulation/flocculation-sand filtration and nanofiltration. Water Resour. Ind. 3, 23–34.

Chapter 3. Fouling behavior and performance of a submerged flat-sheet nanofiltration membrane system for direct treatment of secondary wastewater effluent

3.1. Introduction

The use of recycled water plays an important role in augmenting fresh water supply in urban areas (Michael-Kordatou et al., 2015; Lee et al., 2017). When reclaimed water is used for purposes that may involve contact with the human body, such as recreational use and firefighting, advanced water treatment processes become essential to minimize human health risks that could arise due to the presence of pathogens. They are also necessary to realize positive aesthetics by reducing the unpleasant odors and unnatural color of the reclaimed water. Advanced wastewater treatment usually involves sand filtration pre-treatment, ozonation, and biological activated carbon filtration after conventional wastewater treatment. These approaches have been successfully implemented worldwide (Michael-Kordatou et al., 2015; Liu et al., 2017; Bourgin et al., 2018). Treatment using nanofiltration (NF) membranes is capable of providing similar or better water quality than typical systems that use ozone and activated carbon (Xu et al., 2010; Yang et al., 2010). However, the application of such membranes for full-scale recycling of municipal wastewater is rarely adopted. This can be attributed to the requirement of rigorous pre-treatment (e.g., microfiltration or ultrafiltration) for alleviating membrane fouling (Van der Bruggen et al., 2008).

One of the limitations of the NF membranes is the need for suspended solid removal prior to the NF membrane treatment. Generally, the NF process requires a rigorous pre-treatment process involving a sand filter, microfiltration, or ultrafiltration to minimize membrane fouling (Warsinger et al., 2018). This is because NF membranes are typically supplied in spiral-wound elements that have very narrow feed entries and tight channels. The pre-treatment necessitates both capital and operating costs; thus, any decrease in the cost of these pre-treatment processes can reduce the overall treatment cost (Zhao et al., 2019; Hube et al., 2020). However, direct treatment using NF membranes without pre-treatment processes is challenging due to the presence of suspended solids and organics at high concentrations in wastewater. These can cause the clogging or plugging of the feed channel in NF elements and induce fast membrane fouling that necessitates frequent chemical cleaning.

In water recycling, the alleviation of membrane fouling is key to the success of direct nanofiltration. For example, direct treatment of domestic wastewater by a capillary NF membrane has been previously evaluated at a permeate flux of up to 30 L/m^{2}h (Sayed et al., 2007). However, the NF system required frequent physical cleaning (hydraulic flushing every 15 min) and chemical cleaning (e.g., every 1–4 days), for which high chemical consumption was needed. Common fouling mitigation techniques without high chemical consumptions include the application of high cross-flow velocity, which continuously cleans the membrane surface owing to the application of a shear force (Farhat et al., 2016). Although this high cross-flow velocity is typically applied to waters with high fouling propensity, high energy consumption is one of the limitations of this technique. Another technique that has shown effectiveness in water recycling is the application of low permeate flux (Choi et al., 2005a; Li et al., 2007; He et al., 2017). Although the low permeate flux requires a greater membrane surface area for the generation of a specific permeate flow rate, the application of the low permeate flux can considerably alleviate membrane fouling (Kim et al., 2007). Additionally, the low permeate flux has the advantage of reducing trans-membrane pressure (i.e., reducing energy use) (Bellona et al., 2004; Hilal et al., 2004; Van der Bruggen et al., 2008). However, the efficacy of this low permeate flux approach for membrane fouling mitigation during the direct NF treatment of wastewater has not yet been explored.

Furthermore, the orientation of NF membrane modules is another great concern. In almost all previous studies related to direct NF (Bonné et al., 2003; Choi et al., 2005b; Kramer et al., 2015; Ruigómez Sempere et al., 2020), tubular or capillary membrane modules were applied to avoid clogging or plugging in the feed channel and to enhance physical or chemical cleaning efficiency, with low packing density. Spiral-wound NF membrane elements cannot be utilized without pre-treatment given that the large particles in wastewater can cause clogging of the feed channels. Therefore, for the first time, a flat-sheet submerged NF membrane module was applied for the direct NF treatment of wastewater. In the submerged module orientation, filtration is driven by a vacuum created inside the membrane elements, and a trans-membrane pressure (TMP) of up to 100 kPa can be utilized for filtration (Fujioka et al., 2020). The advantage of the flat-sheet submerged NF membrane module is its simple module structure, which allows for the maximum effectiveness of the physical cleaning process, for example with sponge cleaning, when wastewater with high fouling propensity is used. Our previous study (Fujioka et al., 2021) demonstrated a low membrane fouling propensity of a flat-sheet submerged NF membrane when it was used for direct NF treatment

of water, which was obtained from relatively clean surface water sources, at a drinking water treatment plant over a one month period. However, submerged flat-sheet NF membrane modules have not been applied in any previous study for wastewater recycling; thus, their applicability for treating water with high fouling substances remains unclear.

Therefore, the aim of this study was to evaluate the efficacy of low permeate flux operation and a novel flat-sheet submerged NF membrane module in the realization of the sustainable and low-energy direct nanofiltration of wastewater. The membrane fouling level as well as the quality of the recycled water were assessed over the course of a 48-d direct NF process involving secondary wastewater effluent. The results obtained following the low permeate flux were also compared with those corresponding to a typical permeate flux.

3.2. Methods

3.2.1. Feed solution

This study used secondary wastewater effluent, which was collected from the outlet of an activated sludge treatment process at a municipal wastewater treatment plant in Nagasaki Prefecture, Japan. All of the collected secondary wastewater effluent was stored in a fridge until it was used for filtration tests. The color, E_{254}, total organic carbon (TOC), electrical conductivity, turbidity, and pH values of the secondary wastewater effluent were 46 PCU, 0.12 Abs, 7.3 mg/L, 2.1 mS/cm, 1.5 NTU, and 7.25, respectively. The secondary wastewater effluent was used as a feed solution of direct NF treatment without a sand filtration, microfiltration, or ultrafiltration, which are typical pre-treatment processes applied prior to sending feed solutions to the NF system. A reverse osmosis (RO) system (RTA-200W, AS ONE, Osaka, Japan) was used to filter tap water, and it was called as RO-treated water throughout this study.

3.2.2. NF membrane system

This study used a commercial composite polyamide NF membrane, namely, HYDRApro 402 (Nitto/Hydranautics; Osaka, Japan). The flat-sheet membrane is used for challenging industrial waters with high membrane fouling propensity and is capable of >99.7 % $MgSO_4$ rejection according to the manufacturer's specification (Table 3-1). The NF

membrane sheet was attained from a spiral-wound membrane element and carved into membrane coupons. Thereafter, a flat-sheet submerged membrane module with an effective surface area of 60 cm^2 was fabricated in an outside-in flow orientation using two membrane coupons and a permeate spacer (Fig. 3-1). This study used a submerged NF membrane treatment system (Fig. 3-2a), which is comprised of the NF membrane module, two 2.0-L glass beakers used as the reservoirs of the feed solution or membrane module, a magnetic stirrer (RS-1DN, AS ONE; Osaka, Japan), an automated dosing pump with a level sensor (WLC-SA, AS ONE; Osaka, Japan), a suction pump for transporting the feed to the permeate through the membrane (MP-2000, Tokyo Rikakikai; Tokyo, Japan), a digital pressure gauge (KDM30, Krone corporation; Tokyo, Japan), a digital balance (EK-610i, A&D Company; Tokyo, Japan), a temperature circulator (Thermax TM-1A, AS ONE; Osaka, Japan), and a chiller (NCB-500, Tokyo Rikakikai; Tokyo, Japan). Neither aeration nor stirring were applied in the membrane reservoir.

Table 3-1. Characteristics of the HYDRApro 402 NF membrane provided in a specification of the manufacturer.

Parameter	Value
Membrane Polymer	Composite Polyamide
pH range: continuous (cleaning)	3.0 – 9.0 (1.0 – 11.5)
$MgSO_4$ rejection*	99.7%

*Conditions: 2000 ppm $MgSO_4$, 0.76 MPa applied pressure, 25 °C operating temperature, 15% permeate recovery, 6.5-7.0 feed pH

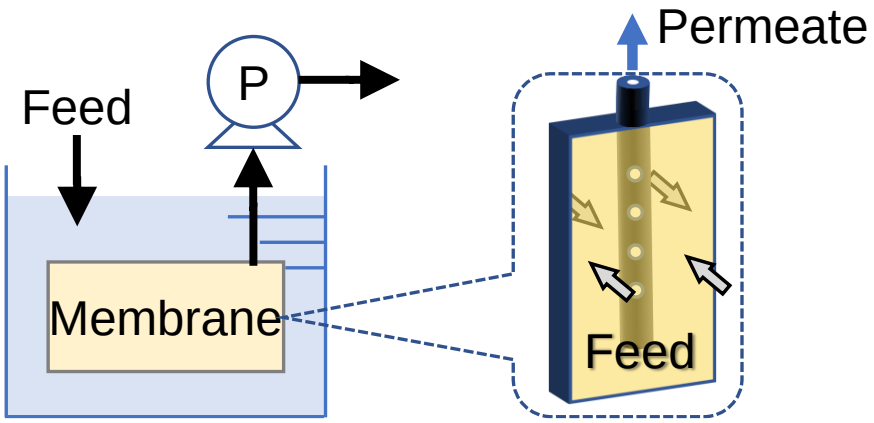

Fig. 3-1. Conceptual image of the flat sheet submerged membrane module.

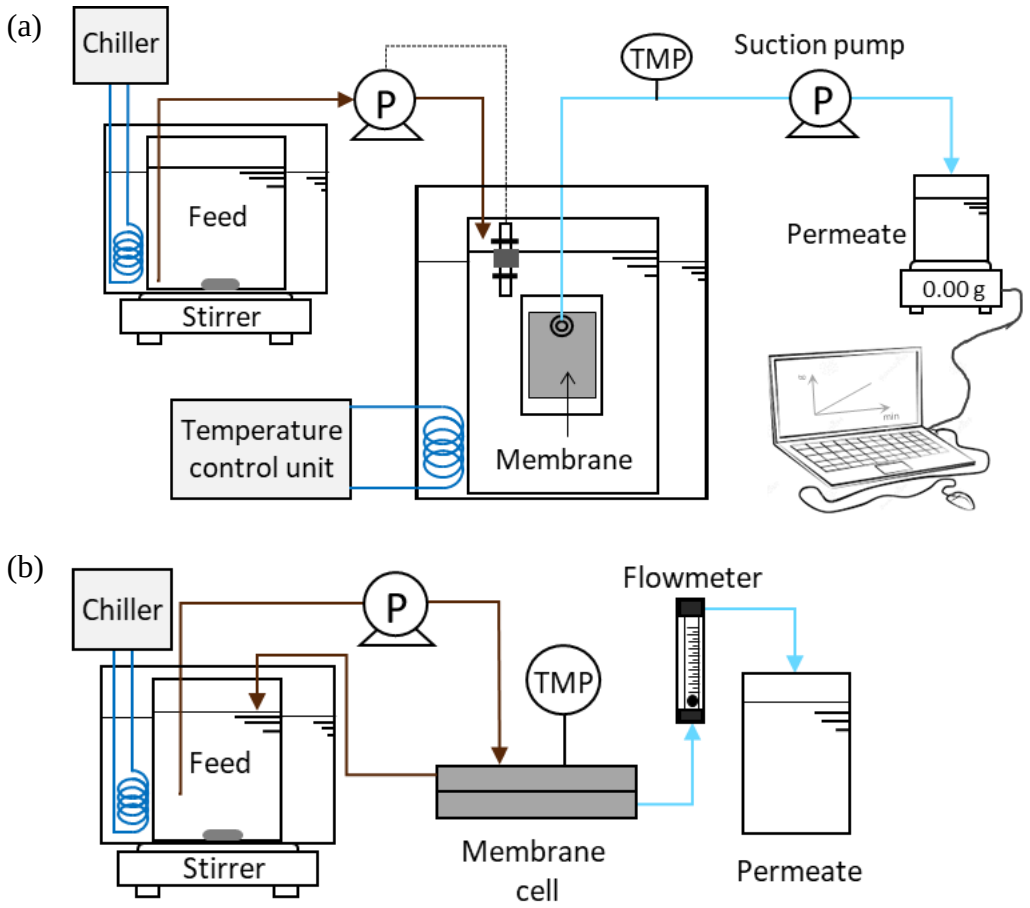

Fig. 3-2. Schematic diagram of (a) the submerged NF system and (b) the pressurized cross-flow NF system for a high permeate flux test.

This study also used a pressurized NF treatment system (Fig. 3-2b) to evaluate the fouling propensity of the HYDRApro membrane under a high permeate flux. The system included a stainless steel cross-flow membrane cell (Iwai Pharma Tech, Tokyo, Japan), high-pressure pump (KP-12, FLOM, Tokyo, Japan), flow meter, pressure regulating valve, and 2-L glass reservoir with a stainless steel heat exchanging coil connected to a temperature control unit (NCB-500, Tokyo Rikakikai, Tokyo, Japan). The membrane cell held a flat-sheet HYDRApro 402 membrane coupon with an effective surface area of 36.3 cm^2.

3.2.3. Experimental protocols

Prior to the experiment using the submerged NF membrane treatment system, the obtained RO-treated water was used to stabilize the submerged NF for 72 h. After the stabilization step, RO-treated water was replaced by the secondary wastewater effluent, and direct NF treatment was conducted over 48-d. A constant permeate flux of 3 L/m^{2}h and a constant feed temperature of 25 °C were maintained throughout the treatment period. Neither aeration nor stirring, which are often applied for mitigating membrane fouling, were intentionally applied to the membrane reservoir throughout the test to minimize energy consumption during direct NF treatment. The volume of feed water in the membrane reservoir was maintained at 1.3 L by automatically supplementing the feed solution from the feed reservoir using a pump integrated with a level sensor. The temperature of the wastewater stored in the feed reservoir was maintained below 7 °C to minimize bacterial growth. The temperature of the feed in the membrane reservoir was maintained at 25 °C during the filtration. Every 6-d, the feed solution in the membrane reservoir was discharged and replaced with fresh secondary wastewater effluent to avoid continuous accumulation of the rejected constituents (approximately two-fold concentration after 6-d operation). The TMP was recorded every 24 h and 1 h after each replacement of feed solution in the membrane reservoir. Feed and permeate samples for water quality analysis were collected every 2 or 3-d. At the end of the 48-d operation, the membrane module was removed from the membrane reservoir. Thereafter, the membrane surface was thoroughly and gently cleaned using a high-quality polyurethane sponge (AMS-363H, AS ONE, Osaka, Japan) and was rinsed with pure water. After reinstalling the membrane module in the membrane reservoir, the direct NF treatment of the secondary wastewater effluent was resumed and continued for the next 5-d.

The high-flux experiment was carried out using the pressurized NF membrane treatment system. The pressurized cross-flow NF experiment was operated at a constant permeate flux of 40 L/m^{2}h and a constant temperature of 30 °C for 48 h. Cross-flow rate and cross-flow velocity were maintained at 30 mL/min and approximately 5 cm/s, respectively, which resulted in a recovery rate of 8%. Throughout the test, the feed and permeate solutions were recirculated into the feed reservoir. Samples for water quality analysis were collected after 1 h operation.

3.2.4. Analysis

Prior to the analysis of E_{254} and color, each sample was pre-filtrated using a 0.45 μm filter (Whatman®, Merck Japan, Tokyo, Japan). The E_{254} and color of each sample were analyzed using a spectrophotometer (UV1280, Shimadzu; Kyoto, Japan) at wavelengths of 455 nm and 254 nm, respectively, in accordance with the USEPA Method 415.3. Quartz sample cuvettes with lengths 10 and 50 mm were used for the analysis of E_{254} and color, respectively. The conductivity and pH of each sample was directly measured using a conductivity meter (Orion Star™ A325, Thermo Fisher Scientific; MA, USA) and a pH meter (MM-41DP, DKK-TOA corporation; Tokyo, Japan), respectively. TOC was analyzed without pre-filtration using a TOC-VSH analyzer (Shimadzu, Kyoto, Japan) and the non-purgeable organic carbon method. Turbidity of each sample was determined using a turbidity meter (2100Q, Hach, Loveland, CO, USA) in accordance with the USEPA Method 180.1. Turbidity of the permeate was measured after leaving the sample to stand for 5 min to eliminate air bubbles. Dissolved organics in feed and permeate water were characterized on the day 46^{th} by using the excitation-emission matrix (EEM) fluorescence spectra by fluorescence spectroscopy (RF-6000, Shimadzu; Kyoto, Japan) (Yan et al., 2000).

3.3. Results and discussion

3.3.1. Membrane fouling

3.3.1.1. Submerged NF treatment

Membrane fouling of the submerged NF system during direct NF treatment of the secondary wastewater effluent was evaluated for 48-d. Typical membrane-based wastewater treatment requires continuous purging of a certain percentage of the concentrate to avoid concentration of rejected constituents in the membrane reservoir. However, only a limited volume of wastewater was available in this bench-scale test in the laboratory; thus, the direct NF treatment was conducted in the dead-end batch mode. As noted in section 3.2.3, the feed solution in the membrane reservoir was replaced every 6-d to avoid excessive accumulation of substances rejected by the NF membrane in the membrane reservoir. Therefore, TMP increase of the submerged NF system during typical operation of wastewater treatment, where the concentrate is continuously discharged, can be less than that in this study.

After commencing the direct NF treatment, the TMP progressively increased until the feed solution in the membrane reservoir was replaced at 6-d (Fig. 3-3). After the replacement of the

feed solution, the TMP dropped to a level close to that of the initial TMP. Similar trends in the TMP change over a 6-d filtration cycle were observed until 48-d. The results indicate that the increased TMP was not due to irreversible membrane fouling. The increased TMP during the filtration can be caused by multiple factors, such as an increase in the osmotic pressure, concentration polarization, and reversible fouling. For example, an increase in osmotic pressure of the feed solution likely occurred due to the increase in the concentration of salts, which were rejected by the NF membrane. This was halted when the feed solutions in the membrane reservoir was replaced every 6-d. In addition, concentration polarization by the rejected ionic constituents could have been enhanced due to the increase in the concentration of organic and inorganic matter on the membrane surface. Further, some foulants deposited on the membrane surface may have been detached from the membrane surface during the feed replacement. For full-scale operation with availability of a large volume of secondary wastewater effluent, continuous operation can be possible by purging a small portion of the feed to avoid the increase in TMP.

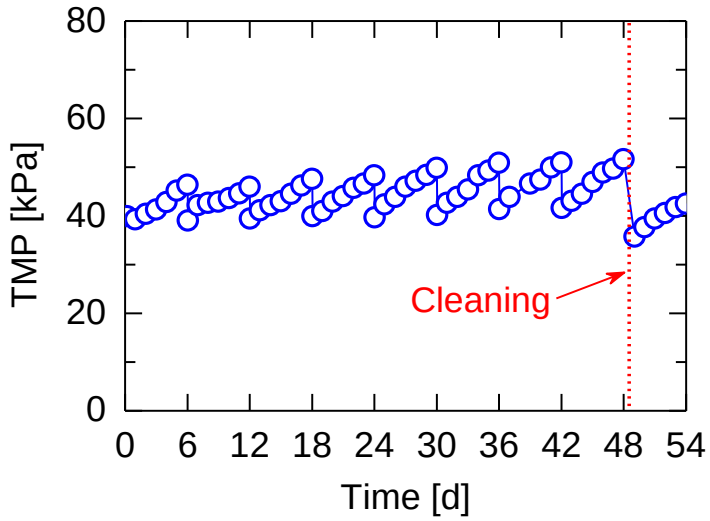

Fig. 3-3. TMP at a constant flux of 3 L/m^{2}h during direct NF treatment of secondary wastewater effluent.

To assess membrane fouling without the impact of the feed concentration, the TMPs that were recorded 1 h after the feed replacement were separately evaluated (Fig. 3-4). The results indicated a minor but linear increase in TMP from 39 to 42 kPa over the 48-d treatment period.

Based on the obtained linear regression formula, the calculated fouling rate was 0.072 kPa/d. This indicates that the TMP after six months of operation can be predicted to reach 52 kPa, which is equivalent to a permeability reduction of 22 %. In other words, direct NF treatment of the secondary wastewater effluent at a permeate flux of 3 L/m^{2}h can be maintained without chemical cleaning during a six-month period.

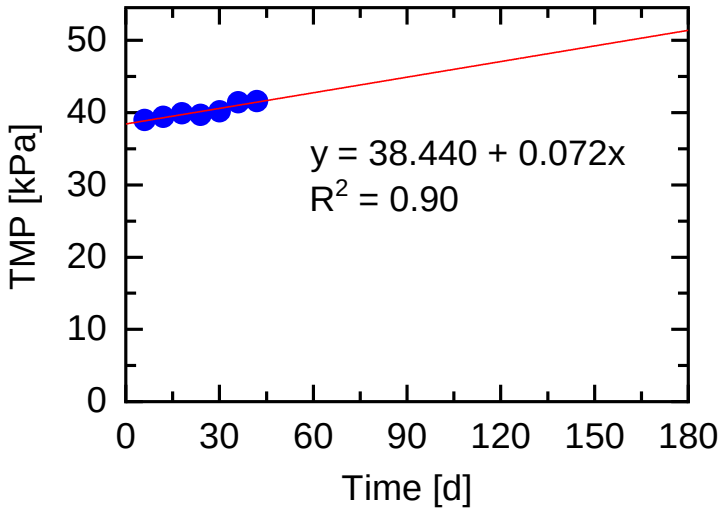

Fig. 3-4. Changes in trans-membrane pressure (TMP) that was recorded 1 h after each replacement of feed solution in the membrane reservoir. TMP after 180 d (i.e., 6 months) can be expected to reach 52 kPa.

Despite the marginal membrane fouling that occurred over 48-d, physical cleaning using a polyurethane sponge was manually performed at the end of 48-d to provide understanding of membrane fouling mechanisms and evaluate the reversibility of the foulants. The removal of the foulants from the membrane surface can also be confirmed through the recovery of TMP after the physical cleaning (Fig. 3-3). The visual observation of the membrane surface before and after the sponge cleaning also revealed the near-complete removal of foulants (Fig. 3-5). In general, pore blocking first occurs during the initial stage of membrane filtration, which is followed by cake-layer formation on the membrane surface (Enfrin et al., 2020; Niu et al., 2020). Cleaning with a polyurethane sponge can only remove the foulants on the membrane surface (Kimura et al., 2016); the recovery of permeability after the sponge cleaning indicates that most foulants contributing to the hydraulic resistance were present on the membrane surface. Therefore, these results suggest that the removal of the cake layer by applying

membrane surface cleaning (e.g., sponge cleaning) can be sufficient to achieve nearly full recovery of membrane permeability.

(a) Before (b) After

Fig. 3-5. Photographs of the membrane surface (a) before and (b) after surface scrubbing.

3.3.1.2. Pressurized NF treatment

Although the stable operation of the submerged NF system at a permeate flux of 3 L/m^{2}h was successfully demonstrated as shown in Fig. 3-3, it can be attributed to the low fouling propensity of the secondary wastewater effluent. To demonstrate that direct NF treatment of secondary wastewater effluent at a typical permeate flux can cause significant membrane fouling, the membrane fouling caused by secondary wastewater effluent, under a typical permeate flux of 40 L/m^{2}h, was evaluated using the pressurized NF system. The initial TMP at t = 0 was 0.55 MPa, and the TMP progressively increased to 2.1 MPa at 48 h (Fig. 3-6). The results indicate that direct NF treatment of the secondary wastewater effluent under typical NF operating conditions can promote fast and significant membrane fouling. It is noted that no spacers were used on the membrane surface for the pressurized NF system to solely evaluate the impact of permeate flux. In general, chemical cleaning using caustic or acidic cleaning agents is conducted after confirming a 10–20 % increase in the TMP (or a 10–20 % drop in the membrane permeability), and the frequency of chemical cleaning at full-scale water reclamation plants is between once every few months and once a year (Regula et

al., 2014). The direct NF treatment in this study reached an 18 % permeability drop (from 7.3–6.0 L/m^{2}hbar) within the first 4 h. This indicates that, under typical operating conditions, chemical cleaning is required a few times a day when directly treating the secondary wastewater effluent, which incurs considerable consumption of chemical agents.

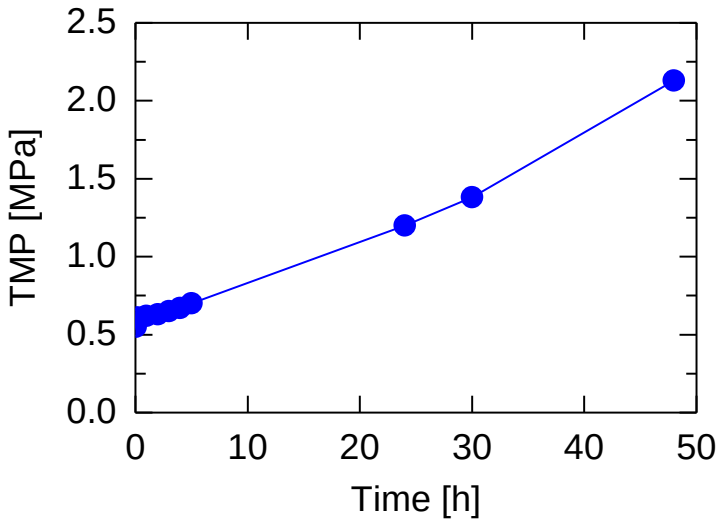

Fig. 3-6. Trans-membrane pressure (TMP) at a constant permeate flux of 40 L/m^{2}h during direct NF treatment of secondary wastewater effluent at 30 °C.

A comparison in different permeate flux values between 3 and 40 L/m^{2}h, in terms of the cumulative treated volume of water (rather than the treatment time), shows that the rate of TMP increase (i.e., hydraulic resistance increase) at a permeate flux of 40 L/m^{2}h was considerably greater than that of 3 L/m^{2}h (Fig. 3-7). At a given cumulative treated water volume, the membranes under 3 and 40 L/m^{2}h underwent the filtration of same feed volume. The TMP, under the permeate flux of 40 L/m^{2}h, increased considerably from 0.55 to 2.1 MPa before reaching the cumulative treated water volume of 7.0 L. In contrast, the TMP, under 3 L/m^{2}h permeate flux, increased by only 2% for the same cumulative treated water volume. Therefore, the results indicate that the deposition of foulants on the membrane can be enhanced at a higher permeate flux, causing a faster increase in the hydraulic resistance. It is noted that the feed water temperatures differed during the tests with different permeate fluxes. The temperatures of the feed waters during tests with permeate fluxes of 3 and 40 L/m^{2}h were 25 °C and 30 °C, respectively. Higher temperatures can reduce the required TMP because the viscosity of water decreases with increasing water temperature. A previous study (Beril

Gönder et al., 2011) reported that a 5 °C difference in feed water temperature during NF treatment can cause a negligible difference. Therefore, despite the difference in their temperature, the feed waters can be expected to show similar overall trends in membrane fouling propensity in the two tests with differing permeate flux values.

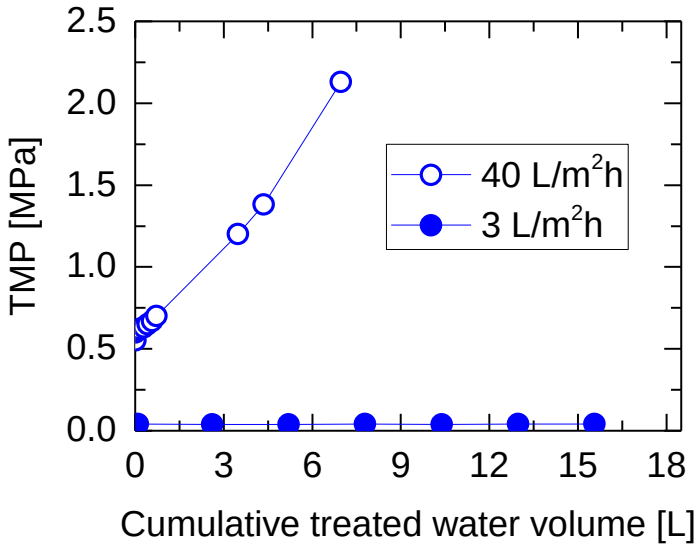

Fig. 3-7. TMP against the cumulative treated water volume during direct NF treatment of the secondary wastewater effluent at constant flux values of 3 and 40 L/m^{2}h, which were conducted using the submerged NF system and the pressurized cross-flow NF system, respectively.

The results align with a previous study (Miller et al., 2014) that reported the role of foulant transport between the bulk feed and the membrane surface by filtration and back diffusion, and suggested that the permeate flux higher than a certain threshold flux can enhance foulant transport from the bulk feed to the membrane surface. Typical foulants in treated wastewater (e.g., polysaccharides, proteins, and humic acid-like substances, which have molecular weights of > 500 g/mol and are larger than the pore size of typical NF membranes (Fujioka et al., 2013), can cause irreversible fouling by getting deposited on the membrane surface as a fouling layer (Choi et al., 2005a). At a high TMP (i.e., high permeate flux), the compaction of the foulant layer can occur, which can induce high hydraulic resistance (Wang and Tang, 2011). In fact, the high permeate flux of 40 L/m^{2}h in this study caused an accelerated increase in hydraulic resistance (i.e., TMP) in a constant permeate flux operation (Fig. 3-7). Overall,

the results indicate the superior performance of the low permeate flux for suppressing membrane fouling during direct NF treatment of the secondary wastewater effluent.

It should be noted that the trend of low membrane fouling propensity at a low permeate flux can be membrane specific. The root-mean-square roughness and contact angle of the HYDRApro 402 NF membrane surface was 14.6 ± 7.2 nm and 45 ± 1°, respectively (Fig. 3-8). These are relatively low among commercial NF membranes; their root-mean-square roughness and contact angle are usually 10–60 nm and 30–90°, respectively (Boussu et al., 2005; Hobbs et al., 2006; Qi et al., 2019). In particular, surface roughness has been reported to directly impact NF membrane permeability: decline in membrane permeability increases with increasing surface roughness (Hobbs et al., 2006). Therefore, it is important to note that the fouling membrane propensity at a low permeate flux can vary depending on the chosen NF membranes in addition to feed water quality.

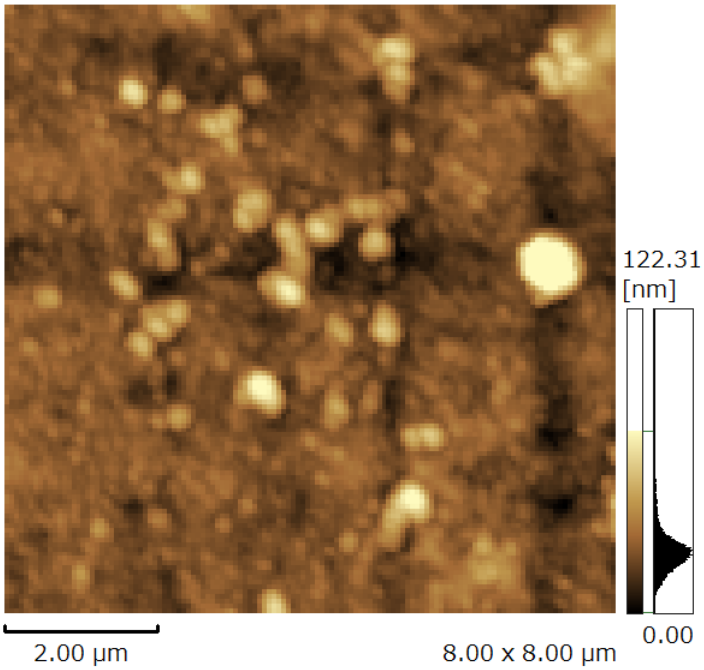

Fig. 3-8. The atomic force microscopy (AFM) image of the HYDRApro 402 NF membrane. Membrane surface roughness was determined using an AFM instrument (SPM-9700, Shimadzu; Kyoto, Japan). The scanning area was 8 × 8 µm, and five samples were analyzed to obtain the average value. The root-mean-square (RMS) of the HYDRApro 402 NF membrane was 14.6 ± 7.2 nm (n = 5). The contact angle of the HYDRApro 402 NF membrane was 45 ± 1° (n = 6), which was analyzed using a Rame-Hart Goniometer (Model 250, Rame-Hart, Netcong, NJ, USA).

3.3.2. Water quality

Water quality during direct NF treatment using the submerged NF system was assessed over 48-d. Throughout the experiment, water quality of the feed solution varied due to the dead-end filtration and the subsequent concentration in the feed reservoir. However, the permeate was of good and stable quality over 48-d: the color, E_{254}, and TOC were 0.7–3.8 PCU, 0.019–0.024 Abs, and 0.7–4.0 mg/L, respectively (Fig. 3-9). The direct NF treatment achieved high rejection of color, $E_{254,}$ and TOC at over 93, 84, and 67 %, respectively (Fig. 3-10). The rejection values were similar to that at a permeate flux of 40 L/m^{2}h (Fig. 3-11), indicating that operation at the low permeate flux did not compensate these water quality parameters. These rejection values were comparable to those reported in previous studies using NF membranes after pre-treatment (Marszałek and Puszczało, 2020; Xu et al., 2020). The high rejection of these water quality parameters by the NF membrane can be fundamentally attributed to the membrane tightness, which governs size exclusion mechanisms (Bellona et al., 2004). The membrane tightness can be represented by a membrane property called the molecular weight cut-off (MWCO); it is the lowest molecular weight which could belong to a solute which can be 90 % rejected by the membrane. The MWCO of HYDRApro 402 NF membrane was determined to be 200 g/mol (Fig. 3-12), which was equivalent to that of other commercial NF membranes; they usually range from 200 to 500 g/mol (Mohammad et al., 2015). The rejection of negatively charged compounds can also be enhanced by electrostatic repulsion. The zeta potential of HYDRApro 402 NF membrane in a solution of pH 6 and 8 was determined to be -20 mV (Fig. 3-13), which was comparable to that of other commercial NF membranes; they usually from -30 to −10 mV at pH 6–8 (Hagmeyer and Gimbel, 1999; Schaep and Vandecasteele, 2001).

In contrast to these major water quality parameters, electrical conductivity in the feed and permeate remained high at approximately 2.0–2.5 mS/cm (Fig. 3-9). Accordingly, the rejection of ions, represented in conductivity removal, remained stable but low at 8–14 % (Fig. 3-10). It should be noted that NF membranes including HYDRApro 402 are not designed for the removal of major ions in wastewater (monovalent ions including sodium and chloride ions), and these ions can readily penetrate through the membrane pores. Therefore, the rejection of NaCl by the HYDRApro 402 NF membrane decreased considerably: NaCl rejection at the permeate fluxes of 40 and 3 L/m^{2}h were 65 % and 18 %, respectively, while $MgSO_4$ rejection at permeate fluxes of 40 and 3 L/m^{2}h were 98 % and 93 %, respectively (Fig. 3-14). The impact of permeate flux on NaCl rejection corresponds with a previous study

(Wijmans and Baker, 1995) where water flux across the membrane decreased with decreasing permeate flux, but solute flux, including NaCl flux, across the membrane showed negligible changes with decreasing permeate flux, which resulted in a higher solute concentration with a lower permeate flux. Based on the mechanisms described above, low rejection at a low permeate flux (e.g., 3 L/m^{2}h) is a trend that is expected when other commercial NF membranes are used during direct NF treatment, which can be a disadvantage of applying the low permeate flux during NF treatment.

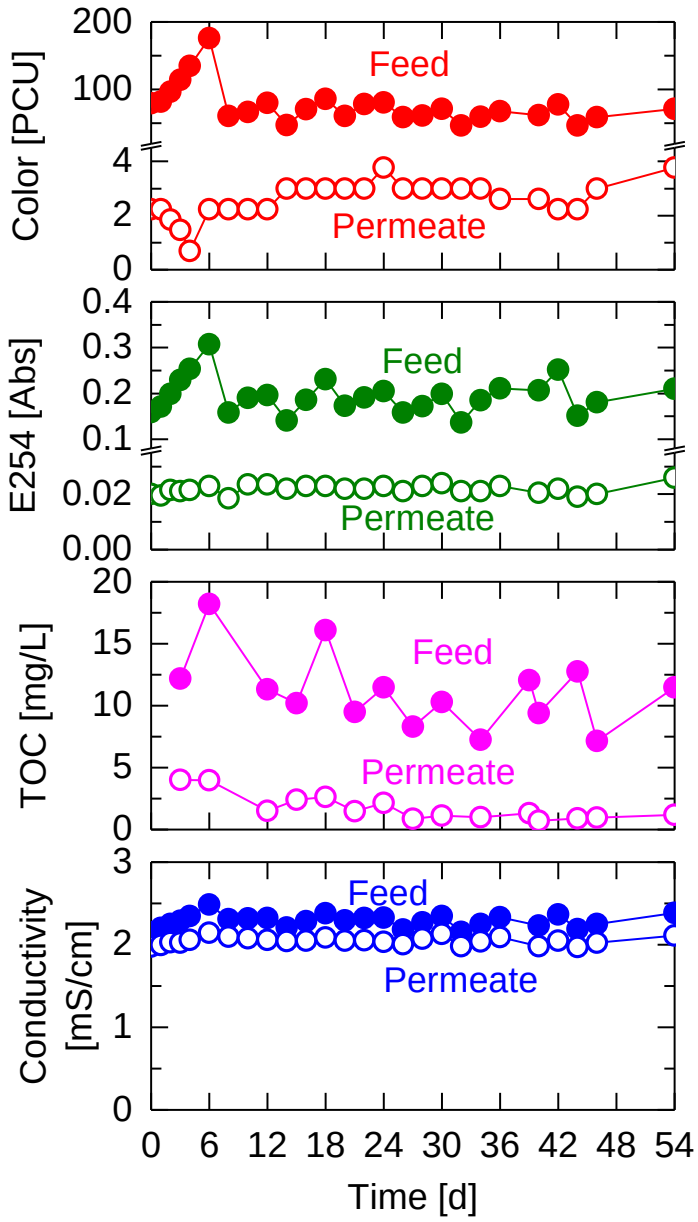

Fig. 3-9. Color, E_{254}, total organic carbon (TOC), and conductivity during the direct NF treatment of the secondary wastewater effluent. The feed water was entirely replaced every 6d.

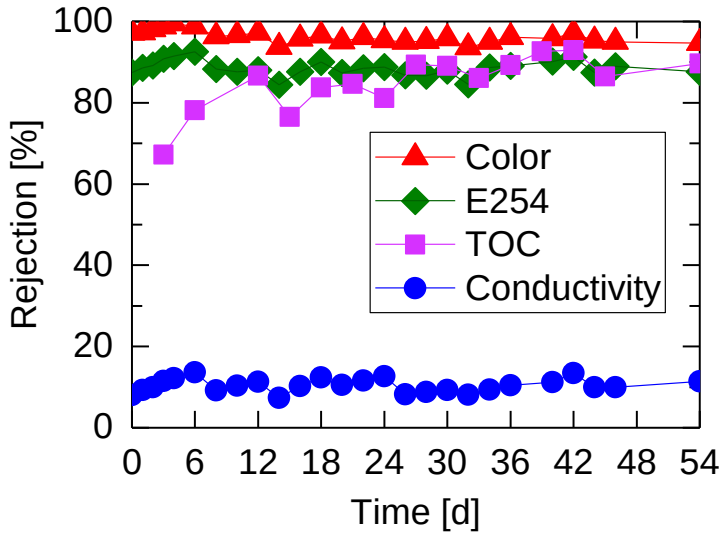

Fig. 3-10. Rejection of color, E_{254}, TOC, and conductivity during direct NF treatment of the secondary wastewater effluent.

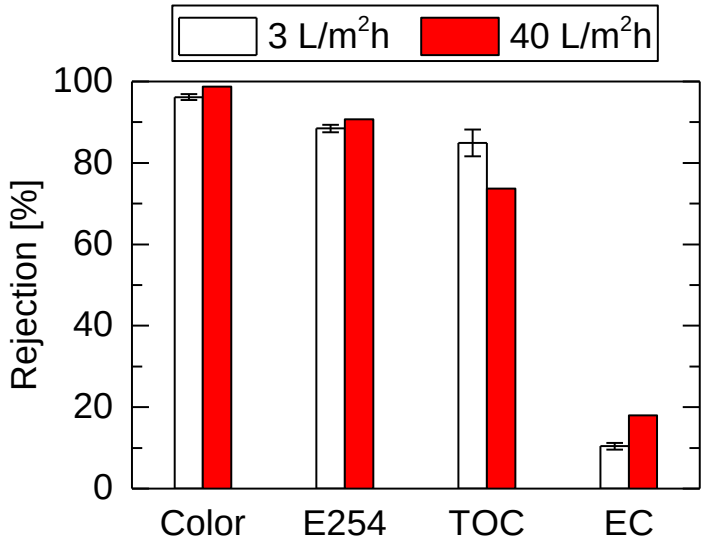

Fig. 3-11. Rejection of water quality parameters between low and high permeate flux (3 and 40 L/m^{2}h, respectively) during direct NF treatment of secondary wastewater effluent. The bar and error bars at the permeate flux of 3 L/m^{2}h show the average and standard deviation of the data presented in Fig. 3-10.

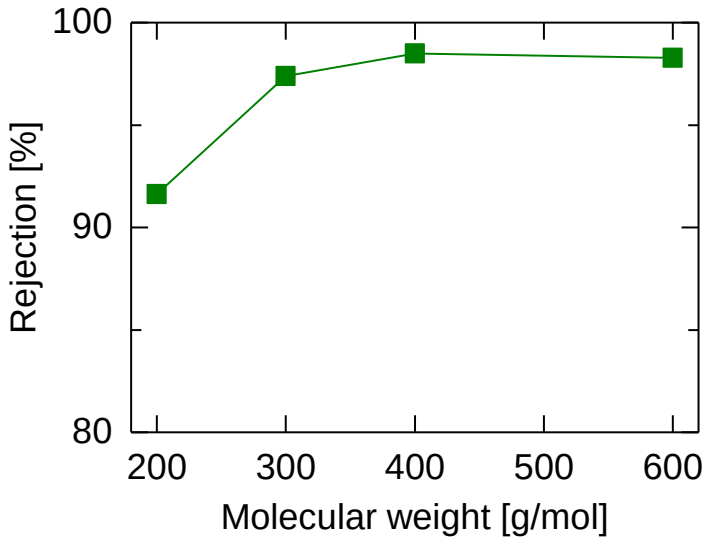

Fig. 3-12. Molecular weight cut-off of the HYDRApro 402 NF membrane. The tests were conducted using the high pressure filtration system and polyethylene glycol with a molecular weight of 200, 300. 400, and 600 g/mol (FUJIFILM Wako Pure Chemical Corporation, Osaka, Japan) at a feed temperature of 25 °C, permeate flux of 40 L/m^{2}h, and NaCl concentration of 10 mM.

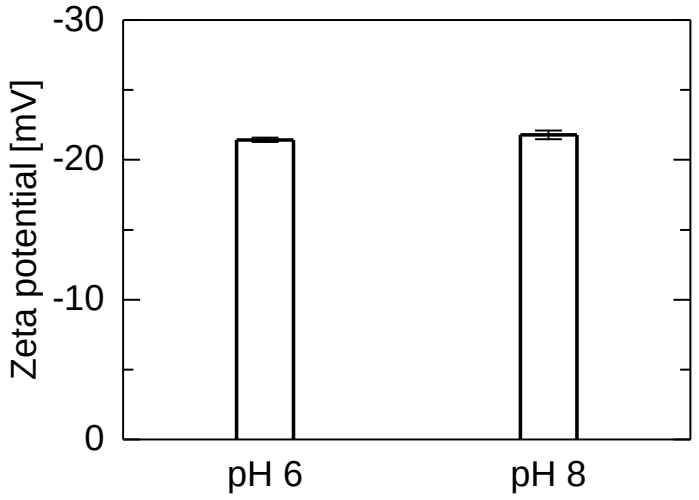

Fig. 3-13. Zeta potential of the HYDRApro 402 NF membrane at a solution pH of 6 and 8. Zeta potential of the membrane was measured in pure water using a zeta potential analyzer (ELSZ-2000, Otsuka Electronics, Osaka, Japan). The zeta potential was calculated from electrophoretic mobility using the Smoluchowski equation.

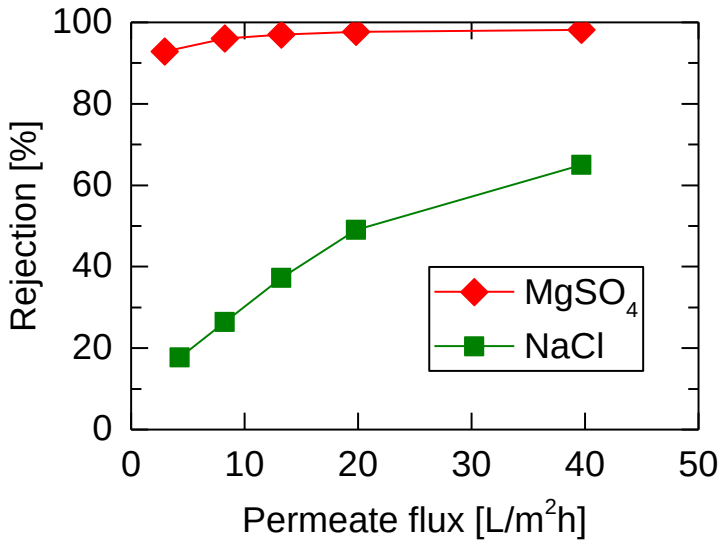

Fig. 3-14. Rejection of NaCl and $MgSO_4$ at variable permeate flux. The tests were conducted using the high-pressure filtration system at a feed temperature of 25 °C, and NaCl or $MgSO_4$ concentrations of 10 mM.

Organics in the NF permeate were further characterized to provide understanding of the variety of organics going through the membrane. The EEM fluorescence spectra of the secondary wastewater effluent in the membrane reservoir showed four major peaks (Fig. 3-15a), which included fluvic acid-like fluorophore (denoted as peak A at Ex/Em of 225–260 nm/400–500 nm), humic acid-like fluorophore (denoted as peak C at Ex/Em of 300–370 nm/400–500 nm), aromatic proteins (denoted as peak B at Ex/Em of 275–280 nm/305–321 nm), and protein-like substances (denoted as peak T at Ex/Em of 225–237 nm/340–381 nm) (Carstea et al., 2016; Derrien et al., 2017; Yoon, 2019). Direct NF treatment considerably reduced the intensity of all peaks (A, B, C, and T) (Fig. 3-15b), whereas the intensity of peaks B and C was relatively higher than that of peaks A and T. Aromatic proteins (peak B) are mainly composed of small organics such as tyrosine (molecular weight =181 Da); thus, they are likely to permeate through the pores of an NF membrane (MWCO of > 200 Da). In contrast, the molecular weights of humic acid-like substances (peak C) in secondary wastewater effluent are relatively high, in the range of 500–3000 Da (Guo et al., 2011), whereas their small fractions may permeate through the membrane. It should be noted that these humic-like substances, including aromatic hydrocarbons and heterocyclic compounds (Ou et al., 2014), can be the source of trihalomethane (THM) precursors, which react with chlorine and form THMs. Because the recycled water may be used for some water

reuse applications that have potential for human contact, the substantial removal of humic acid-like substances by direct NF treatment can be critical for public health protection.

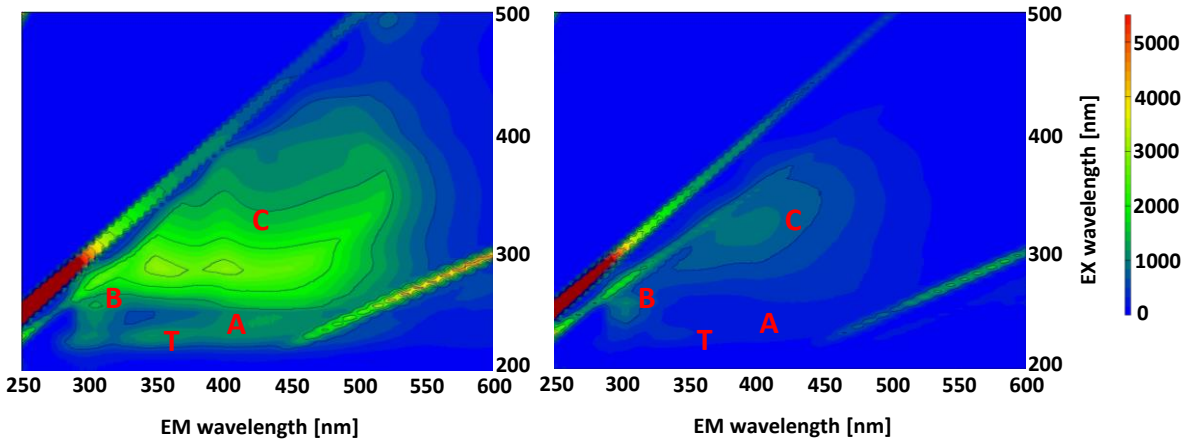

(a) Feed (b) Permeate

Fig. 3-15. Excitation-emission matrix fluorescence spectra of (a) the secondary wastewater effluent in the membrane reservoir (i.e., the feed solution) and (b) permeate values that were collected on day 46.

3.3.3. Full-scale implications

Results from this study demonstrate the potential of direct NF treatment at a low permeate flux of 3 L/m^{2}h without any mixing and air bubbling in the membrane reservoir. Low TMP (approximately 50 kPa) operation could be maintained for six months without membrane cleaning (Fig. 3-4). In addition, the treated water quality except for monovalent ions was not compromised by the low permeate flux. This suggests that direct advanced wastewater treatment (without pre-treatment) using a submerged NF system can be achieved with considerably low energy consumption. A major challenge of applying the low permeate flux is the necessity of large membrane surface areas to produce a specific volume of water, which can result in a high capital cost and large footprint. However, unlike membrane bioreactor (MBR), direct NF treatment does not require aeration and mixing; thus, the fundamental membrane structure can be weaker than the submerged membranes used in MBR. This allows engineers to design flexible membrane structures to further decrease manufacturing costs. The feasibility of direct NF treatment will be explored by comparing the overall capital and

operation costs of each option, including those with pre-treatment processes, in our future study.

3.4. Conclusions

This study evaluated the potential of direct NF treatment using a novel flat-sheet submerged NF membrane module for achieving stable wastewater treatment operations and producing high-quality recycled water. Direct NF treatment of secondary wastewater effluent at a low permeate flux of 3 L/m^{2}h resulted in negligible membrane fouling with a TMP increase of 3 kPa over 48-d, thus demonstrating the advantage of the low permeate flux for suppressing membrane fouling. Membrane fouling was reversible with sponge cleaning; nearly full removal of foulants from the membrane surface and full recovery of permeability were observed. Direct NF treatment was capable of high rejection of color, $E_{254,}$ and TOC by >93 %, >84 %, and >67 %, respectively. Overall, this study demonstrated a stable production of high-quality recycled water using a submerged NF system.

References

Bellona, C., Drewes, J.E., Xu, P., Amy, G., 2004. Factors affecting the rejection of organic solutes during NF/RO treatment - A literature review. Water Res. 38, 2795-2809.

Beril Gönder, Z., Arayici, S., Barlas, H., 2011. Advanced treatment of pulp and paper mill wastewater by nanofiltration process: Effects of operating conditions on membrane fouling. Sep. Purif. Technol. 76, 292-302.

Bonné, P.A.C., Hiemstra, P., van der Hoek, J.P., Hofman, J.A.M.H., 2003. Is direct nanofiltration with air fluxh an alternative for household water production for Amsterdam? Desalination 152, 263-269.

Bourgin, M., Beck, B., Boehler, M., Borowska, E., Fleiner, J., Salhi, E., Teichler, R., von Gunten, U., Siegrist, H., McArdell, C.S., 2018. Evaluation of a full-scale wastewater treatment plant upgraded with ozonation and biological post-treatments: Abatement of micropollutants, formation of transformation products and oxidation by-products. Water Res. 129, 486-498.

Boussu, K., Van der Bruggen, B., Volodin, A., Snauwaert, J., Van Haesendonck, C., Vandecasteele, C., 2005. Roughness and hydrophobicity studies of nanofiltration membranes using different modes of AFM. J. Colloid Interface Sci. 286, 632-638.

Carstea, E.M., Bridgeman, J., Baker, A., Reynolds, D.M., 2016. Fluorescence spectroscopy for wastewater monitoring: A review. Water Res. 95, 205-219.

Choi, H., Zhang, K., Dionysiou, D.D., Oerther, D.B., Sorial, G.A., 2005a. Effect of permeate flux and tangential flow on membrane fouling for wastewater treatment. Sep. Purif. Technol. 45, 68-78.

Choi, J.-H., Fukushi, K., Yamamoto, K., 2005b. Comparison of treatment efficiency of submerged nanofiltration membrane bioreactors using cellulose triacetate and polyamide membrane. Water Sci. Technol. 51, 305-312.

Derrien, M., Yang, L., Hur, J., 2017. Lipid biomarkers and spectroscopic indices for identifying organic matter sources in aquatic environments: A review. Water Res. 112, 58-71.

Enfrin, M., Lee, J., Le-Clech, P., Dumée, L.F., 2020. Kinetic and mechanistic aspects of ultrafiltration membrane fouling by nano- and microplastics. J. Membr. Sci. 601, 117890.

Farhat, N.M., Staal, M., Bucs, S.S., Van Loosdrecht, M.C.M., Vrouwenvelder, J.S., 2016. Spatial heterogeneity of biofouling under different cross-flow velocities in reverse osmosis membrane systems. J. Membr. Sci. 520, 964-971.

Fujioka, T., Khan, S.J., McDonald, J.A., Henderson, R.K., Poussade, Y., Drewes, J.E., Nghiem, L.D., 2013. Effects of membrane fouling on *N*-nitrosamine rejection by nanofiltration and reverse osmosis membranes. J. Membr. Sci. 427, 311-319.

Fujioka, T., Ngo, M.T.T., Makabe, R., Ueyama, T., Takeuchi, H., Nga, T.T.V., Bui, X.-T., Tanaka, H., 2020. Submerged nanofiltration without pre-treatment for direct advanced drinking water treatment. Chemosphere, 129056.

Fujioka, T., Ngo, M.T.T., Makabe, R., Ueyama, T., Takeuchi, H., Nga, T.T.V., Bui, X.-T., Tanaka, H., 2021. Submerged nanofiltration without pre-treatment for direct advanced drinking water treatment. Chemosphere 265, 129056.

Guo, J., Peng, Y., Guo, J., Ma, J., Wang, W., Wang, B., 2011. Dissolved organic matter in biologically treated sewage effluent (BTSE): Characteristics and comparison. Desalination 278, 365-372.

Hagmeyer, G., Gimbel, R., 1999. Modelling the rejection of nanofiltration membranes using zeta potential measurements. Sep. Purif. Technol. 15, 19-30.

He, Z., Miller, D.J., Kasemset, S., Paul, D.R., Freeman, B.D., 2017. The effect of permeate flux on membrane fouling during microfiltration of oily water. J. Membr. Sci. 525, 25-34.

Hilal, N., Al-Zoubi, H., Darwish, N.A., Mohamma, A.W., Abu Arabi, M., 2004. A comprehensive review of nanofiltration membranes:Treatment, pretreatment, modelling, and atomic force microscopy. Desalination 170, 281-308.

Hobbs, C., Seungkwan, H., Taylor, J., 2006. Effect of surface roughness on fouling of RO and NF membranes during filtration of a high organic surficial groundwater. J. Water Supply: Res. Technol. Aqua 55, 559-570.

Hube, S., Eskafi, M., Hrafnkelsdóttir, K.F., Bjarnadóttir, B., Bjarnadóttir, M.Á., Axelsdóttir, S., Wu, B., 2020. Direct membrane filtration for wastewater treatment and resource recovery: A review. Sci. Total Environ. 710, 136375.

Kim, H.-A., Choi, J.-H., Takizawa, S., 2007. Comparison of initial filtration resistance by pretreatment processes in the nanofiltration for drinking water treatment. Sep. Purif. Technol. 56, 354-362.

Kimura, K., Okazaki, S., Ohashi, T., Watanabe, Y., 2016. Importance of the co-presence of silica and organic matter in membrane fouling for RO filtering MBR effluent. J. Membr. Sci. 501, 60-67.

Kramer, F.C., Shang, R., Heijman, S.G.J., Scherrenberg, S.M., van Lier, J.B., Rietveld, L.C., 2015. Direct water reclamation from sewage using ceramic tight ultra- and nanofiltration. Sep. Purif. Technol. 147, 329-336.

Lee, M., Keller, A.A., Chiang, P.-C., Den, W., Wang, H., Hou, C.-H., Wu, J., Wang, X., Yan, J., 2017. Water-energy nexus for urban water systems: A comparative review on energy intensity and environmental impacts in relation to global water risks. Applied Energy 205, 589-601.

Li, Q., Xu, Z., Pinnau, I., 2007. Fouling of reverse osmosis membranes by biopolymers in wastewater secondary effluent: Role of membrane surface properties and initial permeate flux. J. Membr. Sci. 290, 173-181.

Liu, C., Olivares, C.I., Pinto, A.J., Lauderdale, C.V., Brown, J., Selbes, M., Karanfil, T., 2017. The control of disinfection byproducts and their precursors in biologically active filtration processes. Water Res. 124, 630-653.

Marszałek, A., Puszczało, E., 2020. Effect of Photooxidation on Nanofiltration Membrane Fouling During Wastewater Treatment From the Confectionery Industry. Water 12, 793.

Michael-Kordatou, I., Michael, C., Duan, X., He, X., Dionysiou, D.D., Mills, M.A., Fatta-Kassinos, D., 2015. Dissolved effluent organic matter: Characteristics and potential implications in wastewater treatment and reuse applications. Water Res. 77, 213-248.

Miller, D.J., Kasemset, S., Paul, D.R., Freeman, B.D., 2014. Comparison of membrane fouling at constant flux and constant transmembrane pressure conditions. J. Membr. Sci. 454, 505-515.

Mohammad, A.W., Teow, Y.H., Ang, W.L., Chung, Y.T., Oatley-Radcliffe, D.L., Hilal, N., 2015. Nanofiltration membranes review: Recent advances and future prospects. Desalination 356, 226-254.

Niu, C., Pan, Y., Lu, X., Wang, S., Zhang, Z., Zheng, C., Tan, Y., Zhen, G., Zhao, Y., Li, Y.-Y., 2020. Mesophilic anaerobic digestion of thermally hydrolyzed sludge in anaerobic membrane bioreactor: Long-term performance, microbial community dynamics and membrane fouling mitigation. J. Membr. Sci. 612, 118264.

Ou, H.-S., Wei, C.-H., Mo, C.-H., Wu, H.-Z., Ren, Y., Feng, C.-H., 2014. Novel insights into anoxic/aerobic1/aerobic2 biological fluidized-bed system for coke wastewater treatment by fluorescence excitation–emission matrix spectra coupled with parallel factor analysis. Chemosphere 113, 158-164.

Qi, Y., Zhu, L., Gao, C., Shen, J., 2019. A novel nanofiltration membrane with simultaneously enhanced antifouling and antibacterial properties. RSC Advances 9, 6107-6117.

Regula, C., Carretier, E., Wyart, Y., Gésan-Guiziou, G., Vincent, A., Boudot, D., Moulin, P., 2014. Chemical cleaning/disinfection and ageing of organic UF membranes: A review. Water Res. 56, 325-365.

Ruigómez Sempere, I., Gonzalez, E., Rodríguez-Gómez, L., Vera, L., 2020. Direct Membrane Filtration for Wastewater Treatment Using an Intermittent Rotating Hollow Fiber Module. Water 12, 1836.

Sayed, S., Tarek, S., Dijkstra, I., Moerman, C., 2007. Optimum operation conditions of direct capillary nanofiltration for wastewater treatment. Desalination 214, 215-226.

Schaep, J., Vandecasteele, C., 2001. Evaluating the charge of nanofiltration membranes. J. Membr. Sci. 188, 129-136.

Van der Bruggen, B., Mänttäri, M., Nyström, M., 2008. Drawbacks of applying nanofiltration and how to avoid them: A review. Sep. Purif. Technol. 63, 251-263.

Wang, Y.-N., Tang, C.Y., 2011. Protein fouling of nanofiltration, reverse osmosis, and ultrafiltration membranes—The role of hydrodynamic conditions, solution chemistry, and membrane properties. J. Membr. Sci. 376, 275-282.

Warsinger, D.M., Chakraborty, S., Tow, E.W., Plumlee, M.H., Bellona, C., Loutatidou, S., Karimi, L., Mikelonis, A.M., Achilli, A., Ghassemi, A., Padhye, L.P., Snyder, S.A., Curcio, S., Vecitis, C.D., Arafat, H.A., Lienhard, J.H., 2018. A review of polymeric membranes and processes for potable water reuse. Prog. Polym. Sci. 81, 209-237.

Wijmans, J.G., Baker, R.W., 1995. The solution-diffusion model: a review. J. Membr. Sci. 107, 1-21.

Xu, B., Li, D.-P., Li, W., Xia, S.-J., Lin, Y.-L., Hu, C.-Y., Zhang, C.-J., Gao, N.-Y., 2010. Measurements of dissolved organic nitrogen (DON) in water samples with nanofiltration pretreatment. Water Res. 44, 5376-5384.

Xu, R., Qin, W., Zhang, B., Wang, X., Li, T., Zhang, Y., Wen, X., 2020. Nanofiltration in pilot scale for wastewater reclamation: Long-term performance and membrane biofouling characteristics. Chem. Eng. J. 395, 125087.

Yan, Y., Li, H., Myrick, M., 2000. Fluorescence fingerprint of waters: Excitation-emission matrix spectroscopy as a tracking tool. Appl. Spectrosc. 54, 1539-1542.

Yang, J.-S., Yuan, D.-X., Weng, T.-P., 2010. Pilot study of drinking water treatment with GAC, O3/BAC and membrane processes in Kinmen Island, Taiwan. Desalination 263, 271-278.

Yoon, S.-H., 2019. Potential and limitation of fluorescence-based membrane integrity monitoring (FMIM) for reverse osmosis membranes. Water Res. 154, 287-297.

Zhao, Y.-x., Li, P., Li, R.-h., Li, X.-y., 2019. Direct filtration for the treatment of the coagulated domestic sewage using flat-sheet ceramic membranes. Chemosphere 223, 383-390.

Chapter 4. Membrane distillation for achieving high water recovery for potable water reuse

4.1. Introduction

Water treatment using reverse osmosis (RO) membranes is widely employed in many water recycling projects to produce high-quality recycled water for potable reuse. Typical spiral-wound RO membranes can achieve approximately 99% salt removal. To avoid inducing excessive membrane fouling and treating high salinity concentrates, the permeate flux and overall water recovery (ratio of the RO permeate to the RO feed) have been set at conservative values of 20 L/m^{2}h and 85%, respectively (Fujioka et al., 2012; Zhang and Liu, 2020). In recent years, higher water recovery (e.g., 98%) has been attempted in inland areas to gain a higher volume of purified water from the RO feed and minimize the discharge volume of RO (Jiang et al., 2020; Rajwade et al., 2020). However, achieving a high water recovery by treating the RO concentrate is challenging (Wang et al., 2020; Gu et al., 2021), as increasing the water recovery from 85% to 98% represents a considerable increase in the concentration factor (from 6.7 to 50-fold), which incurs ~7.5 times larger osmotic pressure and subsequent feed pressure. Moreover, highly-concentrated impurities in the concentrated feed (i.e., RO concentrate) can induce membrane fouling that necessitates frequent chemical cleaning. Therefore, another treatment technology that can achieve higher water recovery is required.

Among the water treatment technologies for minimizing RO concentrate volume (e.g., electrocoagulation, electrodialysis, and forward osmosis membrane), membrane distillation (MD) can achieve high water recoveries without being limited by initial salinity (Subramani and Jacangelo, 2014). MD is a separation process, in which a hydrophobic membrane allows volatile molecules (e.g., water vapor) to pass through its pores from a high-temperature solution to a low-temperature solution due to the difference in their vapor pressures. Because non-volatile molecules, including salts in wastewater (high temperature solution), do not play a major role in the vapor pressure, a high osmotic pressure in the concentrate does not influence the energy requirement, unlike RO systems. MD has been increasingly used for purifying or concentrating hard-to-treat waters containing high concentrations of organics, such as in beverage industries (Naidu et al., 2020; Kalla, 2021). In recent years, MD has also been applied to municipal wastewater treatment (Caroline Ricci et al., 2021; Patel et al., 2021).

However, it has yet to be comprehensively assessed as a treatment method for potable water reuse with >95% water recovery; thus, many challenges remain.

The uncertainties surrounding MD treatment of municipal wastewater include the propensity for membrane fouling. In general, membrane fouling during MD treatment of wastewater is less likely to occur than in pressure-driven systems, including RO processes (Shi et al., 2019; Rajwade et al., 2020). This is similar to non-pressurized wastewater treatment via the forward osmosis (FO) membrane process, which is based on the difference in salinity between the feed and draw solution phases (Naghdali et al., 2020). MD has an advantage over FO for producing recycled water, as it does not use a draw solution. However, high concentrations of organics in the RO concentrate can cause organic membrane fouling that reduces membrane permeability during MD treatment (Alkhudhiri et al., 2012). Moreover, increasing the concentrations of inorganic components in the concentrate allows them to reach their maximum solubilities, resulting in crystallization on the membrane surface (scaling) (Yun et al., 2006). Although a previous study (Alrehaili et al., 2020) explored the MD treatment of an RO concentrate for achieving an overall water recovery of 95%, the water quality was not comprehensively assessed.

A major concern regarding achieving a high water recovery of >95% using MD treatment is the permeate water quality. In theory, only volatile molecules, particularly water vapor, can move through the pores of hydrophobic membranes from the feed to the permeate streams during MD treatment. Previous studies (Jamil et al., 2020; 71 Piras et al., 2020) have reported that some low molecular weight trace organic chemicals (TOrCs) can readily permeate across RO membranes, making the permeate water quality of the RO concentrate a potential concern for potable water reuse. Although previous studies (Wijekoon et al., 2014; Ren et al., 2018) have assessed TOrC permeation across MD membranes, they have not done so in the context of generating potable water from an RO concentrate.

This study aimed to evaluate the potential of applying MD on RO concentrate to achieve an overall water recovery of 98% during water recycling for potable water reuse. We assessed fouling propensity and water quality during MD treatment of RO concentrate that underwent a 6.7-fold concentration (i.e., 85% system recovery). We examined the feasibility of MD after RO via comparing our results with RO treatment alone and calculating the energy requirement of our method. Our ultimate goal was to determine the potential for increasing water-recycling productivity (i.e., water recovery) using MD membranes without inducing excessive membrane fouling or compromising the water quality. The expected outcome of this study is a

method for producing potable water from pre-treated wastewater, which could reduce the demand for fresh water (e.g., surface water or groundwater) for drinking water purposes.

4.2. Materials and methods

4.2.1. Chemicals

Separation tests were performed on four N-nitrosamines and 42 pharmaceuticals and personal care products (PPCPs) (Table 4-1), categorized as positively and negatively charged ions, zwitterions, neutral hydrophobic, and neutral hydrophilic compounds. Stock solutions of N-nitrosamines or PPCPs were prepared at 1000 and 100 μg/L per chemical, respectively. Tap water was filtered using RO water generation equipment (RTA-200W, AS ONE; Osaka, Japan) to produce pure water for filtration tests. Treated wastewater samples were obtained from a municipal wastewater treatment plant in Kitakyushu, Japan, and were collected after passing through a membrane bioreactor (MBR). The electrical conductivity of the MBR effluent was 1.0–1.1 mS/cm. Another treated wastewater sample was obtained from a municipal wastewater treatment plant in Nagasaki, Japan, and was collected after ultrafiltration (UF) of the secondary wastewater effluent.

4.2.2. Membranes

The RO concentrate was prepared using a polyamide composite RO membrane element, FilmTec™ BW60-1812-75 (DuPont/Filmtec; Midland, MI, USA), with a capacity of 96% minimum salt rejection according to manufacturer specifications. This membrane element was set in a membrane housing.

The MD membranes used to treat RO concentrate were flat sheet polytetrafluoroethylene (PTFE) microfiltration (MF) membranes laminated onto polypropylene netting with a pore size of 0.2 μm (Sterlitech; Kent, WA, US) (Table 4-2). PTFE membranes with a pore size of 0.2 μm were selected for this study, as PTFE provides a higher permeate flux than that of polyvinylidene fluoride (PVDF), and 0.2 μm is one of the most frequently used pore sizes for MD treatment (Ashoor et al., 2016). As a comparison with the MD membranes, polyamide composite flat-sheet RO membranes (ESPA2, Hydranautics; Oceanside, CA, USA) were also used.

Table 4-1. Physicochemical characteristics of the selected chemicals.

Compounds	Structure	MW [Da]	Minimum projection area* [Å^2]	Log *D* at pH 8	Vapor pressure at 25°C [mmHg]	pK_H
Neutral & hydrophilic						
N-nitrosodimethylamine (NDMA)	$C_2H_6N_2O$	74.09	20.1	0.04	4.3	5.74
N-nitrosomethylethylamine (NMEA)	$C_3H_8N_2O$	88.11	22.0	0.40	2.09	6.37
N-nitrosopyrrolidine (NPYR)	$C_4H_8N_2O$	100.12	25.0	0.44	0.264	7.31
N-nitrosomorpholine (NMOR)	$C_4H_8N_2O_2$	116.12	26.9	0.75	0.134	7.61
Acetaminophen	$C_8H_9NO_2$	151.17	21.8	0.89	1.94×10^{-6}	12.19
Antipyrine	$C_{11}H_{12}N_2O$	188.23	32.4	1.22	2.79×10^{-4}	9.18
Caffeine	$C_8H_{10}N_4O_2$	194.19	30.0	-0.55	7.33×10^{-9}	10.45
Cyclophosphamide	$C_7H_{15}Cl_2N_2O_2P$	261.08	45.8	0.10	4.40×10^{-5}	10.87
Trimethoprim	$C_{14}H_{18}N_4O_3$	290.32	51.1	1.23	7.52×10^{-9}	13.62
Griseofulvin	$C_{17}H_{17}ClO_6$	352.77	54.7	2.17	4.35×10^{-8}	11.95
Thiamphenicol	$C_{12}H_{15}Cl_2NO_5S$	356.22	49.3	-0.28	7.18×10^{-14}	18.87
Tylosin	$C_{46}H_{77}NO_{17}$	916.11	120.9	2.25	1.98×10^{-34}	37.24
Neutral & hydrophobic						
N,N-Diethyl-meta-toluamide (DEET)	$C_{12}H_{17}NO$	191.30	39.6	2.50	3.31×10^{-3}	7.68
Crotamiton	$C_{13}H_{17}NO$	203.28	40.2	3.09	4.89×10^{-4}	6.82
Carbamazepine	$C_{15}H_{12}N_2O$	236.27	40.2	2.77	8.80×10^{-8}	9.97
Positively charged						
Salbutamol	$C_{13}H_{21}NO_3$	239.32	41.3	-0.77	8.89×10^{-9}	15.19
Propranolol	$C_{16}H_{21}NO_2$	259.35	42.5	0.92	7.44×10^{-8}	12.10
Atenolol	$C_{14}H_{22}N_2O_3$	266.34	36.9	-1.24	7.69×10^{-10}	17.86
Disopyramide	$C_{21}H_{29}N_3O$	339.48	64.8	1.08	2.14×10^{-8}	15.59
Sulpiride	$C_{15}H_{23}N_3O_4S$	341.43	56.0	-0.21	1.23×10^{-10}	16.82
Lincomycin	$C_{18}H_{34}N_2O_6S$	406.50	61.6	-0.60	1.34×10^{-17}	22.52
Diltiazem	$C_{22}H_{26}N_2O_4S$	414.52	63.0	2.33	2.98×10^{-11}	16.06
Tiamulin	$C_{28}H_{47}NO_4S$	493.75	75.2	2.99	4.15×10^{-14}	15.38
Clarithromycin	$C_{38}H_{69}NO_{13}$	747.96	106.5	2.71	2.35×10^{-25}	28.76
Roxithromycin	$C_{41}H_{76}N_2O_{15}$	837.05	126.8	1.89	No data	No data
Negatively charged						
Ethenzamide	$C_9H_{11}NO_2$	165.19	30.0	1.36	2.79×10^{-5}	9.76
Theophylline	$C_7H_8N_4O_2$	180.16	28.8	-1.11	5.57×10^{-10}	11.77
Clofibric acid	$C_{10}H_{11}ClO_3$	214.65	30.3	-0.60	7.54×10^{-5}	7.66
Naproxen	$C_{14}H_{14}O_3$	230.26	34.8	-0.36	1.27×10^{-6}	9.47
Nalidixic acid	$C_{12}H_{12}N_2O_3$	232.24	34.3	-1.01	6.18×10^{-8}	15.29
Fenoprofen	$C_{15}H_{14}O_3$	242.27	40.6	0.24	2.35×10^{-5}	8.89
Sulfapyridine	$C_{11}H_{11}N_3O_2S$	249.29	44.6	0.12	4.14×10^{-8}	12.97
Sulfamethoxazole	$C_{10}H_{11}N_3O_3S$	253.28	46.1	-0.11	1.30×10^{-7}	12.02
Ketoprofen	$C_{16}H_{14}O_3$	254.29	41.7	0.18	1.46×10^{-6}	10.67
Sulfathiazole	$C_9H_9N_3O_2S_2$	255.30	41.2	0.24	3.24×10^{-8}	13.23
Sulfamerazine	$C_{11}H_{12}N_4O_2S$	264.30	47.4	-0.20	4.17×10^{-9}	9.76
Sulfadimidine	$C_{12}H_{14}N_4O_2S$	278.33	48.8	-0.06	6.82×10^{-9}	9.71
Sulfamonomethoxine	$C_{11}H_{11}N_4NaO_3S$	280.30	47.2	0.09	8.35×10^{-9}	13.62
Sulfadimethoxine	$C_{12}H_{13}N_4NaO_4S$	310.33	49.8	0.52	1.48×10^{-9}	13.89
Furosemide	$C_{12}H_{11}ClN_2O_5S$	330.74	40.9	-1.58	3.06×10^{-11}	15.40
Enrofloxacin	$C_{19}H_{22}FN_3O_3$	359.40	50.1	-0.12	3.06×10^{-12}	17.83
Levofloxacin	$C_{18}H_{20}FN_3O_4$	361.37	45.7	-1.01	1.82×10^{-13}	20.94
Bezafibrate	$C_{19}H_{20}ClNO_4$	361.82	40.4	0.55	6.12×10^{-11}	14.67
Oxytetracycline	$C_{22}H_{24}N_2O_9$	460.40	58.7	-5.46	9.05×10^{-23}	24.77
Zwitterion						
Ciprofloxacin	$C_{17}H_{18}FN_3O_3$	331.35	43.0	-0.91	2.85×10^{-13}	18.29
Tetracycline	$C_{22}H_{24}N_2O_8$	444.44	62.3	-4.16	2.08×10^{-21}	23.33

Chemical properties were obtained from ChemAxon (https://www.chemaxon.com/).

Table 4-2. Characteristics of membrane distillation (MD) and reverse osmosis (RO) systems.

System	MD	ESPA2 RO
Manufacturer	Sterlitech, WA, US	Hydranautics, CA, US
Materials	Polytetraflouroethylene (PTFE)	Polyamide composite
Pore size (µm)	0.2	Not available
Total membrane area (cm^2)	120	36.3
Membrane cell material	Acrylic resin	Stainless steel

Both MD and RO systems was used in the treatment of the RO concentrate.

4.2.3. Treatment system

The RO treatment system (Fig. 4-1) comprised a membrane module containing the BW60-1812-75 membrane element, diaphragm pump (CDP 8800, Aquatec International, Inc., Irvine, CA, USA), flow indicators, pressure gauge, 5 L feed and permeate collection tanks, as well as a coil pipe connected to a temperature-controlled water bath (Thermax Water Bath, TM-1A, AS-ONE, Osaka, Japan).

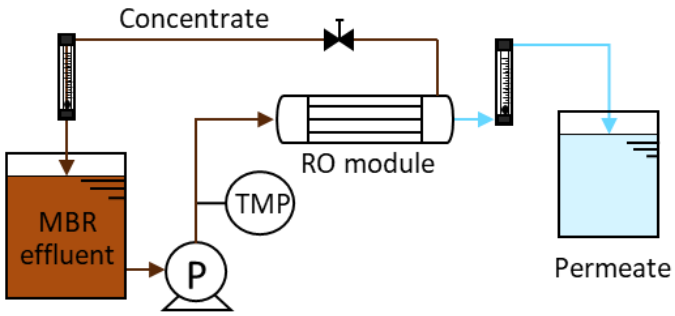

Fig. 4-1. Schematic diagram of the reverse osmosis (RO) unit for the preparation of the RO concentrate. RO system was operated at a constant permeate flux of 20 L/m^2h, a feed temperature of 20 °C, and water recovery of 85%.

The direct-contact MD system for treating RO concentrate (Fig. 4-2) comprised two acrylic resin membrane cells (C10-T, Nitto, Osaka, Japan) containing a flat sheet of the PTFE MF membrane (Sterlitech; Kent, WA, US), two 5 L medium PYREX® bottles (AS ONE; Osaka, Japan), two diaphragm pumps (CDP 8800, Aquatec International, Inc.; Irvine, CA, USA), two flow meters with ranges of 0.4–4.0 L/min (AS ONE; Osaka, Japan), low-temperature circulator (CCA-1112, Tokyo Rikakikai; Tokyo, Japan), water bath (EW-100R, AS ONE;

Osaka, Japan), digital balance (EK-6100i, A&D Company; Tokyo, Japan) connected to a computer, two thermometers (WT100, AS ONE; Osaka, Japan), two stainless steel cooling coils with heat transfer areas of 0.11 m^2 (AS ONE; Osaka, Japan), and PTFE pipes (inner diameter = 6 mm) that connected each apparatus. Each membrane cell holds a flat sheet membrane with an effective membrane area of 60 cm^2.

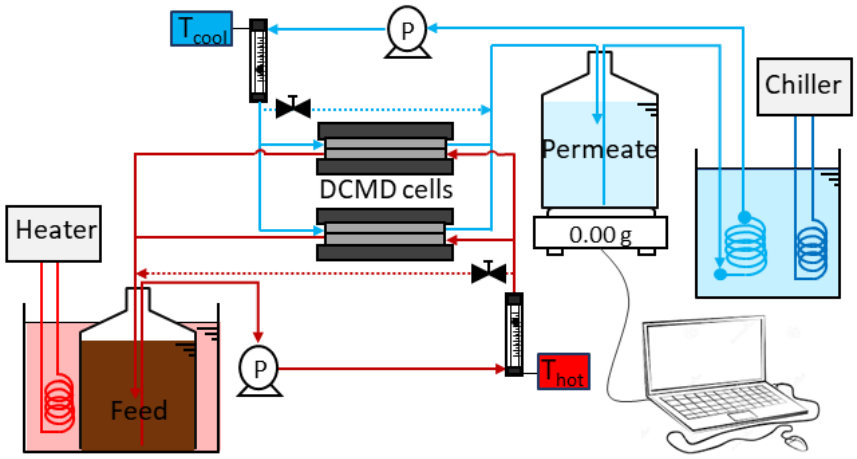

Fig. 4-2. Schematic diagram of the MD unit.

The RO treatment system (Fig. 4-3) consisted of a stainless-steel membrane cell with an integrated magnetic stirrer (Iwai Pharma Tech, Tokyo, Japan) containing ESPA2 RO membrane coupons, high-pressure pump (KP-12, FLOM; Tokyo, Japan), two flow meters, pressure gauge, pressure relief valve, and temperature control unit (NCB-500, Tokyo Rikakikai; Tokyo, Japan). The membrane cell contained a flat-sheet membrane with an effective area of 36.3 cm^2.

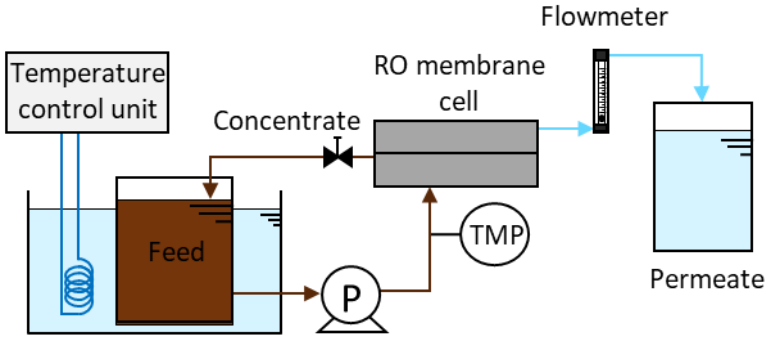

Fig. 4-3. Schematic diagram of the RO unit.

4.2.4. Experimental protocols

4.2.4.1. Preparation of RO concentrate

To prepare RO concentrate, MBR- or UF-treated wastewater was filtered until water recovery reached 85%. The filtration system using the BW60-1812-75 RO membrane element was first stabilized using pure water, then operated at a constant transmembrane pressure (TMP) of 0.6 MPa and a cross-flow rate of 1.0 L/min. The RO concentrate was recirculated into the feed tank, while the RO permeate was collected in another container. After reaching 85% water recovery, RO concentrate was at 15% of initial wastewater volume and stored in the refrigerator. It was then spiked with a stock solution of N-nitrosamines (the 1st experiment) or PPCPs (the 2nd experiment) at 1.0 μg/L and 100 μg/L, respectively, before being used for subsequent MD or RO treatments.

4.2.4.2. MD treatment

The major operating conditions in the MD treatment (feed temperature and cross-flow velocity [CFV]) were first optimized using pure water. The effects of feed temperature on permeate flux were assessed at feed temperatures of 40, 50, and 55 °C under a constant distillate temperature of 20 °C. During the assessment, CFVs of the feed and distillate streams in the membrane cell were maintained at 0.40 and 0.53 m/s, respectively, corresponding to a flow rate of 1.0 L/min in both streams. The effects of CFV on permeate flux were also assessed at feed CFVs of 0.24, 0.32, 0.40, and 0.48 m/s, as well as distillate CVFs of 0.32, 0.42, 0.53, and 0.63 m/s. During the assessment, solution temperatures in the feed and distillate streams were maintained at 50 °C and 20 °C, respectively.

Treatment using the direct-contact MD system continued until 98% overall water recovery. Reverse-osmosis concentrate (3.0 L) was placed in the feed container, and 1.0 L of pure water was placed in the distillate container. Initial permeate flux was set to approximately 25 L/m^{2}h. Throughout the tests, temperatures of the feed and distillate streams were maintained at 50 and 20 °C, while their CFVs were maintained at 0.40 and 0.53 m/s, respectively. Pure-water permeate flux was measured before and after each treatment.

4.2.4.3. RO treatment

The RO concentrate was also passed through an RO treatment system to achieve higher water recovery. First, 0.9 L of RO concentrate was placed in a feed container. Permeate flux was maintained at 25 L/m^{2}h. Throughout the tests, feed temperature and CFV were maintained at 25 °C and 0.047 m/s, respectively. Pure-water permeate flux was measured at a TMP of 1.0 MPa before and after each treatment. RO treatment was also conducted on the MBR-treated wastewater for 96 h to compare the membrane fouling speed with that of the RO concentrate. The same operating conditions as those used to treat the RO concentrate were applied. During the RO treatment of the MBR-treated wastewater, both the permeate and concentrate were re-circulated into the feed tank to evaluate the propensity for membrane fouling.

4.2.5. Analysis

Electrical conductivity was determined using an Orion Star A325 (Thermo Fisher Scientific, MA, USA). Dissolved organics in the feed, permeate, and concentrate were analyzed using fluorescence spectroscopy (RF-6000, Shimadzu; Kyoto, Japan). The 3D excitation-emission matrix (EEM) spectra were obtained at fluorescence excitation and emission wavelengths of 200–500 nm and 250–600 nm, respectively. An optical device (Narishige, Japan) was used to estimate contact angles of membranes before and after treatment. Membrane surface images were obtained using atomic force microscopy (AFM) (SPM-9700, Shimadzu; Kyoto, Japan) and a scanning electron microscope (SEM, JSM-7500FAM, Japan Electronic Computer Company, Tokyo, Japan). N-nitrosamine concentrations were measured by high-performance liquid chromatography-photochemical reaction-chemiluminescence (HPLC-PR-CL) (Kodamatani et al., 2018). An ACQUNITY ultra-performance liquid chromatography (UPLC) equipped with an atmospheric pressure ionization (API) tandem mass spectrometer (Waters, MA, USA) was used for PPCP analysis (Narumiya et al., 2013).

4.2.6. Energy requirement calculations

4.2.6.1. MD treatment

The energy requirement during MD treatment was estimated based on specific energy consumption (SEC, kWh/m^3) (Fig. 4-4). The SEC in direct-contact MD is calculated as follows (Christie et al., 2020):

$$\mathrm{SEC} = \frac{P}{\Delta Q} \tag{4-1}$$

$$P = C_f Q_{f,in} \Delta T \tag{4-2}$$

$$\Delta Q = \frac{\eta C_f Q_{f,in} (\Delta T - \Delta T_{\mathrm{MD}})}{H_v} \tag{4-3}$$

where P is thermal energy (kW), ΔQ is distillate flow rate (kg/s), C_f is specific heat capacity of the feed (kJ/kg °C), $Q_{f,in}$ is inflow rate of the feed stream (m^3/s), η is thermal efficiency, H_v is average enthalpy of vaporization of feed and distillate streams (kJ/kg), ΔT is temperature difference (°C) between feed and distillate streams in bulk solutions, and ΔT_{MD} is temperature difference (°C) at membrane interfacial surfaces. The trans-membrane temperature difference (ΔT_{MD}) (°C) is expressed as (Christie et al., 2020):

$$\Delta T_{\mathrm{MD}} = T_{f,m} - T_{d,m} \tag{4-4}$$

where $T_{f,m}$, $T_{d,m}$ are interfacial temperatures (°C) of feed and distillate at the membrane surface, respectively. Membrane surface temperatures are calculated as follows (Martínez-Díez and Vázquez-González, 1999):

$$T_{f,m} = T_{f,in} - \frac{\left(T_{f,in} - T_{d,in}\right)\frac{1}{h_f}}{\frac{1}{h_v + \frac{k_m}{\delta}} + \frac{1}{h_f} + \frac{1}{h_d}} \tag{4-5}$$

$$T_{d,m} = T_{d,in} - \frac{\left(T_{f,in} - T_{d,in}\right)\frac{1}{h_d}}{\frac{1}{h_v + \frac{k_m}{\delta}} + \frac{1}{h_f} + \frac{1}{h_d}} \tag{4-6}$$

where $T_{f,in}$ and $T_{d,in}$ are influent temperatures (°C) of feed and distillate streams, respectively; h_v, h_f, and h_d are heat transfer coefficients (W/m^{2}K) for the vapor, feed, and distillate streams, respectively; k_m is membrane thermal conductivity (W/mK); and δ is membrane thickness (m).

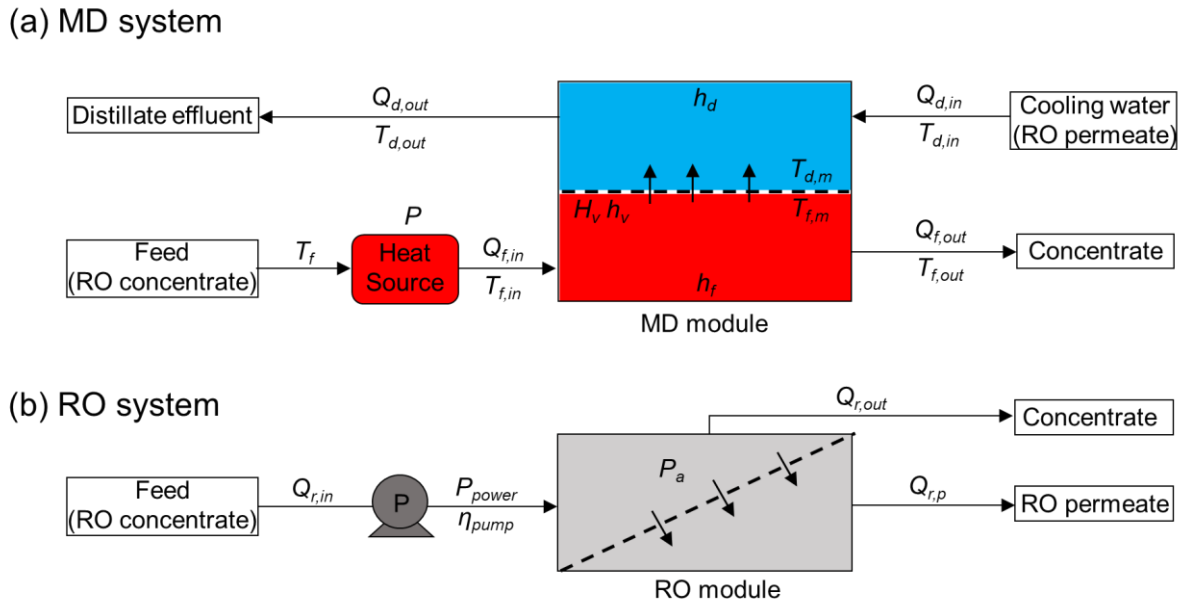

Fig. 4-4. Schematic diagram of (a) membrane distillation (MD) and (b) reverse osmosis (RO) treatment system: feed temperature (T_f); thermal energy (P); feed inflow rate ($Q_{f,in}$), outflow rate ($Q_{f,out}$); feed influent temperature ($T_{f,in}$), feed outflow temperature ($T_{f,out}$) of the feed; average enthalpy of vaporization of feed and distillate streams (H_v); heat transfer coefficients for the vapor (h_v), feed (h_f), and distillate (h_d); interfacial temperatures at the membrane surface of the feed ($T_{f,m}$) and distillate ($T_{d,\mathrm{m}}$); influent distillate temperature ($T_{d,in}$), outflow distillate temperature ($T_{d,out}$); distillate inflow rate ($Q_{d,in}$), distillate outflow rate ($Q_{d,out}$); flow rate of the RO feed ($Q_{r,in}$); power consumption (P_{power}); pump efficiency (η_{pump}); feed pressure (P_a); permeate flow rate ($Q_{r,p}$); and concentrate flow rate ($Q_{r,out}$).

4.2.6.2. RO treatment

Specific energy consumption (SEC) in the RO system was calculated using the following formula (Li, 2011; Nagy, 2018):

$$\mathrm{SEC} = \frac{P_{\mathrm{power}}}{Q_{r,p} \times 3600} \tag{4-7}$$

$$P_{\mathrm{power}} = \frac{P_a \times Q_{r,in}}{\eta_{\mathrm{pump}}} \times 10^2 \tag{4-8}$$

where P_{power} is power consumption (kW), $Q_{r,p}$ is permeate flow rate (m^3/s), $Q_{r,in}$ is inflow rate of the feed stream (m^3/s), η_{pump} is pump efficiency, P_a is feed pressure (bar).

The pressure requirement during the RO-concentrate treatment was calculated using the Integrated Membrane Solutions Design (IMSDesign) software (Hydranautics; Oceanside, CA, USA). The overall water recovery was assumed to increase from 85 to 98% through the RO-concentrate treatment.

4.3. Results and discussion

4.3.1. Fundamental performance using pure water

Prior to treatment of RO concentrate, we optimized MD operational conditions using pure water. In this study, typical procedures for municipal wastewater treatment were employed: feed temperatures of 40–60 °C and CFVs of 0.005–0.27 m/s (Jacob et al., 2015; Kim et al., 2015; Kim et al., 2016; Guo et al., 2018). Because crystals can form on the membrane at a feed temperature of ≥60 °C during water recycling (Liu et al., 2019), a maximum feed temperature of 55 °C was set in this study. In general, an increase in feed temperature from 40 to 55 °C corresponded to an increase in permeate flux from 16 to 42 L/m^2h (Fig. 4-5a), presumably induced by the increased transfer of water molecules (Damtie et al., 2019). In contrast to the feed temperature, CFV increases in both the feed and distillate streams only caused a slight elevation in permeate flux (Fig. 4-5b), likely due to reductions of both the thermal boundary layer and concentration polarization layer (Warsinger et al., 2015). As increases in feed and distillate CFVs do not enhance the permeate flux, typical CFVs of 0.4 m/s (feed) and 0.53 m/s (distillate) were selected as the standard conditions. Although a feed temperature of 55 °C provides the highest permeate flux, such a high temperature requires considerable heat energy and can potentially induce more volatile TOrC permeation. Therefore, the following evaluations were conducted at a feed temperature of 50 °C. To examine the feasibility of high temperatures (i.e., ≥55 °C), future research should assess the impact of the feed temperature on energy consumption and permeate water quality.

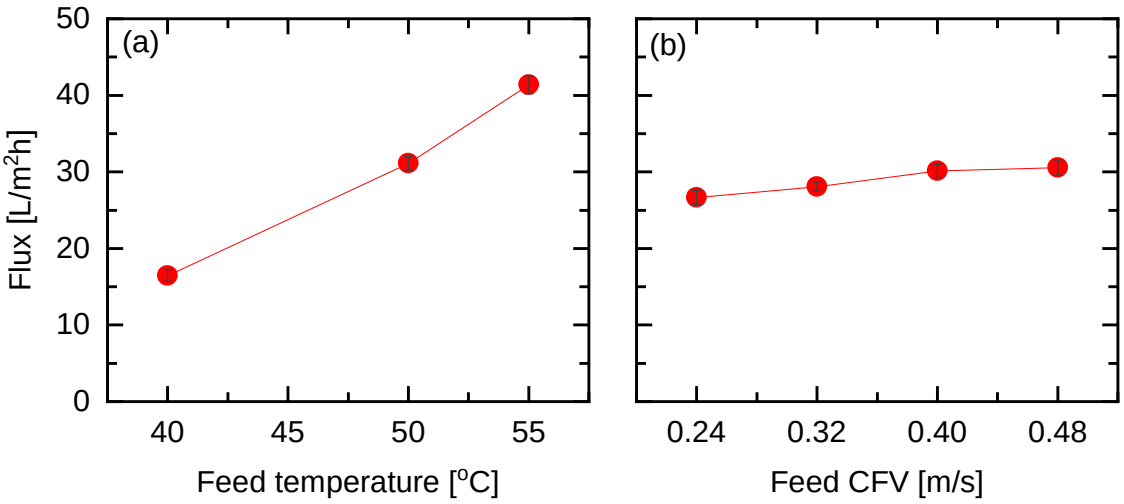

Fig. 4-5. Permeate flux against (a) variable feed temperatures (distillate temperature of 20°C, feed cross-flow velocity [CFV] of 0.4 m/s, distillate CFV of 0.53 m/s) and (b) variable CFV of the feed stream (feed temperature of 50°C, distillate temperature of 20°C). The average and ranges are the results of duplicated tests.

4.3.2. Membrane fouling propensity

With the aim of achieving a 98% overall water recovery, we treated the RO concentrate with MD membranes for over 8 h, and observed a negligible reduction in permeate flux from 26 to 25 L/m^{2}h (Fig. 4-6). In addition, the pure-water permeate flux of the MD membrane exhibited negligible variations after the test (~1% increase from 25 to 25.3 L/m^{2}h). These results indicate that negligible membrane fouling occurred over 8 h of MD treatment. To confirm membrane fouling propensity, we repeated the filtration cycles three times (Fig. 4-7) and observed approximately a 16% reduction in the permeate flux from 25 to 21 L/m^{2}h. Despite this reduction, the permeate flux fully recovered to the initial flux when switching from the 25-fold concentrated wastewater (i.e., 98% recovery) to pure water for the analysis of pure-water permeate flux. The recovery indicates that a cross-flow of pure water readily detaches foulants deposited on the membrane surface.

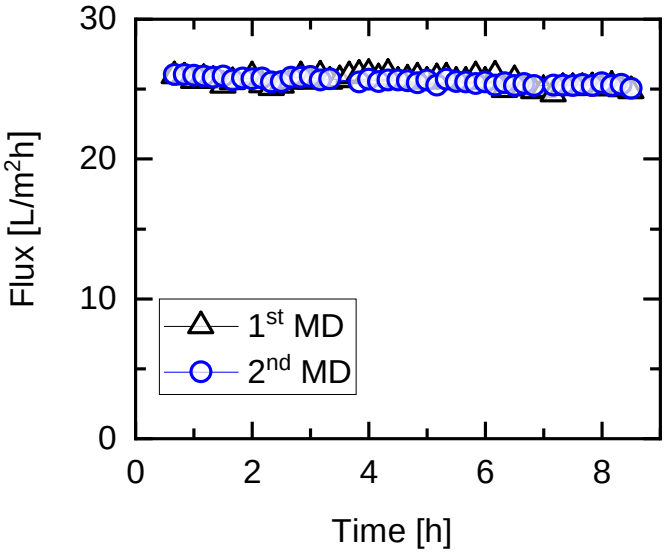

Fig. 4-6. Permeate flux during membrane distillation (MD) treatment of reverse osmosis (RO) concentrate to achieve 98% overall water recovery (feed temperature of 50°C, permeate temperature of 20°C, feed cross-flow velocity (CFV) of 0.4 m/s, and permeate CFV of 0.53 m/s). The experiment was performed twice. Symbols represent average fluxes in 10 min.

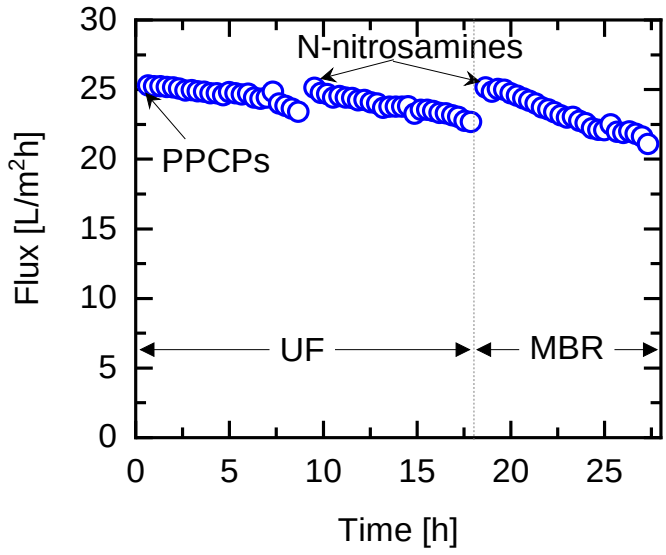

Fig. 4-7. Variation of permeate flux over the time during the reverse osmosis (RO) concentrate treatment by membrane distillation (MD). The membrane was at a feed temperature of 50°C, the distillate temperature was 20°C, the feed cross-flow velocity (CFV) of 0.4 m/s, and the distillate CFV was 0.53 m/s. The RO concentrate was prepared using ultrafiltration (UF) or membrane bioreactor effluent (MBR) as the RO treatments. The experiment was performed once. The symbols represent the average fluxes in 20 min.

In contrast to MD treatment, membrane permeance changed considerably during RO treatment of the RO concentrate. Variation in TMP was monitored at a constant permeate flux of 25 L/m^{2}h. During the 1.5–1.7 h operation, TMP peaked at 4.5 MPa (Fig. 4-8), resulting in an overall recovery of only 88%, from 85%. This could partly be due to an increase in osmotic-pressure difference through further concentration of the wastewater. Membrane fouling is another factor that influences TMP levels. Pure-water permeability decreased considerably from 5.7 to 1.5–2.4 L/m^{2}hbar (58–73%) after RO treatment of the RO concentrate. In contrast, direct RO treatment of MBR effluent without pre-concentration did not cause membrane fouling, even when operated under the same conditions (Fig. 4-9). This outcome indicates that concentrated wastewater can intensify membrane fouling.

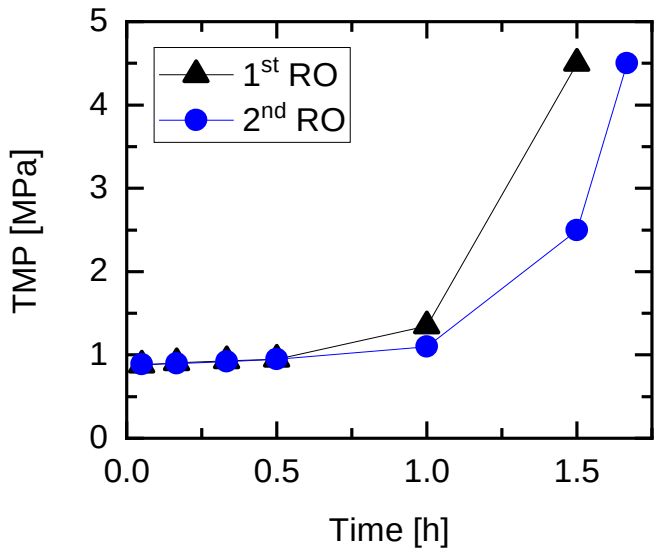

Fig. 4-8. Variation of transmembrane pressure (TMP) over time during the reverse osmosis (RO) treatment of the RO concentrate at a feed temperature of 20°C and a permeate flux of 25 L/m^{2}h. The experiment of RO concentrate treatment was performed twice.

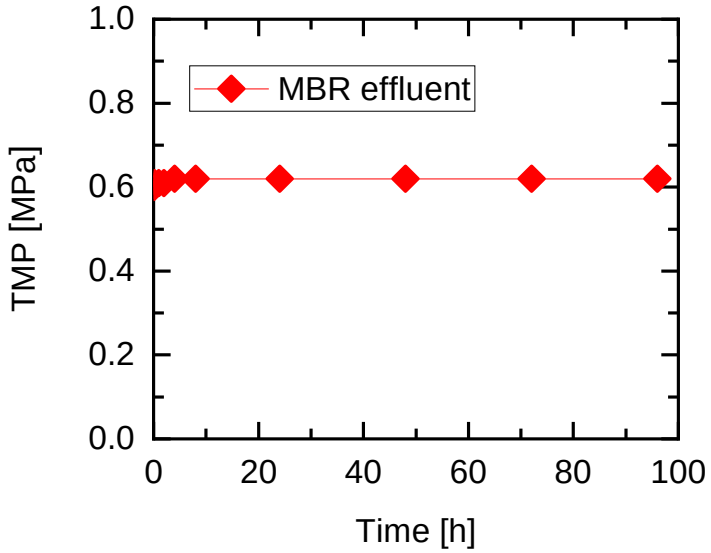

Fig. 4-9. Variation of transmembrane pressure (TMP) over time during reverse osmosis treatment of membrane bioreactor effluent (MBR) at a permeate flux of 25 L/m^{2}h and a feed temperature of 20°C. The experiment was performed once.

Normalized permeability data plotted against overall water recovery clearly show that MD caused far less membrane fouling than RO (Fig. 4-10). This finding is in line with previous studies that compared membrane-fouling levels of RO and MD wastewater treatment (Tow et al., 2018; Anwar and Rahaman, 2020). We also identified membrane fouling through SEM images of the membrane surface before and after treatment. A dense layer of foulants fully covered the RO membrane surface, while only scaling was observed on the MD membrane (Fig. 4-11). It is important to note that the cracks observed on the fouled ESPA2 RO membrane occurred during sample preparation prior to SEM imaging (drying process); thus, the cracks were not related to the membrane fouling propensity or separation performance. An AFM analysis of both membranes also indicated changes in the membrane surface morphology (Fig. 4-12). However, the compositions of the major foulants could not be determined using AFM analysis. Despite the changes in the appearance of the membrane surface, the hydrophobicity (i.e., contact angle) of the PTFE membrane remained high before and after the treatment (121° and 127°, respectively) (Table 4-3). These results indicate that membrane fouling that reduced the membrane permeability during MD treatment was negligible. The high hydrophobicity of PTFE membranes exhibits a high wetting resistance owing to the surface tension force (Rezaei et al., 2018; Lu et al., 2019). Therefore, foulants in the feed stream may not approach the membrane surface. However, the membrane's

hydrophobic properties can deteriorate or be lost during long-term operation (Chew et al., 2017), which can result in foulants attaching to the membrane surface and can cause operational changes from the MD treatment to the microfiltration treatment. Although long-term tests are still required, the MD treatment exhibited a strong potential for achieving 98% overall recovery without considerable membrane fouling, unlike RO treatment.

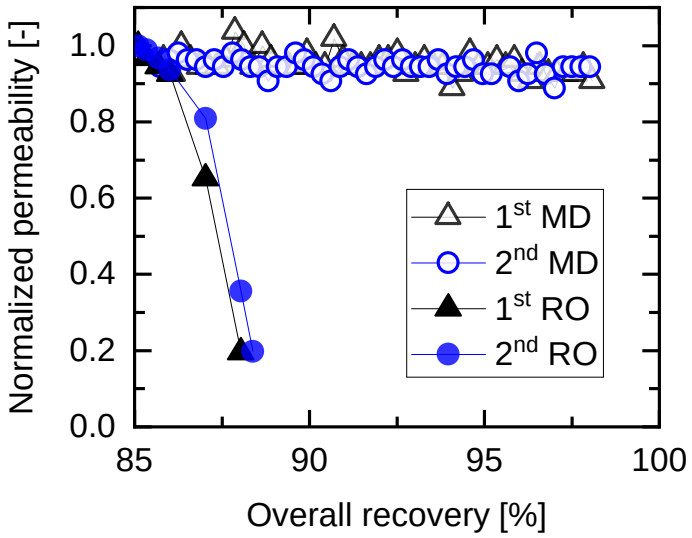

Fig. 4-10. Normalized permeability against overall water recovery during the reverse osmosis (RO) concentrate treatment. The experiment was performed twice. The results of Figs. 4-6 and 4-8 were standardized against overall water recovery.

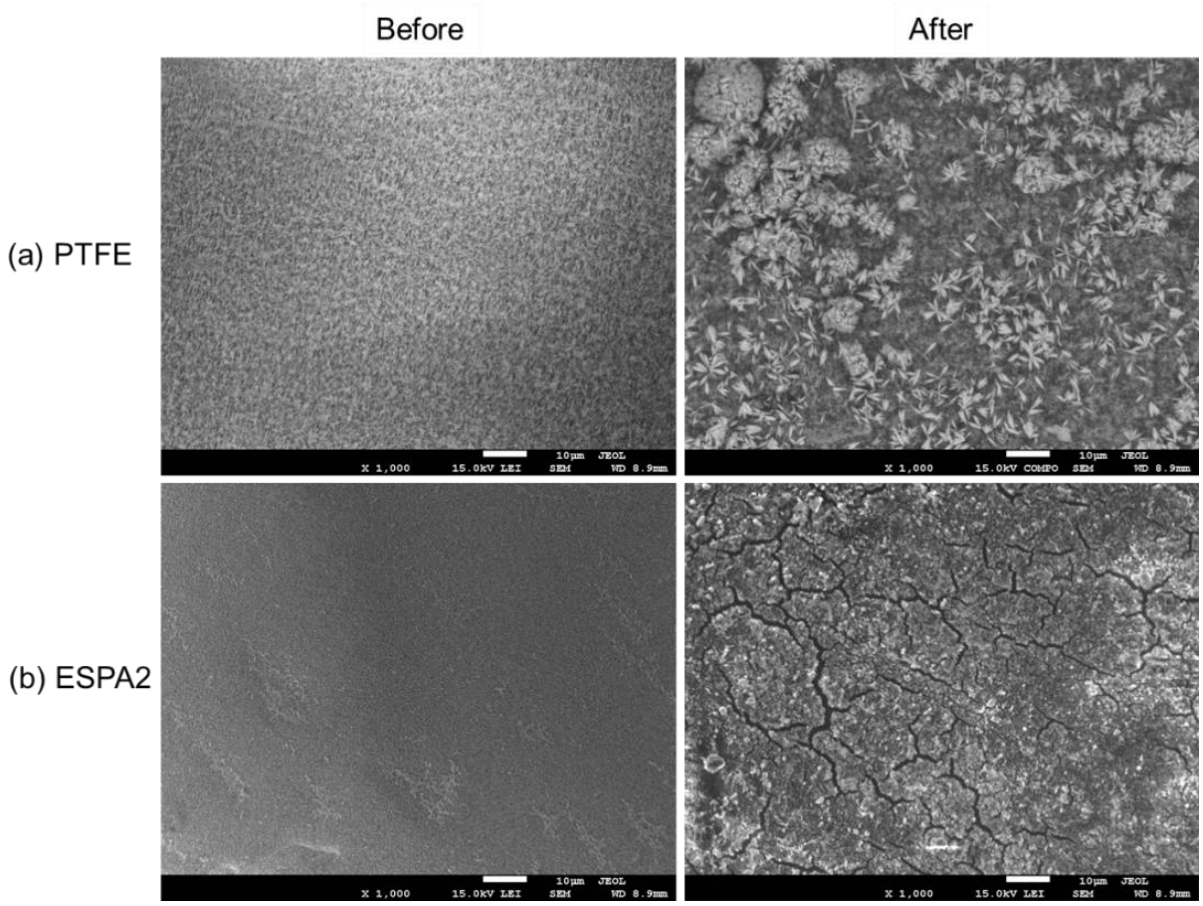

Fig. 4-11. Scanning electronic microscope (SEM) photographs of the membrane surface before and after the RO concentrate treatment at a permeate flux of 25 L/m^{2}h: (a) PTFE (microfiltration membrane used for MD treatment) (b) ESPA2 (RO) membranes.

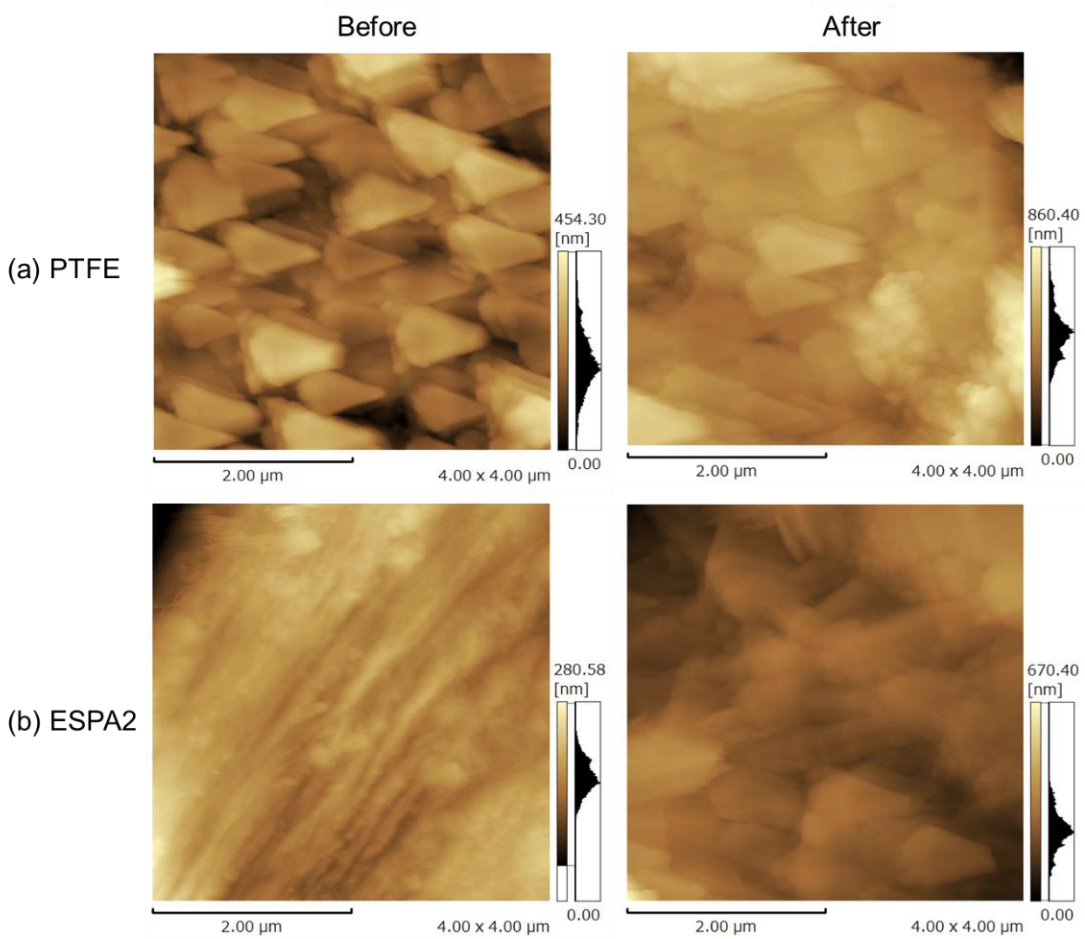

Fig. 4-12. Atomic force microscopy images of the membrane surface before and after the reverse osmosis (RO) concentrate treatment at a permeate flux of 25 L/m^{2}h: (a) PTFE (microfiltration membrane used for membrane distillation (MD) treatment) and (b) ESPA2 RO membranes.

Table 4-3. Contact angle (CA) of membranes before and after the treatment.

Treatment	Feed water	CA value (˚)*	
		before	after
MD	RO-concentrate + *N-nitrosamines*	126.5 ± 1.9	119.3 ± 2.1
	RO concentrate + PPCPs		124.2 ± 2.1
RO	RO-concentrate + *N-nitrosamines*	47.6 ± 2.3	40.6 ± 2.2
	RO-concentrate + PPCPs		34.6 ± 2.3

* For each membrane sample, six different locations were analyzed at a membrane area of 20 × 30 mm to obtain the average value. The water contact angle of the membrane was determined using ImageJ software.

4.3.3. Separation capacity

Reverse osmosis of the RO concentrate achieved 98.9% removal of electrical conductivity (Fig. 4-13), in line with what is typically observed during wastewater treatment (Fujioka et al., 2019; Roback et al., 2019). In contrast, MD treatment of the RO concentrate reached an even higher removal rate (99.8%), achieving an electrical conductivity of 7.3–8.4 μS/cm in the MD permeate. A similar electrical conductivity (<15 μS/cm) of the MD permeate during RO concentrate treatment has been reported by previous studies (Naidu et al., 2017; Rajwade et al., 2020) (Table 4-4). As MD membranes only allow volatile molecules to pass through the hydrophobic layer, almost all of the ions remain in the feed solution (i.e., high temperature stream), which ultimately results in high electrical conductivity rejection (Drioli et al., 2015).

We also used EEM spectra to evaluate dissolved-organics removal (Fig. 4-14). The assay detected three main peaks in the RO concentrate and the permeate, including aromatic proteins (peak A, 225–250/280–330 nm), protein-like substances (peak B, 260–280/300–380 nm), and humic acid-like substances (peak C, 250–400/380–550 nm) (Carstea et al., 2016; Yoon, 2019; Wang et al., 2021). Peak C was present at a high intensity (>15,000) in the RO concentrate, but disappeared after MD or RO treatment. The results indicate that both RO and MD treatments commonly have high capacities for removing humic acid-like substances.

High separation performance is important when MD treatment is used in potable reuse, as the humic-like substances can be precursors of disinfection by-products (DBPs), such as trihalomethanes (THMs), during chlorination (Ou et al., 2014). For the other major organics (peak A aromatic proteins and peak B protein-like substances), notable peaks in fluorescence intensities were observed after the MD and RO treatments. Aromatic protein and protein-like substances can contain small molecules, including tyrosine (molecular weight = 181 g/mol) and tryptophan (molecular weight = 204 g/mol), respectively (Hua et al., 2015), that may permeate the RO and MD membranes compared to humic acid-like substances (molecular weight >500 g/mol).

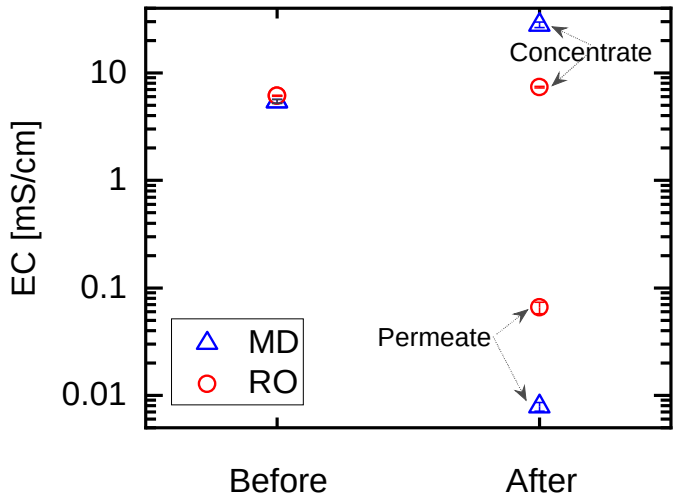

Fig. 4-13. Electrical conductivity (EC) of treated wastewater before and after treatment using membrane distillation (MD) and reverse osmosis (RO) membrane. The electrical conductivity in the distillate of MD treatment was converted to the concentration of the MD permeate by taking account of dilution effect.

Table 4-4. Comparison of separation performance in reverse osmosis (RO) treatment of the effluent from municipal wastewater.

Feed solution	Permeate flux (L/m^2h)	Water recovery (%)	EC in permeate (µS/cm)	TOrCs rejection (%)	References
RO concentrate	~16	85	10–15	96–99 (50–88 for propylparaben, salicylic acid, benzophenone, triclosan, bisphenol A, and atrazine)	(Naidu et al., 2017)
Effluent from an osmotic anaerobic MBR	1–2	-	(>99.6%)	>96 for PPCPs	(Caroline Ricci et al., 2021)
MBR-treated wastewater	17.5	70	<10	>95 (50–70 for 4-tert-octylphenol, 4-tert-butylphenol and benzophenone)	(Wijekoon et al., 2014)
RO concentrate	~25	98	7–8 (99.9%)	>99.6 (5–70 for *N*-nitrosamines)	This study

MBR: membrane bioreactor, EC: electrical conductivity, TOrCs: trace organic compounds and PPCPs: pharmaceuticals and personal care products.

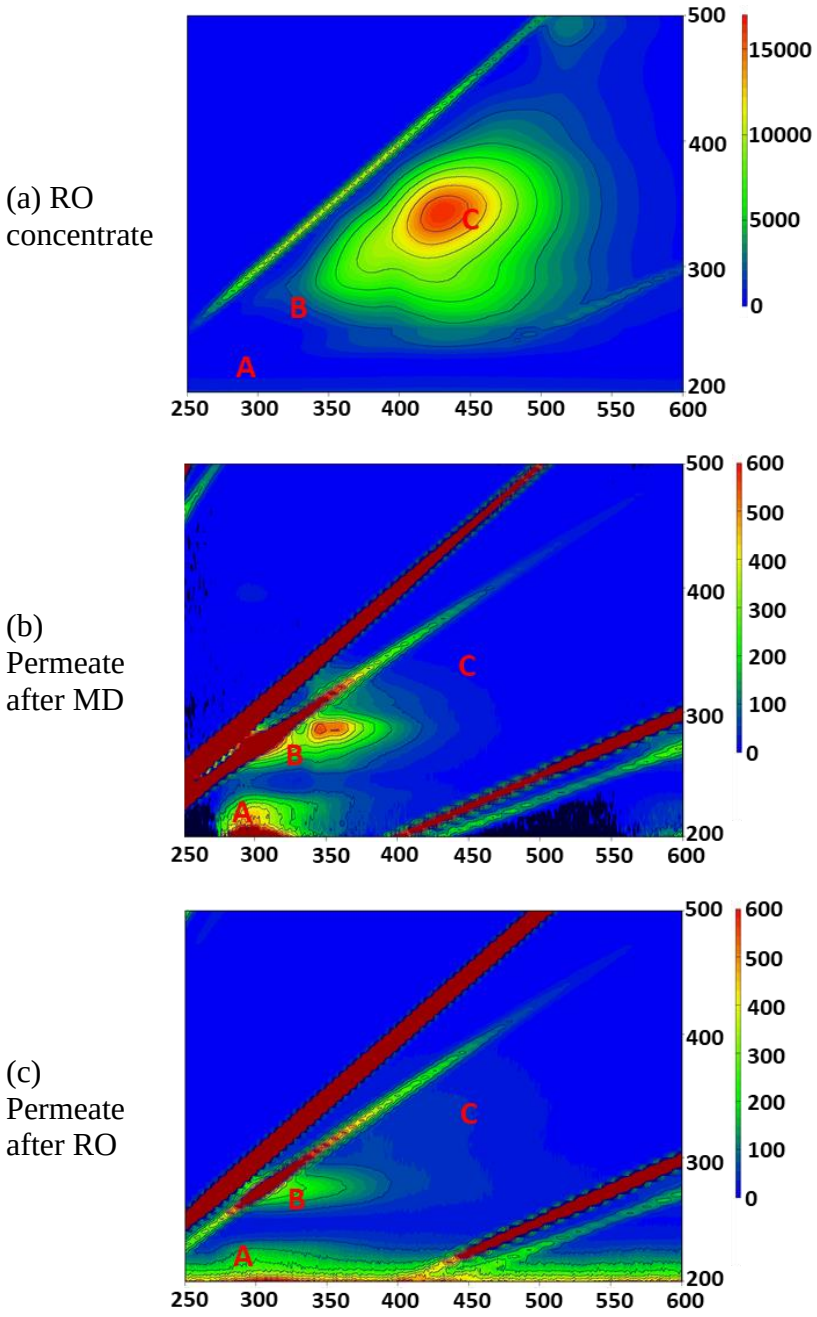

Fig. 4-14. Excitation-emission matrix fluorescence (EEM) spectra of (a) reverse osmosis (RO) concentrate prepared from membrane bioreactor effluent, (b) permeate after membrane distillation (MD), and (c) permeate after RO treatment.

Membrane-distillation rejection of most uncharged TOrCs in the RO concentrate was generally 100%, similar to rejection under RO treatment (Fig. 4-15). However, six TOrCs (*N*-nitrosodimethylamine [NDMA], *N*-nitrosomethyelthylamine [NMEA], *N*-nitrosopyrrolidine [NPYR], *N*-nitrosomorpholine [NMOR], crotamiton, and *N*,*N*-diethyl-meta-toluamide

[DEET]) had lower rejection under MD than RO. Details of chemical rejection are provided in Fig. 4-16. The ability of an RO membrane to remove uncharged TOrCs is governed by its minimum projection area (MPA), which is defined as the area of the compound projection with the minimum plane of its circular disk, based on the van der Waals radius (Fujioka et al., 2018; Fujioka et al., 2020). In other words, their removal is influenced by the clearance between the uncharged TOrCs and the membrane free volume hole. However, under MD treatment, the rejection of uncharged TOrCs was clearly governed by their volatility, represented as the log Henry's law constant (pK_H) (Fig. 4-17). Previous studies have also demonstrated low rejections of highly volatile TOrCs at $pK_H < 9$ (Wijekoon et al., 2014; Jeong et al., 2021). Notably, a hydrophobic membrane only allows vapor to cross its pores. As highly volatile chemicals (i.e., chemicals with low pK_H values) can evaporate even at low temperatures, they readily pass through the MD membrane, driven by the difference in partial pressure leading to their low rejection. In contrast to uncharged TOrCs, both MD and RO processes had high (>99.4%) rejection of charged TOrCs (Fig. 4-15). Overall, MD was inferior to RO in the removal of TOrCs with high volatility.

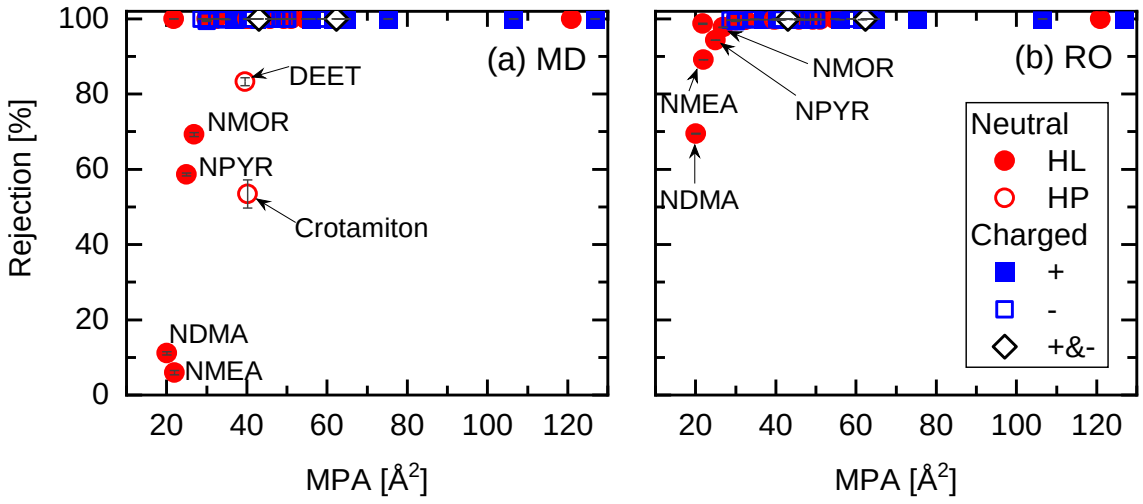

Fig. 4-15. Rejection of neutral hydrophilic (HL), neutral hydrophobic (HP), positively (+) and negatively (-) charged trace organic compounds (TOrCs) against their minimum projection area (MPA) under (a) membrane distillation (MD) treatment and (b) reverse osmosis (RO) treatment. *N*-nitrosodimethylamine (NDMA), *N*-nitrosomethyelthylamine (NMEA), *N*-nitrosopyrrolidine (NPYR), *N*-nitrosomorpholine (NMOR), and *N*,*N*-Diethyl-meta-toluamide (DEET). Each symbol shows the average and error ranges of triplicate samples collected at the end of the experiment.

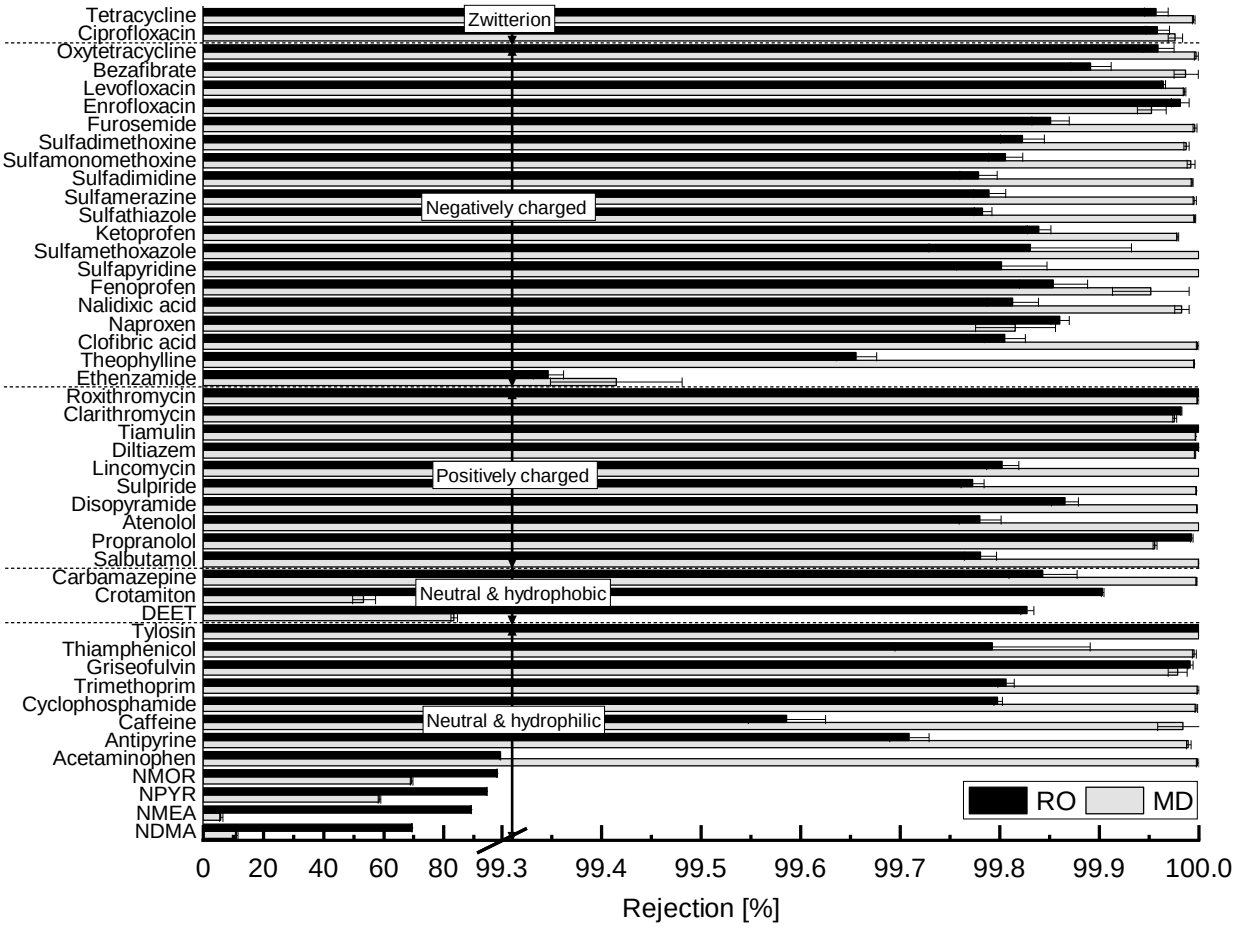

Fig. 4-16. Chemical rejection by membrane distillation (MD) treatment (reverse osmosis (RO) concentrate from the RO treatment of membrane bioreactor (MBR) effluent, a feed temperature of 50°C, a distillate temperature of 20°C, a feed cross-flow velocity (CFV) of 0.4 m/s and a distillate CFV of 0.53 m/s) and RO treatment (RO concentrate from the RO treatment of MBR effluent, a feed temperature of 20°C and a permeate flux of 25 L/m^{2}h).

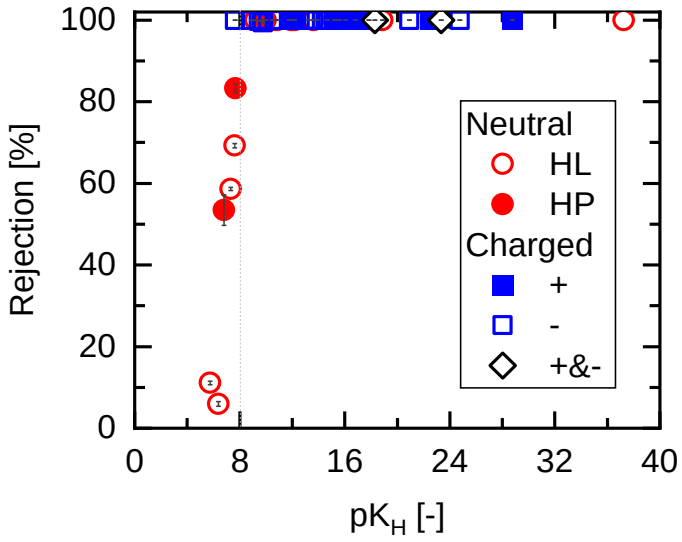

Fig. 4-17. The rejection of chemicals by membrane distillation (MD) as a function of their pK_H: hydrophilic (HL) – neutral, hydrophobic (HP) – neutral, positively (+) and negatively (-) charged, and zwitterionic (+&-) chemicals. The reverse osmosis (RO) concentrate was used as a feed solution that is prepared from membrane bioreactor (MBR) effluent. Each symbol shows the average and error ranges of triplicate samples collected at the end of the experiment.

At full-scale plants, both RO and MD permeate will be diluted with RO permeate produced from the main RO system, which achieved 85% water recovery. Water reclaimed from RO concentrate via RO or MD treatment has an additional flow rate (13% of the RO feed) that is less than the flow rate of the main RO system (85% of the RO feed). Therefore, the water quality of RO concentrate in MD or RO permeates generally has a small impact. However, residual NDMA concentrations in MD-treated wastewater require further evaluation, because they may be at concentrations higher than the regulated 10 ng/L in recycled water for potable water reuse (Plumlee et al., 2008; Hatt et al., 2013). Thus, post treatment of the main RO process, such as UV or UV-based advanced oxidation, will play an important role in removing residual NDMA and complying with existing regulations.

4.3.4. Energy consumption

4.3.4.1. Calculations for specific energy consumption in RO and MD

To calculate specific energy consumption (SEC) for additional water recovery from 85% to 98%, we assumed an advanced wastewater treatment plant with a production capacity of 100,000 m^3/d. At this plant, an RO concentrate of 15,000 m^3/d can be discharged from the main RO system with 85% water recovery.

❖ For direct contact MD system

The theoretical flux (J, $kgm^{-2}s^{-1}$) can be calculated by the following relation (Yun et al., 2006; Lee and Drioli, 2020):

$$J = B \times (P_{f,m} - P_{d,m}) \tag{4-9}$$

where $P_{f,m}$ and $P_{d,m}$ are the vapor pressures at the membrane surface on feed and distillate side, respectively. The membrane characteristic parameter B is determined using Knudsen diffusion (k_n >1), molecular diffusion (k_n <0.01), or combined Knudsen and molecular diffusion models ($0.01 \leq k_n \leq 1$) depending on the pore size and mean free path of water molecules. Based on the kinetic theory of gases, mean free path of water molecules can be calculated (Lee and Drioli, 2020):

$$l = \frac{K_B T_v}{\sqrt{2}\pi (d_{H2O})^2 P} = \frac{1.38 \times 10^{-23}\text{JK}^{-1} \times \frac{\text{Nm}}{\text{J}} \times (273+35)\text{K}}{\sqrt{2}\pi \times (2.641 \times 10^{-10})^2\ \text{m}^2 \times 1.013 \times 10^5 \text{Nm}^{-2}} = 1.3 \times 10^{-7}(\text{m}) \tag{4-10}$$

where K_B is the Boltzmann constant (1.38×10^{-23} JK^{-1}), T_v is an average temperature at the membrane (35°C), d_{H2O} is the diameter of water molecules (2.641×10^{-10} m) and P is the total pressure (1.013×10^5 Nm^{-2}).

Therefore, ratio of the mean free path of water molecules (l) and the membrane pore diameter (Lee and Drioli, 2020):

$$k_n = \frac{l}{r} = \frac{1.3 \times 10^{-7}\text{m}}{0.2 \times 10^{-6}\text{m}} = 0.65 \tag{4-11}$$

where r is the mean pore size of the PTFE membrane (0.2×10^{-6} m).

Therefore, the main physical transport mechanism in direct contact MD is the combination of Knudsen diffusion and molecular diffusion (Lee and Drioli, 2020):

$$B = \left[\frac{3\tau\delta}{2\varepsilon r}\left(\frac{\pi R T_{ave}}{8M_w}\right)^{1/2} + \frac{\tau\delta}{\varepsilon}\frac{Y_{ln}}{P D_{WA}}\frac{RT_{ave}}{M_w}\right]^{-1} \tag{4-12}$$

where δ is the membrane thickness (150 μm), ε is the porosity (80%), τ is the tortuosity factor ($\tau = \frac{1}{\varepsilon} = \frac{1}{0.8} = 1.25$) and r is the mean membrane pore (0.2×10^{-6} m), R is the universal gas constant (8314 $J.K^{-1}.kmol^{-1}$), T_{ave} is an average temperature at the membrane (35°C), M_w is the molecular weight of water (18 $kg.kmol^{-1}$), Y_{ln} is the log mean partial pressure of air, P is the total pressure and D_{WA} is the molecular diffusion coefficient. D_{KA} can be calculated by (Yun et al., 2006):

$$D_{WA} = 1.19 \times 10^{-4} \times \frac{(T_{ave} + 273)^{1.75}}{P} \tag{4-13}$$

The Antoine equation can be applied to calculate the vapor pressure P at any temperature T with the values of the constants followed by (Gryta et al., 1997):

$$P_i = e^{\left(23.238 - \frac{3841.273}{T_i - 45}\right)} \tag{4-14}$$

Assuming that $T_{f,m}$ = 40.4°C and $T_{d,m}$ = 32.9°C

$$P_{f,m} = e^{\left(23.238 - \frac{3841.273}{T_{f,m} - 45}\right)} = e^{\left(23.238 - \frac{3841.273}{273+40.4-45}\right)} = 7527$$

$$P_{d,m} = e^{\left(23.238 - \frac{3841.273}{T_{d,m} - 45}\right)} = e^{\left(23.238 - \frac{3841.273}{273+32.9-45}\right)} = 4988$$

where $T_{f,m}$ and $T_{d,m}$ are the temperature at the membrane surface on feed and distillate side respectively.

Therefore, log mean partial pressure of air at the membrane surface, Y_{ln}, is calculated (Lee and Drioli, 2020):

$$Y_{ln} = \frac{P_{f,m} - P_{d,m}}{ln\left(\frac{P_{f,m}}{P_{d,m}}\right)} = \frac{7527 - 4988}{ln\left(\frac{7527}{4988}\right)} = 6171 \tag{4-15}$$

From Eq. (4-12), (4-13) and (4-15):

$$B = \left[\frac{3 \times 1.25 \times 150 \times 10^{-6}}{2 \times 80\% \times 0.2 \times 10^{-6}}\left(\frac{\pi \times 8314 \times (273 + 35)}{8 \times 18}\right)^{1/2} + \frac{1.25 \times 150 \times 10^{-6}}{80\%} \frac{6171}{1.19 \times 10^{-4} \times (273 + 35)^{1.75}} \frac{8314 \times (273 + 35)}{18}\right]^{-1}$$

$$= 2 \times 10^{-6}$$

From Eq. (4-9):

$$J = B \times \left(P_{f,m} - P_{d,m}\right) = 2 \times 10^{-6} \times (7527 - 4988) = 0.005 \left(\frac{\text{kg}}{\text{m}^2\text{s}}\right)$$

In addition, the vapor enthalpy (H_v) can be calculated by using the following thermodynamic relationship at any temperature T (Phattaranawik et al., 2003):

$$H_v = 1.7535T + 2024.3 \tag{4-16}$$

From Eq. (4-16):

$$H_{ave} = 1.7535T + 2024.3 = 1.7535 \times 35 + 2024.3 = 2085 \left(\frac{\text{kJ}}{\text{kg}}\right) = 2085 \times 10^3 \left(\frac{\text{J}}{\text{kg}}\right)$$

The heat transfer coefficient for vapor flow through the membrane, h_v, can be calculated (Martínez-Díez and Vázquez-González, 1999):

$$h_v = \frac{J \times H_v}{T_{f,m} - T_{d,m}} \tag{4-17}$$

where H_v is the enthalpy of vapor at the average temperature of the membrane surface.

From Eq. (4-9), (4-16) and (4-17):

$$h_v = \frac{J\, H_v}{T_{f,m} - T_{d,m}} = \frac{0.005 \frac{\text{kg}}{\text{m}^2\text{s}} \times (2085 \times 10^3) \frac{\text{J}}{\text{kg}} \times \frac{\text{W}}{\text{Js}^{-1}}}{(40.4 - 32.9)\text{K}} = 1412 \left(\frac{\text{W}}{\text{m}^2\text{K}}\right)$$

The thermal conductivity of the membrane (k_m, $\text{Wm}^{-1}\text{K}^{-1}$) can be calculated (Martínez-Díez and Vázquez-González, 1999):

$$k_m = \varepsilon k_a + (1 - \varepsilon) k_p \tag{4-18}$$

where k_a and k_p are the thermal conductivities of air and membrane material (polymer), respectively. In this case, the membrane material is PTFE, therefore, k_p = 0.28 $\text{Wm}^{-1}\text{K}^{-1}$. The thermal conductivity of air, k_a, can be calculated (Adnan et al., 2012):

$$k_a = -3.393 \times 10^{-9} \times T^2 + 9.456 \times 10^{-6} \times \text{T} + 1.063 \times 10^{-4} \tag{4-19}$$

At 50°C, Eq. (4-19) becomes:

$$K_a = -3.393 \times 10^{-9} \times (273 + 50)^2 + 9.456 \times 10^{-6} \times (273 + 50) + 1.063 \times 10^{-4}$$
$$= 0.0028 \left(\frac{\text{W}}{\text{mK}}\right)$$

Eq. (4-18) becomes:

$$k_m = \varepsilon k_a + (1-\varepsilon)k_p = 80\% \times 0.0028 + (1-80\%) \times 0.28 = 0.058 \left(\frac{\mathrm{W}}{\mathrm{mK}}\right)$$

A flat-sheet membrane module is assumed to have a channel width of 1 m and a channel height of 0.005 m. Therefore, the hydraulic diameter is calculated by (Lee and Drioli, 2020):

$$D_h = \frac{2WH}{W+H} = \frac{2 \times 0.005 \times 1}{0.005 + 1} = 0.01 \text{ (m)}$$

Therefore, the Reynold number of the feed side (Re_f) and distillate side (Re_d)

For feed stream (50°C) (Gryta et al., 1997):

$$Re_f = \frac{v_f \rho_f D_h}{\varepsilon \mu} = \frac{0.1 \text{ m.s}^{-1} \times 988 \text{ kg.m}^{-3} \times 0.01 \text{ m}}{0.8 \times 1.0016 \times 10^{-3} \text{ kg.m}^{-1}.\text{s}^{-1}} = 1233$$

For distillate stream (20°C) (Gryta et al., 1997):

$$Re_d = \frac{v_d \rho_d D_h}{\varepsilon \mu} = \frac{0.05 \text{ m.s}^{-1} \times 998 \text{ kg.m}^{-3} \times 0.01 \text{ m}}{0.8 \times 0.5465 \times 10^{-3} \text{ kg.m}^{-1}.\text{s}^{-1}} = 1141$$

The thermal conductivity of water can be calculated (Adnan et al., 2012):

$$k_w = -1.861 \times 10^{-9} \times T^3 - 0.000008078 \times T^2 + 0.0057255 \times T - 0.432 \quad (4\text{-}20)$$

For feed stream (50°C):

$$k_{fw} = -1.861 \times 10^{-9} \times (273+50)^3 - 0.000008078 \times (273+50)^2 + 0.0057255 \times (273+50) - 0.432 = 0.512 \left(\frac{\mathrm{W}}{\mathrm{mK}}\right)$$

For distillate stream (20°C):

$$k_{dw} = -1.861 \times 10^{-9} \times (273+20)^3 - 0.000008078 \times (273+20)^2 + 0.0057255 \times (273+20) - 0.432 = 0.505 \left(\frac{\mathrm{W}}{\mathrm{mK}}\right)$$

The Prandtl number can be calculated by (Gryta et al., 1997):

$$Pr_i = \frac{\mu_i C_f}{k_{iw}} \quad (4\text{-}21)$$

Where μ is dynamic viscosity and C_p is heat capacity of water.

For feed stream (50°C):

$$Pr_f = \frac{1.0016 \times 10^{-3} \text{kg.m}^{-1}.\text{s}^{-1} \times 4180\ \text{J.kg}^{-1}.\text{K}^{-1}}{0.512\ \text{W.m}^{-1}.\text{K}^{-1} \times \frac{\text{J.s}^{-1}}{\text{W}}} = 8.1$$

For distillate stream (20°C):

$$Pr_d = \frac{0.5465 \times 10^{-3} \text{kg.m}^{-1}.\text{s}^{-1} \times 4180\ \text{J.kg}^{-1}.\text{K}^{-1}}{0.505\ \text{W.m}^{-1}.\text{K}^{-1} \times \frac{\text{J.s}^{-1}}{\text{W}}} = 4.5$$

The Nusselt number can be calculated in the laminar region (*Re* < 2100) (Gryta et al., 1997):

$$Nu_i = 0.13 \times {Re_i}^{0.64} \times {Pr_i}^{0.38} \tag{4-22}$$

For feed stream (50°C):

$$Nu_f = 0.13 \times 1233^{0.64} \times 8.1^{0.38} = 27.4$$

For distillate stream (20°C):

$$Nu_d = 0.13 \times 1141^{0.64} \times 4.5^{0.38} = 20.8$$

Theoretically, heat transfer coefficients can be calculated by the following general expression (Martínez-Díez and Vázquez-González, 1999):

$$h_i = \frac{Nu_i \times k_{iw}}{D_h} \tag{4-23}$$

For feed stream (50°C):

$$h_f = \frac{27.4 \times 0.512 \frac{\text{W}}{\text{mK}}}{0.01\ \text{m}} = 1402\ \left(\frac{\text{W}}{\text{m}^2\text{K}}\right)$$

For distillate stream (20°C):

$$h_d = \frac{20.8 \times 0.505 \frac{\text{W}}{\text{mK}}}{0.01\ \text{m}} = 1050\ \left(\frac{\text{W}}{\text{m}^2\text{K}}\right)$$

The corresponding temperatures at the membrane surfaces can be calculated by the following equations (Martínez-Díez and Vázquez-González, 1999):

$$T_{f,m} = T_{f,in} - \frac{\left(T_{f,in} - T_{d,in}\right) \times \frac{1}{h_f}}{\frac{1}{h_v + \frac{k_m}{\delta}} + \frac{1}{h_f} + \frac{1}{h_d}} = 50 - \frac{30 \times \frac{1}{1402}}{\frac{1}{1536 + \frac{0.058}{150 \times 10^{-6}}} + \frac{1}{1402} + \frac{1}{1050}} = 40.4℃ \tag{4-24}$$

$$T_{d,m} = T_{d,in} + \frac{(T_{f,in} - T_{d,in}) \times \frac{1}{h_d}}{\frac{1}{h_v + \frac{k_m}{\delta}} + \frac{1}{h_f} + \frac{1}{h_d}} = 20 + \frac{30 \times \frac{1}{1050}}{\frac{1}{1536 + \frac{0.058}{150 \times 10^{-6}}} + \frac{1}{1402} + \frac{1}{1050}} \quad (4\text{-}25)$$

$$= 32.9℃$$

The obtained temperatures at the membrane surface of the feed and distillate sides ($T_{f,m}$ and $T_{d,m}$) are the same as we assume ($T_{f,m}$ = 40.4℃ and $T_{d,m}$ = 32.9°C).

The trans-membrane temperature difference in the MD system (ΔT_{MD}) is (Christie et al., 2020):

$$\Delta T_{\mathrm{MD}} = T_{f,m} - T_{d,m} = 40.4 - 32.9 = 7.5℃$$

Because the interfacial temperature of feed side is lower than bulk feed solution and interfacial temperature of distillate side is higher than distillate bulk solution. It means that effective temperature gradient of two sides of the membrane (ΔT_{MD} = 7.5°C) is lower than the temperature difference between the bulk solutions *(*$\Delta T = T_{f,in} - T_{d,in}$ = 30°C).

Assuming that ΔT_{MD} is constant during MD process. As there is no recirculation in both feed streams, the inflow temperature of the feed is constant: $T_{f,in}$ = 20 °C. Therefore, the temperature gain of the feed stream in the heat source is given by:

$$\Delta T_{feed-gain} = T_{f.in} - T_f \quad (4\text{-}26)$$

The thermal power of heat absorbed in the heat source for the first stage is (Christie et al., 2020):

$$P = C_f Q_{f,in}(T_{f,in} - T_f) = \frac{4.2\ \mathrm{kJ}}{\mathrm{kg℃}} \times 0.174\ \frac{\mathrm{m}^3}{\mathrm{s}} \times \frac{1000\ \mathrm{kg}}{\mathrm{m}^3} \times (50 - 20)℃ = 21{,}875\left(\frac{\mathrm{kJ}}{\mathrm{s}}\right) \quad (4\text{-}27)$$

$$= 21{,}875\ (\mathrm{kW})$$

where C_f is specific heat capacity of the feed solution (kJ/kg°C), $Q_{f,in}$ is the inflow rate of the feed (0.026 m^3/s).

$$Q_{f,out} = Q_{f,in} - \Delta Q$$

Along the feed stream, the temperature drop of feed stream is the difference of inflow ($T_{f,in}$) and outflow ($T_{d,in} + \Delta T_{MD}$) temperature:

$$T_{f,in} - (T_{d,in} + \Delta T_{MD}) = \Delta T - \Delta T_{MD}$$

Hence, the heat loss along the feed stream is $C_f \times Q_{f,in} \times (\Delta T - \Delta T_{\mathrm{MD}})$

Part of the heat loss is for transferring phase of water from liquid to vapor (known as latent heat). The latent heat can be calculated as $\Delta Q \times H_v$ with H_v is the enthalpy of vaporization (kJ/kg):

$$\eta \times C_f \times Q_{f,in} \times (\Delta T - \Delta T_{MD}) = \Delta Q \times H_v$$

$$\Delta Q = \frac{\eta \times C_f \times Q_{f,in} \times (\Delta T - \Delta T_{\mathrm{MD}})}{H_v}$$

$$= \frac{0.85 \times \frac{4.2\ \mathrm{kJ}}{\mathrm{kg°C}} \times 0.174\ \frac{\mathrm{m}^3}{\mathrm{s}} \times \frac{1000\ \mathrm{kg}}{\mathrm{m}^3} \times (30 - 7.5)\mathrm{°C}}{2085\,\frac{\mathrm{kJ}}{\mathrm{kg}} \times 10^3 \mathrm{kg/m}^3}$$

$$= 0.0067\left(\frac{\mathrm{m}^3}{\mathrm{s}}\right)$$

where H_v is the average enthalpy of vaporization of feed stream and distillate stream (kJ/kg) and η (thermal efficiency) is the percentage of latent heat in total heat loss of feed stream.

Therefore, the outflow temperature of feed stream ($T_{f,out}$) and distillate stream ($T_{d,out}$) (Christie et al., 2020):

$$T_{f,out} = T_{d,in} + \Delta T_{\mathrm{MD}} = 20\mathrm{°C} + 7.5\mathrm{°C} = 27.5\mathrm{°C}$$

$$T_{d,out} = T_{f,in} - \Delta T_{\mathrm{MD}} = 50\mathrm{°C} - 7.5\mathrm{°C} = 42.5\mathrm{°C}$$

Therefore, to obtain 98% overall water recovery, 51 stages can be used in a series type. The specific energy consumption (*SEC*) is (Christie et al., 2020):

$$SEC = \frac{P}{\Delta Q} = \frac{374729\ \mathrm{kW}}{0.150\ \frac{\mathrm{m}^3}{\mathrm{s}} \times \frac{3600\mathrm{s}}{\mathrm{h}}} = 694\ (\mathrm{kWh/m}^3)$$

- For RO system

The composition of real RO-concentrate from RO treatment of municipal wastewater at a water recovery of 85% can be shown as follows (Naidu et al., 2017; Deng, 2020):

Composition	Unit	Value
pH	-	8
EC	µS/cm	6210
Turbidity	NTU	1.1
Calcium	mg/L	120
Magnesium	mg/L	100
Sodium	mg/L	938
Potassium	mg/L	100
Sulphate	mg/L	200
Chloride	mg/L	1880
Fluoride	mg/L	3
Nitrate	mg/L	12

Based on IMSdesign software for RO design from Hydranautics, to obtain the overall water recovery of 98%, the feed pressure of the RO system (P_a) can be calculated as 17.7 bar at a permeate flux of 25 L/m^{2}h, a feed temperature of 20°C. Therefore, the power consumption (Li, 2011):

$$P_{\text{power}} = \frac{P_a \times Q_{r,in}}{\eta_{pump}} = \frac{17.7\ \text{bar} \times 0.174 \frac{\text{m}^3}{\text{s}}}{0.85} = 3.62 \times [10^5 \times \text{Pa}] \times \frac{\text{m}^3}{\text{s}}$$

$$= 3.62 \times \left[10^5 \times \frac{\text{N}}{\text{m}^2}\right] \times \frac{\text{m}^3}{\text{s}} = 3.62 \times 10^5 \times \frac{\text{Nm}}{\text{s}} = 3.62 \times 10^5 \times \frac{\text{J}}{\text{s}}$$

$$= 3.62 \times 10^5\ \text{W} = 362\ (\text{kW})$$

where $Q_{r,in}$ is feed flow rate (m^3/s) and η_{pump} is the pump efficiency.

The specific energy consumption (SEC) of RO system (Li, 2011):

$$\text{SEC} = \frac{P_{power}}{Q_{r,p}} = \frac{362\ \text{kW}}{0.15 \frac{\text{m}^3}{\text{s}} \times \frac{3600\text{s}}{\text{h}}} = 0.7\ (\text{kWh/m}^3)$$

where $Q_{r,p}$ is permeate flow rate (m^3/s).

Summaries of design assumptions and calculated results of SEC were presented in table 4-5.

Table 4-5. Design assumptions and calculations for specific energy consumption in reverse osmosis (RO) and membrane distillation (MD) plants with a capacity of 15,000 m^3/d.

Parameters	Symbol	Unit	Equation	Value
Inflow rate of the feed	Q_f	m^3/s		0.174
MD				
Membrane thickness	δ	m		150×10^{-6}
Porosity	ε	%		80
Tortuosity factor	τ	-		1.25
Mean pore size	r	m		0.2×10^{-6}
Thermal conductivity of PTFE	k_p	W/mK		0.28
Specific heat capacity of the feed solution	C_f	kJ/kg°C		4.2
Log mean partial pressure of air at the membrane surface	Y_{ln}	-	$Y_{ln} = \frac{P_{f,m} - P_{d,m}}{ln\left(\frac{P_{f,m}}{P_{d,m}}\right)}$	6171
Membrane characteristic parameter	B	-	$B = \left[\frac{3\tau\delta}{2\varepsilon r}\left(\frac{\pi RT_{ave}}{8M_w}\right)^{1/2} + \frac{\tau\delta}{\varepsilon}\frac{Y_{ln}}{PD_{WA}}\frac{RT_v}{M_w}\right]^{-1}$	2×10^{-6}
Average enthalpy of vaporization of feed and distillate stream (35°C)	H_v	kJ/kg	$H_v = 1.7535T + 2024.3$	2085
Heat transfer coefficient for vapor across the membrane	h_v	W/m^2K	$h_v = \frac{J \times H_v}{T_{f,m} - T_{d,m}}$	1412
Thermal conductivity of air	K_a	W/mK	$k_a = -3.393\times10^{-9}\times T^2 + 9.456\times10^{-6}\times \mathrm{T} + 1.063\times10^{-4}$	0.0028
Thermal conductivity of the membrane	k_m	W/mK	$k_m = \varepsilon k_a + (1-\varepsilon)k_p$	0.058
Thermal conductivity of feed stream	K_{fw}	W/mK	$k_{iw} = -1.861\times10^{-9}\times T^3 - 0.000008078\times T^2 + 0.0057255\times T - 0.432$	0.512
Thermal conductivity of distillate stream	K_{dw}	W/mK		0.505
Hydraulic diameter	D_h	m	$D_h = \frac{2WH}{W+H}$	0.01
Reynold number of the feed side	Re_f	-	$Re_f = \frac{v_f\rho_f D_h}{\varepsilon\mu}$	1233
Reynold number of the distillate side	Re_d	-	$Re_d = \frac{v_d\rho_d D_h}{\varepsilon\mu}$	1141
Prandtl number for feed stream	Pr_f	-	$Pr_f = \frac{\mu_f C_f}{k_{fw}}$	8.1
Prandtl number for distillate stream	Pr_d	-	$Pr_d = \frac{\mu_d C_f}{k_{dw}}$	4.5
Nusselt number for feed stream	Nu_f	-	$Nu_f = 0.13\times {Re_f}^{0.64}\times {Pr_f}^{0.38}$	27.4
Nusselt number for	Nu_d	-	$Nu_d = 0.13\times {Re_d}^{0.64}\times {Pr_d}^{0.38}$	20.8

distillate stream				
Heat transfer coefficients for feed stream	h_f	W/m^{2}K	$h_f = \frac{Nu_f \times k_{fw}}{D_h}$	1402
Heat transfer coefficients for distillate stream	h_d	W/m^{2}K	$h_d = \frac{Nu_d \times k_{dw}}{D_h}$	1050
Temperature at the membrane surface on feed side	$T_{f,m}$	°C	$T_{f,m} = T_{f,in} - \frac{(T_{f,in} - T_{d,in}) \times \frac{1}{h_f}}{\frac{1}{h_v + \frac{k_m}{\delta}} + \frac{1}{h_f} + \frac{1}{h_d}}$	40.4
Temperature at the membrane surface on distillate side	$T_{d,m}$	°C	$T_{d,m} = T_{d,in} + \frac{(T_{f,in} - T_{d,in}) \times \frac{1}{h_d}}{\frac{1}{h_v + \frac{k_m}{\delta}} + \frac{1}{h_f} + \frac{1}{h_d}}$	32.9
Outflow temperature of feed stream	$T_{f,out}$	°C	$T_{f,out} = T_{d,in} + \Delta T_{\mathrm{MD}}$	27.5
Outflow temperature of distillate stream	$T_{d,out}$	°C	$T_{d,out} = T_{f,in} - \Delta T_{\mathrm{MD}}$	42.5
Trans-membrane temperature difference	ΔT_{MD}	°C	$\Delta T_{\mathrm{MD}} = T_{f,m} - T_{d,m}$	7.5
Temperature gain of the feed stream in the heat source	$\Delta T_{\text{feed-gain}}$	°C	$\Delta T_{feed-gain} = T_{f.in} - T_f$	30
Thermal power of heat absorbed in the heat source	P	kW	$P = C_f Q_{f,in}(T_{f,in} - T_f)$	374729
Transmembrane flowrate for each stage	ΔQ_i	m^3/s	$\Delta Q_i = \frac{\eta \times C_f \times Q_{f,in} \times (\Delta T - \Delta T_{\mathrm{MD}})}{H_v}$	-
Number of stages	n	-	$\Delta Q = Q_1 + Q_2 + \cdots + Q_n = 0.150$	51
Specific energy consumption	SEC	kWh/m^3	$SEC = \frac{P}{\Delta Q}$	694
RO				
Pump efficiency	η_{pump}	%		85
Permeate flux	J_w	L/m^{2}h		25
Flow rate of permeate	$Q_{r,p}$	m^3/s		0.150
Feed temperature	T_f	°C		20
Applied pressure	P_a	bar		17.7
Power consumption	P_{power}	kW	$P_{power} = \frac{P_a \times Q_{r,in}}{\eta_{pump}} \times 10^2$	362
Specific energy consumption	SEC	kWh/m^3	$SEC = \frac{P_{power}}{Q_{r,p} \times 3600}$	0.7

Assumption: an advanced wastewater treatment plant with a production capacity of 100,000 m^3/d and an RO concentrate (15,000 m^3/d) discharged from the main RO system with 85% water recovery.

4.3.4.2. Assessment of energy consumption

For RO, the main source of energy consumption is electricity required for running high-pressure pumps, while the energy required for MD is mostly heat used to increase feed temperature. The SEC for RO treatment using ESPA2 RO membranes was calculated as 0.7 kWh/m^3. The MD treatment required 694 kWh/m^3 to achieve a feed temperature of 50 °C and MD-distillate temperature of 20 °C (Table 4-5). In general, MD had a significantly higher energy requirement than RO for treating RO concentrate. Previous research has also described a high SEC value in direct-contact MD (>350 kWh/m^3) (Table 4-6). High thermal energy consumption by MD during RO concentrate treatment can potentially be overcome by utilizing solar heat or industrial heat waste (e.g., power plants) (Naidu et al., 2018). This can reduce the electricity consumption required for heating during MD treatment. For example, applying waste heat to MD treatment has been reported to significantly reduce the total operating cost of fresh water production by 84% (e.g., from \$5.70/m^3 to \$0.74/m^3, (Tavakkoli et al., 2017)). Therefore, the feasibility of MD treatment of an RO concentrate may be dependent on the industries located near the advanced wastewater treatment plant. To assess the economic impact of MD treatment, future studies should conduct pilot-scale validation studies.

Despite the challengingly high energy requirement of MD treatment, achieving >85% water recovery using RO has such elevated fouling propensity that the resultant frequency in chemical cleaning makes the RO process infeasible. According to the RO membrane manufacturer's guidelines, chemical cleaning of the membranes is typically performed after the membrane permeability is reduced by 10–15%. The rapid membrane fouling observed during RO treatment of the RO concentrate suggests that chemical cleaning will be required several times per day to achieve 98% water recovery. However, the multiple chemical cleaning steps (i.e., dosing with a pre-heated chemical solution, recirculation, soaking, and flushing) typically require <10 h, and maintaining RO treatment operations by conducting several rounds of chemical cleaning per day is not practical. Therefore, MD treatment is a potential option when high water recovery is essential.

Table 4-6. Specific energy consumption (SEC) for reverse osmosis (RO) and direct-contact membrane distillation (MD) treatment.

Feed solution	Feed temperature (°C)	SEC in MD (kWh/m^3)	SEC in RO (kWh/m^3)	References
Synthetic water	35–65	689–1,037	-	(Elmarghany et al., 2019)
Wastewater	60	1,500	-	(Dow et al., 2016)
Synthetic water	80	<800	-	(Jantaporn et al., 2017)
RO brine	<50	350	6	(Alrehaili et al., 2020)
RO concentrate	-	-	1.3–2.3	(Tufa et al., 2019)
RO concentrate	50	694	0.7	This study

4.4. Conclusions

We successfully demonstrated that MD treatment can achieve 98% water recovery. Membrane distillation of RO concentrate only caused a minor reduction (4%) in membrane permeability, and this reduction was fully recovered during the pure water test. In contrast, RO treatment caused a considerable reduction in membrane permeability (73%), making it infeasible. Scaling was identified on the PTFE membrane surface used for MD. Despite negligible contribution to membrane fouling, scaling can become a major challenge for long-term operation. Therefore, future pilot studies are necessary to examine water recovery under MD treatment of RO concentrate. Both MD and RO resulted in similar water quality. Electrical conductivity rejection was very high (99.8%) for MD, but the treatment led to high permeation of TOrCs with high volatility, particularly NDMA. Post-treatment (e.g., advanced oxidation) after RO and MD processes may be needed to comply with NDMA regulations. Although MD requires far more energy than RO, the latter's high fouling propensity makes it unlikely to be a viable option for achieving 98% overall water recovery. Therefore, we recommend MD treatment as an alternative for high water-recovery processes. The management of energy sources (e.g., waste heat) will be key to MD feasibility in potable water reuse.

References

Adnan, S., Hoang, M., Wang, H., Xie, Z., 2012. Commercial PTFE membranes for membrane distillation application: Effect of microstructure and support material. Desalination 284, 297-308.

Alkhudhiri, A., Darwish, N., Hilal, N., 2012. Membrane distillation: A comprehensive review. Desalination 287, 2-18.

Alrehaili, O., Perreault, F., Sinha, S., Westerhoff, P., 2020. Increasing net water recovery of reverse osmosis with membrane distillation using natural thermal differentials between brine and co-located water sources: Impacts at large reclamation facilities. Water Res. 184, 116134.

Anwar, N., Rahaman, M.S., 2020. Membrane desalination processes for water recovery from pre-treated brewery wastewater: Performance and fouling. Sep. Purif. Technol. 252, 117420.

Ashoor, B.B., Mansour, S., Giwa, A., Dufour, V., Hasan, S.W., 2016. Principles and applications of direct contact membrane distillation (DCMD): A comprehensive review. Desalination 398, 222-246.

Caroline Ricci, B., Santos Arcanjo, G., Rezende Moreira, V., Abner Rocha Lebron, Y., Koch, K., Cristina Rodrigues Costa, F., Paulinelli Ferreira, B., Luiza Costa Lisboa, F., Diniz Miranda, L., Vieira de Faria, C., Celina Lange, L., Cristina Santos Amaral, M., 2021. A novel submerged anaerobic osmotic membrane bioreactor coupled to membrane distillation for water reclamation from municipal wastewater. Chem. Eng. J. 414, 128645.

Carstea, E.M., Bridgeman, J., Baker, A., Reynolds, D.M., 2016. Fluorescence spectroscopy for wastewater monitoring: A review. Water Res. 95, 205-219.

Chew, N.G.P., Zhao, S., Loh, C.H., Permogorov, N., Wang, R., 2017. Surfactant effects on water recovery from produced water via direct-contact membrane distillation. J. Membr. Sci. 528, 126-134.

Christie, K.S.S., Horseman, T., Lin, S., 2020. Energy efficiency of membrane distillation: Simplified analysis, heat recovery, and the use of waste-heat. Environ. Int. 138, 105588.

Damtie, M.M., Woo, Y.C., Kim, B., Park, K.-D., Hailemariam, R.H., Shon, H.K., Choi, J.-S., 2019. Analysis of mass transfer behavior in membrane distillation: Mathematical modeling under various conditions. Chemosphere 236, 124289.

Deng, H., 2020. A review on the application of ozonation to NF/RO concentrate for municipal wastewater reclamation. J. Hazard. Mater. 391, 122071.

Dow, N., Gray, S., Li, J.-d., Zhang, J., Ostarcevic, E., Liubinas, A., Atherton, P., Roeszler, G., Gibbs, A., Duke, M., 2016. Pilot trial of membrane distillation driven by low grade waste heat: Membrane fouling and energy assessment. Desalination 391, 30-42.

Drioli, E., Ali, A., Macedonio, F., 2015. Membrane distillation: Recent developments and perspectives. Desalination 356, 56-84.

Elmarghany, M.R., El-Shazly, A.H., Salem, M.S., Sabry, M.N., Nady, N., 2019. Thermal analysis evaluation of direct contact membrane distillation system. Case Studies in Thermal Engineering 13, 100377.

Fujioka, T., Khan, S.J., Poussade, Y., Drewes, J.E., Nghiem, L.D., 2012. N-nitrosamine removal by reverse osmosis for indirect potable water reuse – A critical review based on observations from laboratory-, pilot- and full-scale studies. Sep. Purif. Technol. 98, 503-515.

Fujioka, T., Kodamatani, H., Nghiem, L.D., Shintani, T., 2018. Transport of N-nitrosamines through a reverse osmosis membrane: role of molecular size and nitrogen atoms. Environmental Science & Technology Letters 6, 44-48.

Fujioka, T., Kodamatani, H., Yujue, W., Yu, K.D., Wanjaya, E.R., Yuan, H., Fang, M., Snyder, S.A., 2020. Assessing the passage of small pesticides through reverse osmosis membranes. J. Membr. Sci. 595, 117577.

Fujioka, T., Makabe, R., Mori, N., Snyder, S.A., Leddy, M., 2019. Assessment of online bacterial particle counts for monitoring the performance of reverse osmosis membrane process in potable reuse. Sci. Total Environ. 667, 540-544.

Gryta, M., Tomaszewska, M., Morawski, A.W., 1997. Membrane distillation with laminar flow. Sep. Purif. Technol. 11, 93-101.

Gu, H., Plumlee, M.H., Boyd, M., Hwang, M., Lozier, J.C., 2021. Operational optimization of closed-circuit reverse osmosis (CCRO) pilot to recover concentrate at an advanced water purification facility for potable reuse. Desalination 518, 115300.

Guo, J., Farid, M.U., Lee, E.-J., Yan, D.Y.-S., Jeong, S., Kyoungjin An, A., 2018. Fouling behavior of negatively charged PVDF membrane in membrane distillation for removal of antibiotics from wastewater. J. Membr. Sci. 551, 12-19.

Hatt, J.W., Lamy, C., Germain, E., Tupper, M., Judd, S.J., 2013. NDMA formation in secondary wastewater effluent. Chemosphere 91, 83-87.

Hua, G., Reckhow, D.A., Abusallout, I., 2015. Correlation between SUVA and DBP formation during chlorination and chloramination of NOM fractions from different sources. Chemosphere 130, 82-89.

Jacob, P., Phungsai, P., Fukushi, K., Visvanathan, C., 2015. Direct contact membrane distillation for anaerobic effluent treatment. J. Membr. Sci. 475, 330-339.

Jamil, S., Loganathan, P., Kandasamy, J., Listowski, A., McDonald, J.A., Khan, S.J., Vigneswaran, S., 2020. Removal of organic matter from wastewater reverse osmosis concentrate using granular activated carbon and anion exchange resin adsorbent columns in sequence. Chemosphere 261, 127549.

Jantaporn, W., Ali, A., Aimar, P., 2017. Specific energy requirement of direct contact membrane distillation. Chem. Eng. Res. Des. 128, 15-26.

Jeong, S., Song, K.G., Kim, J., Shin, J., Maeng, S.K., Park, J., 2021. Feasibility of membrane distillation process for potable water reuse: A barrier for dissolved organic matters and pharmaceuticals. J. Hazard. Mater. 409, 124499.

Jiang, W., Lin, L., Gedara, S.H., Schaub, T.M., Jarvis, J.M., Wang, X., Xu, X., Nirmalakhandan, N., Xu, P., 2020. Potable-quality water recovery from primary effluent through a coupled algal-osmosis membrane system. Chemosphere 240, 124883.

Kalla, S., 2021. Use of membrane distillation for oily wastewater treatment – A review. Journal of Environmental Chemical Engineering 9, 104641.

Kim, H.-C., Shin, J., Won, S., Lee, J.-Y., Maeng, S.K., Song, K.G., 2015. Membrane distillation combined with an anaerobic moving bed biofilm reactor for treating municipal wastewater. Water Res. 71, 97-106.

Kim, S., Lee, D.W., Cho, J., 2016. Application of direct contact membrane distillation process to treat anaerobic digestate. J. Membr. Sci. 511, 20-28.

Kodamatani, H., Roback, S.L., Plumlee, M.H., Ishida, K.P., Masunaga, H., Maruyama, N., Fujioka, T., 2018. An inline ion-exchange system in a chemiluminescence-based analyzer for direct analysis of N-nitrosamines in treated wastewater. J. Chromatogr. A 1553, 51-56.

Lee, Y., Drioli, E., 2020. MEMBRANE DISTILLATION : materials and processes. NOVA Science.

Li, M., 2011. Reducing specific energy consumption in Reverse Osmosis (RO) water desalination: An analysis from first principles. Desalination 276, 128-135.

Liu, C., Chen, L., Zhu, L., Wu, Z., Hu, Q., Pan, M., 2019. The effect of feed temperature on biofouling development on the MD membrane and its relationship with membrane performance: An especial attention to the microbial community succession. J. Membr. Sci. 573, 377-392.

Lu, K.J., Chen, Y., Chung, T.-S., 2019. Design of omniphobic interfaces for membrane distillation – A review. Water Res. 162, 64-77.

Martínez-Díez, L., Vázquez-González, M.I., 1999. Temperature and concentration polarization in membrane distillation of aqueous salt solutions. J. Membr. Sci. 156, 265-273.

Naghdali, Z., Sahebi, S., Mousazadeh, M., Jamali, H.A., 2020. Optimization of the forward osmosis process using aquaporin membranes in chromium removal. Chemical Engineering & Technology 43, 298-306.

Nagy, E., 2018. Basic equations of mass transport through a membrane layer. Elsevier.

Naidu, G., Jeong, S., Choi, Y., Vigneswaran, S., 2017. Membrane distillation for wastewater reverse osmosis concentrate treatment with water reuse potential. J. Membr. Sci. 524, 565-575.

Naidu, G., Tijing, L., Johir, M.A.H., Shon, H., Vigneswaran, S., 2020. Hybrid membrane distillation: Resource, nutrient and energy recovery. J. Membr. Sci. 599, 117832.

Naidu, G., Zhong, X., Vigneswaran, S., 2018. Comparison of membrane distillation and freeze crystallizer as alternatives for reverse osmosis concentrate treatment. Desalination 427, 10-18.

Narumiya, M., Nakada, N., Yamashita, N., Tanaka, H., 2013. Phase distribution and removal of pharmaceuticals and personal care products during anaerobic sludge digestion. J. Hazard. Mater. 260, 305-312.

Ou, H.-S., Wei, C.-H., Mo, C.-H., Wu, H.-Z., Ren, Y., Feng, C.-H., 2014. Novel insights into anoxic/aerobic1/aerobic2 biological fluidized-bed system for coke wastewater treatment by fluorescence excitation–emission matrix spectra coupled with parallel factor analysis. Chemosphere 113, 158-164.

Patel, A., Arkatkar, A., Singh, S., Rabbani, A., Solorza Medina, J.D., Ong, E.S., Habashy, M.M., Jadhav, D.A., Rene, E.R., Mungray, A.A., Mungray, A.K., 2021. Physico-chemical and biological treatment strategies for converting municipal wastewater and its residue to resources. Chemosphere 282, 130881.

Phattaranawik, J., Jiraratananon, R., Fane, A.G., 2003. Heat transport and membrane distillation coefficients in direct contact membrane distillation. J. Membr. Sci. 212, 177-193.

Piras, F., Santoro, O., Pastore, T., Pio, I., De Dominicis, E., Gritti, E., Caricato, R., Lionetto, M.G., Mele, G., Santoro, D., 2020. Controlling micropollutants in tertiary municipal wastewater by O3/H2O2, granular biofiltration and UV254/H2O2 for potable reuse applications. Chemosphere 239, 124635.

Plumlee, M.H., López-Mesas, M., Heidlberger, A., Ishida, K.P., Reinhard, M., 2008. N-nitrosodimethylamine (NDMA) removal by reverse osmosis and UV treatment and analysis via LC–MS/MS. Water Res. 42, 347-355.

Rajwade, K., Barrios, A.C., Garcia-Segura, S., Perreault, F., 2020. Pore wetting in membrane distillation treatment of municipal wastewater desalination brine and its mitigation by foam fractionation. Chemosphere 257, 127214.

Ren, J., Li, J., Chen, Z., Cheng, F., 2018. Fate and wetting potential of bio-refractory organics in membrane distillation for coke wastewater treatment. Chemosphere 208, 450-459.

Rezaei, M., Warsinger, D.M., Lienhard V, J.H., Duke, M.C., Matsuura, T., Samhaber, W.M., 2018. Wetting phenomena in membrane distillation: Mechanisms, reversal, and prevention. Water Res. 139, 329-352.

Roback, S.L., Ishida, K.P., Plumlee, M.H., 2019. Influence of reverse osmosis membrane age on rejection of NDMA precursors and formation of NDMA in finished water after full advanced treatment for potable reuse. Chemosphere 233, 120-131.

Shi, J., Dang, Y., Qu, D., Sun, D., 2019. Effective treatment of reverse osmosis concentrate from incineration leachate using direct contact membrane distillation coupled with a NaOH/PAM pre-treatment process. Chemosphere 220, 195-203.

Subramani, A., Jacangelo, J.G., 2014. Treatment technologies for reverse osmosis concentrate volume minimization: A review. Sep. Purif. Technol. 122, 472-489.

Tavakkoli, S., Lokare, O.R., Vidic, R.D., Khanna, V., 2017. A techno-economic assessment of membrane distillation for treatment of Marcellus shale produced water. Desalination 416, 24-34.

Tow, E.W., Warsinger, D.M., Trueworthy, A.M., Swaminathan, J., Thiel, G.P., Zubair, S.M., Myerson, A.S., Lienhard V, J.H., 2018. Comparison of fouling propensity between reverse osmosis, forward osmosis, and membrane distillation. J. Membr. Sci. 556, 352-364.

Tufa, R.A., Noviello, Y., Di Profio, G., Macedonio, F., Ali, A., Drioli, E., Fontananova, E., Bouzek, K., Curcio, E., 2019. Integrated membrane distillation-reverse electrodialysis system for energy-efficient seawater desalination. Applied Energy 253, 113551.

Wang, L., Zhang, X., Chen, S., Meng, F., Zhang, D., Liu, Y., Li, M., Liu, X., Huang, X., Qu, J., 2021. Spatial variation of dissolved organic nitrogen in Wuhan surface waters: Correlation with the occurrence of disinfection byproducts during the COVID-19 pandemic. Water Res. 198, 117138.

Wang, Z., Deshmukh, A., Du, Y., Elimelech, M., 2020. Minimal and zero liquid discharge with reverse osmosis using low-salt-rejection membranes. Water Res. 170, 115317.

Warsinger, D.M., Swaminathan, J., Guillen-Burrieza, E., Arafat, H.A., Lienhard V, J.H., 2015. Scaling and fouling in membrane distillation for desalination applications: A review. Desalination 356, 294-313.

Wijekoon, K.C., Hai, F.I., Kang, J., Price, W.E., Cath, T.Y., Nghiem, L.D., 2014. Rejection and fate of trace organic compounds (TrOCs) during membrane distillation. J. Membr. Sci. 453, 636-642.

Woldemariam, D., Kullab, A., Fortkamp, U., Magner, J., Royen, H., Martin, A., 2016. Membrane distillation pilot plant trials with pharmaceutical residues and energy demand analysis. Chem. Eng. J. 306, 471-483.

Yoon, S.-H., 2019. Potential and limitation of fluorescence-based membrane integrity monitoring (FMIM) for reverse osmosis membranes. Water Res. 154, 287-297.

Yun, Y., Ma, R., Zhang, W., Fane, A.G., Li, J., 2006. Direct contact membrane distillation mechanism for high concentration NaCl solutions. Desalination 188, 251-262.

Zhang, X., Liu, Y., 2020. Reverse osmosis concentrate: an essential link for closing loop of municipal wastewater reclamation towards urban sustainability. Chem. Eng. J., 127773.

Chapter 5. Conclusions and further works

5.1. Conclusions

Research on the assessment of membrane fouling behavior of nanofiltration and membrane distillation for water reuse was conducted in this doctoral dissertation. Nanofiltration (NF), reverse osmosis (RO), and membrane distillation (MD) membranes were used for evaluating membrane fouling in the treatment of secondary wastewater effluent and RO concentrate that was generated from concentrating municipal wastewater using RO membranes. The direct NF treatment of secondary wastewater effluent was applied using a submerged membrane module at low permeate flux (3 L/m^2h) for alleviating membrane fouling. During a 48-d operation, direct NF treatment resulted in an insignificant membrane fouling with the transmembrane pressure (TMP) increase of only 3 kPa. Direct NF treatment stably achieved high removal of organics during the test period with the rejection of color, $E_{254,}$ and total organic carbon at over 93, 84, and 67%, respectively. In the case of RO concentrate treatment, the membrane fouling propensity and water quality were compared during the treatment of the RO concentrate by MD and RO membrane at a permeate flux of 25 L/m^2h. Increasing overall water recovery from 85% to 98% did not significantly reduce the permeate flux (~4%) for MD treatment. However, the considerable increase in TMP in only 1.5 h indicates that the treatment of the RO concentrate by RO allowed only 88% of overall water recovery. MD rejection of most uncharged trace organic chemicals in the RO concentrate was generally 100%, similar to rejection under RO treatment. In general, this study demonstrated the efficacy of the direct NF treatment using a submerged NF and the feasibility of MD in RO concentrate treatment for achieving a stable operation and producing high-quality recycled water.

5.2. Further works

In this research, a submerged nanofiltration membrane module was adopted at permeate flux of 3 L/m^2h during the direct NF treatment to alleviate membrane fouling. Despite the successful suppression of membrane fouling, the employed permeate flux is considerably low compared to common cross-flow systems with extensive pretreatment. Moreover, the incomplete design of the submerged membrane module that was caused by the mismatch

between the membrane reservoir and membrane module resulted in the obtained water recovery of only <67%. Hence, further pilot-scale study with improved membrane module design and a larger membrane area is necessary to enhance the permeate flux and justify the applicability of the novel submerged NF membrane system on large scale for non-potable purposes. In addition, only a limited volume of wastewater was available in this bench-scale test in the laboratory; thus, the direct NF treatment was conducted in the dead-end batch mode. In particular, the feed solution in the membrane reservoir was replaced every 6-d to avoid the excessive accumulation of substances rejected by the NF membrane in the membrane reservoir. Therefore, continuous discharge of a certain percentage of the concentrate to avoid the concentration of rejected constituents in the membrane reservoir can limit the transmembrane pressure increase of the submerged NF system during a typical operation of wastewater treatment. An on-site test should be conducted at a municipal wastewater treatment plant for a long-term period to investigate membrane fouling propensity without influencing factors on the transmembrane pressure.

For the study on membrane distillation, although membrane fouling that reduced the membrane permeability during MD treatment was negligible, scaling was still found on the surface of the hydrophobic membrane. Moreover, low rejection of *N*-nitrosamines and other volatile compounds can cause membrane wetting for long-term operation. Therefore, another study should focus on modifying a hydrophobic surface or fabricating an ideal membrane to gain high wetting and fouling resistance in wastewater treatment for potable reuse. In addition, a considerably high energy requirement was found based on the calculation of specific energy consumption. Although taking advantage of solar energy or heat waste can address the energy problem in MD treatment, other limitations may arise, such as the inconsistent supply of waste heat and solar energy or the unavailability of renewable energy sources. Further study should be performed by incorporating photothermal materials (e.g., plasmonic metallic nanomaterials, inorganic semiconductor solar absorber materials, or carbon-based nanomaterials) with the membrane surface to maintain and increase the membrane surface temperature and then reduce energy consumption.

List of publications

(1) My Thi Tra Ngo, Binh Quoc Diep, Hideaki Sano, Yasuhiro Nishimura, Sandrine Boivin, Hitoshi Kodamatani, Haruka Takeuchi, Satya Candra Wibawa Sakti, Takahiro Fujioka*; Membrane distillation for achieving high water recovery for potable water reuse, *Chemosphere*, In Press (Chapter 4).

(2) My Thi Tra Ngo, Tetsuro Ueyama, Ryo Makabe, Xuan-Thanh Bui, Long D. Nghiem, Tran Thi Viet Nga, Takahiro Fujioka*; Fouling behavior and performance of a submerged flat-sheet nanofiltration membrane system for direct treatment of secondary wastewater effluent, *Journal of Water Process Engineering*, Vol. 41, pp. 101991 (2021.06) (Chapter 3).

(3) Takahiro Fujioka*, My Thi Tra Ngo, Ryo Makabe, Tetsuro Ueyama, Haruka Takeuchi, Tran Thi Viet Nga, Xuan-Thanh Bui, Hiroaki Tanaka; Submerged nanofiltration without pre-treatment for direct advanced drinking water treatment, *Chemosphere*, Vol. 265, pp. 129056 (2021.02).

(4) Takahiro Fujioka*, My Thi Tra Ngo, Ryo Makabe, Sandrine Boivin, Keisuke Ikehata; Pretreatment of Surface Waters and Wastewater by a Hemodiafilter for Online Bacterial Counting, *ACS ES&T Water*, Vol. 1, pp. 101–107 (2021.01).

(5) Takahiro Fujioka*, My Thi Tra Ngo, Tanki Mochochoko, Sandrine Boivin, Naoki Ohkuma, Hidenari Yasui, Mitsuharu Terashima; Biofouling control of a forward osmosis membrane during single-pass pre-concentration of wastewater, *Chemosphere*, Vol. 257, pp. 127263 (2020.10).

(6) Takahiro Fujioka*, My Thi Tra Ngo, Sandrine Boivin, Kengo Kawahara, Akihiro Takada, Yuki Nakamura, Hiro Yoshikawa; Controlling biofouling and disinfection by-product formation during reverse osmosis treatment for seawater desalination, *Desalination*, Vol. 488, pp. 114507 (2020.08).